PhD thesis
David Brian Noirat

Investigation of the role of glycerol in the mixtures with water or 1-propanol

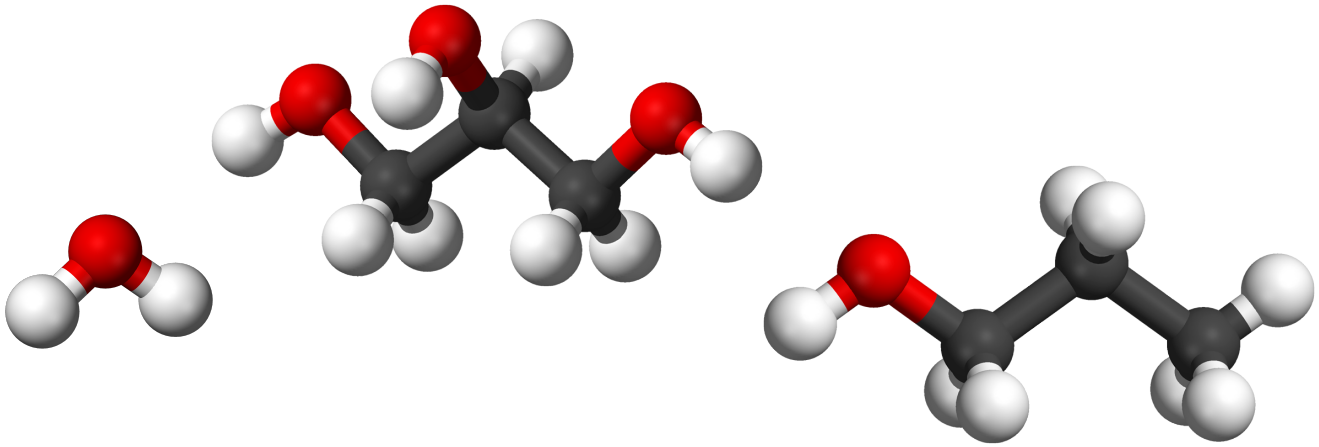

Roskilde University
INM, Glass & Time

Supervisor:
Kristine Niss

Institut Laue-Langevin
Spectroscopy

Supervisor:
Markus Appel

Roskilde University

NEUTRONS FOR SOCIETY

Investigation of the role of glycerol in the mixtures with water or 1-propanol

David Noirat

31 march 2023

Abstract

The general orientation of this thesis is the analysis of hydrogen bonded liquids by testing the shoving model, trying to expand the realm of prediction of the isomorph theory and trying to gather a better understanding of the microscopic contributions of the different parts of the molecule 1-propanol to its macroscopic dynamics.

We first test 1-propanol and a mixture with 10 % mol ratio glycerol in quasi elastic neutron scattering, with the tool of selective deuteration, to measure the contribution of the hydrogens in the hydrogen bonding network. We test its total local dynamic spectra at short timescale, pico to nano seconds, and try to link it to its slower macroscopic dynamics seen in dielectric spectroscopy. For this experiment, a new simultaneous neutron scattering and dielectric spectroscopy cell was developed. We found that the hydrogens in the alcohols do participate mostly in a slow mode, which we fitted to a Lorentzian function in inelastic fixed window scans. We found also that the shoving model does not predict well the mean squared displacement around the glass transition temperature.

We then test on two mixtures of glycerol water, 40 and 70 % mol ratio glycerol, the shoving model and with selective deuteration try to find some probable micro phase separation of either neat glycerol or neat water in the mixtures. No separate dynamics is seen and the shoving model's mean squared displacement prediction is not disproved for these mixtures of highly bonded liquids. We show also that once scaled to their respective timescale, the two mixtures have isochronal superposition, showing similar behavior.

Lastly, we test over a pressure range of 0.1 - 400 MPa isochronal superposition and the isomorph theory on the same two glycerol water mixtures. We show that with dielectric spectroscopy slightly above the glass transition temperature, isochronal superposition is not present. The deviation from superposition is more pronounced for the 40 % mixture. But at the nanosecond timescale and high temperature in neutron scattering, we do observe a rather good superposition of dynamics. We also show that the dielectric isoconductivity is a rather good indication for finding isochrones at high temperature.

Acknowledgment

I first want to thank my two supervisors, Kristine Niss and Markus Appel, for guiding me along my journey that brought me to the conclusion of my PhD. The support was present anytime I required and definitely accompanied me in the rich area of neutron scattering and the study of liquid dynamics. This to the point of allowing me by the end of this journey to be able to manage a beam time from the start to the near end all by myself without problems. I am also very thankful towards Bernhard Frick with whom I shared a lot, from the beginning as IN16 instrument manager to later times, once retired from the ILL, improving designs on dielectric cells for neutron scattering. And not forgetting the instrument's technician Jérôme Rimet who was very available even on last minute requests to help.

I am very thankful to the Institut Laue-Langevin, both financing this thesis and by allowing me to work in its leading facility. This granted me easy and direct access to a plethora of skilled engineers and top class scientist on different instruments. Scientists from IN5's Jacques Ollivier to WASP's Bela Fargo, from D4's Gabriel Cuello to ESRF ID31's Veijo Honkimäki, or technicians on pressure Claude Payre and cryogenics Yohan Memphis and the IT support for the implementation of dielectric spectroscopy into ILL's instrument control, Yannick Le Goc.

I am very thankful to Roskilde University's IMFUFA and Glass & Time group with whom I spend time exchanging and integrated well, even though being based 1250 km away and going through a pandemic that limits travel is quite a hindrance. I want to thank warmly the physics workshop who supported me. Producing small parts I needed for experiments and more crucially the cells I used for simultaneous dielectric spectroscopy and neutron scattering that I designed with their help. Namely, Bo Jakobsen who did the bridge between the science and the technicians, Bjarne Christensen who created the plans for the cell and the rest of the team who produced the cells.

Contents

Chapter 1

Introduction

The study of glass forming liquids has been something that physicists have been at for a long time and that is slowly delivering its secrets. Glasses have been known in the prehistory and were already a sought after material, used as gifts and traded around the world. In the last decades, advances in materials, engineering and the associated tools at our disposition gave us more possibilities to try to understand the underlying processes of glasses and supercooled liquids. These are for example, dielectric spectroscopy or rheology and more recently, neutron scattering, dynamic light scattering, nuclear magnetic resonance.

This thesis originated from the work of Henriette Hansen [1] and Mikkel Jensen [2]. Henriette studied dipropylene glycol under pressure to test some models in the low hydrogen bonded liquid dipropylene glycol. She showed that even though it is a hydrogen bonded liquid with clear directional bonding, isochronal superposition is still partly present. For her work, she developed a pressure cell for simultaneous dielectric spectroscopy and neutron scattering. Mikkel Jensen did rheological studies of glycerol-water mixtures and found an additional slow mode that was concentration dependent with a threshold, $\approx 55\%$, under which it mostly disappeared. It is speculated that small clusters of neat glycerol, or water dependent on the concentration, is present with a micro phase separation. Coming from a speculation about micro phase separation in glycerol water mixtures, the interest of digging deeper in that subject with neutron scattering and using the new tool of simultaneous dielectric spectroscopy and neutron scattering, this project formed.

The study of mono alcohol came during the course of this thesis while working on dielectric spectroscopy of glycerol and researching literature on 1-propanol and its peculiar dielectric spectra. Since it is said that these molecules do form chain-like structures, the idea of introducing glycerol with its three carbon backbone and three alcohol groups, which we already were using, as a source of cross linking and possible disruption of the long chains of mono alcohol, all while increasing the density of alcohol groups in the mixture. Glycerol made the choice of 1-propanol seem natural. We kept then all molecules with a three carbon backbone and so, a rather similar length of molecule.

This thesis starts by giving a short theoretical introduction to the experimental techniques used, then goes to glasses, a specific elastic model, the shoving model, and the isomorph theory. We then present some specificity about hydrogen bonded liquids and more specifically about mono hydroxy alcohols. Following that, a brief explanation about the different experimental techniques used in neutron scattering and broadband dielectric spectroscopy. Before presenting the results, we list the instruments used with the samples and their origin. The results come in three chapters about mixtures of glycerol with: 1-propanol in chapter 5, water at atmospheric pressure with selective deuteration in chapter 6 and water under pressure in chapter 7. We finally finish with some concluding discussion about our results.

Chapter 2

Experimental techniques

In this chapter, the experimental techniques that were used for this work and the observables that are associated with will be introduced. Then in the next chapter, we will talk about the theories underlining our work and hypothesis.

2.1 Neutron Scattering

2.1.1 Quasi elastic neutron scattering

We will present here some of the neutron scattering concepts, following books [3–5], publication [6] and presentation from the Hercules school and Oxford neutron scattering school. Neutron scattering encompasses a broad range of techniques that can study the structure or dynamics of a system. We will introduce here the concepts that will be useful to understand the work of this study and the techniques used during this thesis.

Neutron scattering starts at the very beginning from having neutrons free from a nucleus. This step is achieved in large scale facilities by either nuclear reactor, which uses highly enriched uranium 235 that naturally releases neutron as part of its radioactive decay; or by spallation, where a particle accelerator collides high energy protons into heavy atoms to break them into smaller atoms and gather some neutrons in the process. After freeing these neutrons, they need to be slowed down to the desired energy, wavelength or temperature. For this, a moderator material, as D_2O, is used where the neutrons will bounce against and lose energy to get to the moderator's temperature. For our experiments, we use cold neutrons which are

moderated additionally with liquid D_2, which associated temperature are in the 20-50 K, energies of 0.3-10 meV or wavelengths of 10-4 Å.

The wavelength associated with the a particle of mass m and velocity v is called the de-Broglie wavelength and is described as:

$$\lambda = \frac{h}{mv} \tag{2.1}$$

$$p = mv = \hbar k \tag{2.2}$$

with k being the wave vector so we can rewrite it like:

$$\lambda = \frac{2\pi}{k} \tag{2.3}$$

From this incoming neutron, the general principle is to have it scatter from the nucleus of atoms to changes direction and sometimes energy. Then comparing the incoming k_i and outgoing k_f wave vector. The scattering vector Q, defined as $Q = k_i - k_f$, can give us our information about the dynamics and structure. In elastic scattering, no energy is transferred from the atom to the neutron, so $|k_i| = |k_f|$, like shown in the figure below.

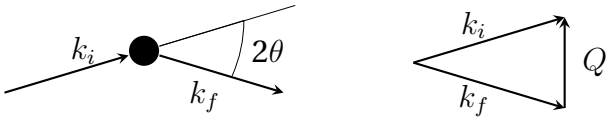

Figure 2.1: sketch of (left) incoming neutron vector k_i and outgoing neutron vector k_f with the angle of scattering and (right) how the Q vector is calculated.

If we are in inelastic scattering, then energy is transferred in the amount

$$\hbar\omega = E_i - E_f = \frac{\hbar^2}{2m}(k_i^2 - k_f^2) \tag{2.4}$$

What is actually measured during neutron scattering is the cross section, meaning a number of scattered neutrons in a solid angle as a function of energy. The differential cross section gives us the probability that a neutron will scatter in a given solid angle Ω.

$$\frac{\partial\sigma}{\partial\Omega} \tag{2.5}$$

with σ being the scattering cross section.

The scattering double-differential cross-section gives us then the probability that a neutron with energy E_f scatters in a solid angle Ω with energy transfer if $\hbar\omega$

$$\frac{\partial^2\sigma}{\partial\Omega\partial E} = \frac{1}{\hbar}\frac{\partial^2\sigma}{\partial\Omega\partial\omega}. \tag{2.6}$$

The scattering cross section is composed of a coherent and an incoherent part, referring to a collective and a self-motion part respectively.

$$\sigma = \sigma_{coh} + \sigma_{inc} \tag{2.7}$$

The values for each component are very isotope dependent and in general, $\sigma_{coh} > \sigma_{inc}$, but at least in the case of ^1H $\sigma_{inc} > \sigma_{coh}$.

The dynamic structure factor, $S(Q,\omega)$, which is what we probe in neutron scattering experiments, contains the spatial and dynamic properties of the probed sample. The double-differential cross-section can be rewritten as

$$\frac{\partial^2\sigma}{\partial\Omega\partial\omega} = \frac{k_f}{k_i}\frac{\hbar}{4\pi}\left(\sigma_{coh}S_{coh}(Q,\omega) + \sigma_{inc}S_{inc}(Q,\omega)\right). \tag{2.8}$$

The dynamic structure factor is linked to the intermediate scattering function through a time Fourier transformation and is the information that is measured in spin echo techniques.

$$S(Q,\omega) = \frac{1}{2\pi}\int_{-\infty}^{\infty} I(Q,t)\exp(-i\omega t)dt \tag{2.9}$$

The intermediate scattering function I is correlated to the pair distribution function $G(r,t)$ through a space Fourier transformation

$$G(r,t) = \frac{1}{(2\pi)^3}\int_{-\infty}^{\infty} I(Q,t)\exp(-iQ\cdot r)dQ \tag{2.10}$$

This function also has its coherent and incoherent part. The coherent pair distribution function $G_{coh}(r,t)$ tells then us the probability that with an atom with a position at the origin at time = 0, the same , or another scatterer can be found at a distance r at time = t. The incoherent pair distribution function $G_{inc}(r,t)$ tells then us the probability the same exact scatterer with a position at the origin at time = 0 can be found at a distance r at time = t.

About the separation of motions

The position vector of the scattering atoms $r(t)$ can be, in ideal system, separated in 2 components. $r_e(t)$ represents the equilibrium position relative to an external reference, which depends on time and $u(t)$ represents the displacement of the atom in the molecule, due to vibration, bending relative to chemical bonds which depends on internal and external timescale.

$$r(t) = r_e(t) + u(t) \tag{2.11}$$

For a liquid, these motions are mostly translations and rotations around the center of mass. The exact calculation of the intermediate scattering function, taking into account all types of motion is very difficult. So, the usual method is to separate it into factors of different motions. Here, we will separate between an intramolecular vibration part V and a reorientation term R.

$$I_{inc}(Q,t) = I^R_{inc}(Q,t) \cdot I^V_{inc}(Q,t) \tag{2.12}$$

And from this, the dynamic structure factor is a convolution of the reorientation and vibration terms.

$$S_{inc}(Q,\omega) = S^R_{inc}(Q,\omega) \otimes S^V_{inc}(Q,\omega) \tag{2.13}$$

For liquids close to or under the glass transition, due to their high viscosity, it can be assumed that the non moving parts contribute by a constant to the intermediate scattering function and a delta function in the $S(Q,\omega)$. We can then simplify

$$I_{inc}(Q,t) = \langle \exp(2Q \cdot u) \rangle \,. \tag{2.14}$$

In amorphous solids, isotropy is assumed which gives the average $\langle Q \cdot u \rangle$ direction independent. So again for a time $\to \infty$, using the Debye-Waller factor $\exp(-Q^2 < u^2 >)$, we see the following expression that we will come again soon at.

$$I_{inc} = \exp\left(-\frac{Q^2\langle u^2\rangle}{3}\right) \tag{2.15}$$

Neutron instrumentation

Time of flight (TOF)

Time of flight instruments are also called direct geometry instruments, where incoming neutron energy is selected and the outgoing one gives information with angle and the time the neutron took to interact with the detector. In TOF, the energy or velocity of a neutron is obtained by measuring the time it takes for a neutron to fly from the scattering event to the detector. With incoming neutrons before the scattering event coming all with the same energy in a very short pulse, inelastic scattering will give the neutrons a distribution of energies after it, thus a distribution of speed and time of arrival at the detector.

The TOF instrument used for this experiment was IN5 from the ILL as an example to detail the working of a typical instrument. For the incoming neutron beam, a pair of choppers cuts the continuous incoming beam of neutrons into short pulses, which give the scattering event a very thinly time dispersed distribution and also a buffer to not have slower neutrons arriving at the detectors overlapping with faster neutrons from the following packet. Then a second group of choppers will select the energy of the neutron in the incoming packet. After the scattering, the flight path until the detectors is 4 m. IN5 instrument has the time range 10^{-12} to 10^{-10} s, with energy resolution of about 100 μeV, energy transfer of -10 to 1.5 meV and Q range of 0.2-11 Å^{-1}.

Backscattering

The neutron backscattering spectrometer is an inverted geometry instrument, where the incoming neutron energy is broad and the selectivity happens after the scattering process. In this process, a crystal analyzer

using the Si111 reflection is placed after the scattering event and uses a Bragg angle of 90° to increase the energy resolution well into the sub μeV range. Unfortunately, this high selectivity in energy resolution means also a very low neutron count. Thus, instruments have to balance the resolution versus count rate of the instrument. On IN16B, the neutrons coming from the reactor are pulsed in packets by choppers that are monochromatized and reflected on a Doppler monochromator. The monochromator can be moved with finite velocity such that the selected neutron wavelength is shifted accordingly. the selected neutrons then scatter from the sample and hits the analyzer crystals. Neutrons with selected energy will be reflected back to the detectors. IN16B with Si111 in high flux settings has an energy resolution of 0.8 μeV, energy transfer of $\pm$30 μeV and Q range of 0.1-1.8 Å^{-1}.

IN16B allows also for 2 specific modes. Namely fixed window scans (FWS), which is presented in Frick et al. [7], and a mix of backscattering and time of flight (BATS), presented in Appel et al. [8][9]. FWS is a mode where the incoming neutrons come with a fixed wavelength. Depending on the selection of the incoming wavelength, in conjunction with the selectivity of the crystal analyzer, it is possible to focus the measurement on a specific energy transfer value. If the incoming and outgoing energy selected are the same, we measure the elastic scattering (EFWS) by measuring $S(Q,0)$. This the calculation of the mean squared displacement, which will be looked more in depth in the following section 3.4.2. If a different energy is selected, an inelastic scattering (IFWS) permits to look at a specific timescale process. This mode allows also for a higher count rate, allowing quasi dynamics measurements like cooling or heating ramps while still having acceptable statistics. The second specific mode, BATS, mixes parts of backscattering, the crystal analyzer and time of flight, another set of choppers to create the t_0 pulse. The Doppler monochromator is then not present. The mix of those 2 techniques allows for a bridge in the energy window of standard TOF and backscattering. with an energy resolution of 1.5-8 μeV, energy transfer of $\pm$ 250 μeV and Q range of 0.2-1.8 Å^{-1}.

Spin echo

Neutron spin echo is a time of flight technique that measure the intermediate scattering function. The main parts of a spin echo instrument is the presence of a spin polarizer, 2 spin flippers and magnetic coils sur-

rounding the sample. After going through a polarizer, the first coil flips all the spins perpendicular to the first coil's field. After the analyzer another coil of inverse magnetic field is placed before a second spin flipper. Then a polarization analyzer is place before the detectors.

If the neutron is passing through a magnetic field, it will start to precess around the magnetic field with its Larmor frequency $\omega_l = \gamma B$ with B the magnetic field's strength γ and the gyromagnetic ratio of the neutron. Knowing the speed of the neutrons and the distance traveled, its precession angle at that position should be $\phi = \gamma \frac{l}{v}$.

For elastic scattering, the total precession angle will be zero, as the energy, thus the speed of the neutron will be the same and they will spend the same time in the 2 coils. If the scattering is inelastic, the velocity of the neutrons after scattering will be different and the time it will take to travel up to the second coil will be of different time, giving a polarization that is different from neutrons that scatter only elastically. The polarization at the analyzer is a cosine of the phase angle of the neutron $P = \cos\phi$ which is related the the intermediate scattering function

$$P(Q,t) = \frac{\int_{-\infty}^{\infty} S(Q,\omega)\cos(\omega t)d\omega}{\int_{-\infty}^{\infty} S(Q,\omega)d\omega} \tag{2.16}$$

We see that P is the cosine of the transform of $S(Q,\omega)$. This is equal only to the real part of the intermediate scattering function $\Re eI(Q,t)$. We can rewrite then the polarization as

$$P(Q,t) = \frac{\Re eI(Q,t)}{I(Q,0)} \tag{2.17}$$

Spin echo accesses the intermediate Scattering function $I(Q,t)$ which in turn can be analyzed by doing a Fourier transform to $S(Q,\omega)$ which is the equivalent that we access by time of flight and back scattering.

2.1.2 Deuteration

Incoherent neutron scattering allows for a wonderful tool to discriminate parts of hydrogen containing samples. As written above, ^1H and ^2H have very different ratio between coherent and incoherent scattering cross section.The incoherent scattering length of hydrogen being $\approx$ 80 barn and

deuterium ≈2 barn. This makes deuterium mostly invisible in incoherent scattering while hydrogen has a strong signal. Some special attention is needed with highly deuterated samples. The appearance of a coherent scattering signal becomes non negligible anymore as its relative intensity compared to the incoherent signal grows.

Some problems arise also when one wishes to only partially deuterate a liquid. It is widely known that the protons of alcohol or of water are labile and exchange between molecules. Specific exchange of protons et deuterons has been studied early on, like by Hine and Thomas [10] and other already in the 1950's, where the exchange between the mono alcohols studied were at the limit of their instrument's speed. So, for the purpose of neutron scattering which require acquisition time from minutes to hours, the fast kinetics of the exchange of protons and deuterons limits the selective deuteration of hydrogen bonds to all be H or D in the liquid.

Some additional problems can also arise with deuteration of molecules as the change of mass between proton and deuteron can have significant effect on the dynamics of the sample. The most known example is the difference between light and heavy water. At atmospheric pressure, light water has a melting point of 0 °C and at 20 °C a dynamic viscosity of 1.002 mPa·s and heavy water has a melting point of 3.8 °C and at 20 °C a dynamic viscosity of 1.246 mPa·s. For study about dynamics, this effect needs to be investigated for all samples when hydrogen bonding is present and might be deuterated. This is important as deuterated samples might behave slightly different from fully protonated ones. If, for example, the dynamics of a sample changes due to the different hydrogen bonding strengths, an additional layer of analysis needs to be done to scale the processes before looking at potential dynamic mode disappearance due to deuteration.

2.1.3 SANS

Small angle neutron scattering is a diffraction technique, not a spectroscopy technique, like all other techniques that were presented until now. SANS focuses on the low to very low angle of diffraction, typically between 0.1 and 20°[11]. this translates roughly into Q values of 0.1 to 0.001 Å^{-1}. Since $Q = (2\pi/\lambda)sin(\theta/2)$, the small angle simplifies a value to $Q = (4\pi\theta/\lambda)$, giving in real space, sizes of nm to several μm. SANS measures density-density correlation function which can give structural and macro structural infor-

mation which in our case, we tried to test if some structure becomes visible in the partially deuterated samples.

2.2 Dielectric spectroscopy

In this section is presented a brief overview and a more complete introduction can be read in a textbook like Broadband Dielectric Spectroscopy by Kremer and Schönhals [12].

Dielectric spectroscopy is the analysis of the dielectric properties of a medium. The most common instruments work from the interaction of an oscillating electric field with the dipole moment of the measured sample. Standard experiments involve an alternative current flowing through a capacitor with the sample as the insulator between the two capacitor plates. Commercial equipment allow already for broadband measurement, i.e. 10^{-5} to 10^{7} Hz with high accuracy.

2.2.1 Parallel-plate capacitors

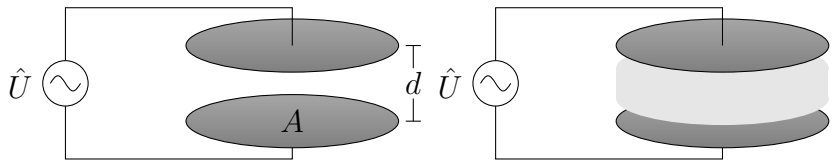

(a) With empty space (b) With dielectric

Figure 2.2: Schematic drawing of parallel-plate capacitor.

A parallel-plate capacitor, shown in figure 2.2, consists of two conducting plates connected to an electric current, aligned in such a way that the plates are not touching but are parallel with a small separation distance d. In the simple model, A is much larger compared to the separation, so that the electric field can be considered uniform throughout the space between the two plates and discard the boundary effects. If the capacitor is filled with a material with a relative permittivity of ϵ_r, the capacitance C of the setup can be found as:

$$C = \epsilon_r \epsilon_0 \frac{A}{d} = \epsilon_r C_0 = (\epsilon' + i\epsilon'')C_0 \tag{2.18}$$

ϵ' represents a storage of energy, while ϵ'' represents a loss of energy [12]. If we were in the vacuum, then ϵ_r would be 1 and the capacitance would just be

$$C_0 = \epsilon_0 \frac{A}{d}. \tag{2.19}$$

The capacitance C is a measure for the ratio between the voltage difference over the capacitor and the charges stored on the plates.

$$Q = CU \tag{2.20}$$

Where Q is the charge on the plates and U is the voltage over the capacitor.

In a direct current circuit, components have a resistance, classified through Ohm's law as the ratio of the voltage and the current. In alternating current circuits, certain components such as capacitors or inductors can also alter the phase of the current. A convenient way to describe amplitude and phase is the use of complex numbers for the mathematical description of such circuits. In reality, the voltages and currents that occur correspond only to the real part of these complex numbers.

The concept of complex impedance, $\hat{Z}$, must be introduced as the ratio between the (complex) voltage and (complex) current. As such the generalized Ohm's law becomes $\hat{U} = \hat{Z}\hat{I}$.

Taking the time derivative of equation 2.20, the relationship between the voltage and the current over a capacitor is apparent.

$$\frac{dQ}{dt} = \hat{I} = \hat{C}\frac{d\hat{U}}{dt} \tag{2.21}$$

The harmonically oscillating voltage of an alternating current can be written as the complex voltage

$$\hat{U} = U_0 e^{i(\omega t + \phi_U)} \tag{2.22}$$

where ω is the frequency and ϕ_U is a phase shift. Then, the time derivative of the voltage is

$$\frac{d\hat{U}}{dt} = i\omega U_0 e^{i(\omega t + \phi_U)} = i\omega\hat{U}. \tag{2.23}$$

The impedance of the capacitor is then:

$$\hat{Z} = \frac{\hat{U}}{\hat{I}} = \frac{1}{i\omega\hat{C}} \tag{2.24}$$

This can also be written as:

$$\hat{C} = -i\frac{1}{\omega\hat{Z}} \tag{2.25}$$

For a real life capacitor, there will be both storage of energy as well as some conduction. For a capacitor filled with a dielectric the conduction could arise from free charges in the dielectric, while dipoles in the dielectric also adds a contribution to the storage of energy. The impedance of the conduction can be considered a purely ohmic resistor of constant resistance, that is $\hat{C}_{cond} = -i/(\omega R_C)$, where R_C is a real number.

The real part of the capacitance would then be $\mathrm{Re}(\hat{C}_{conduction}) = \epsilon' = 0$. This shows us that the energy storage is independent of the conduction. The imaginary part is:

$$\mathrm{Im}(\hat{C}_{conduction}) = \epsilon'' = -\frac{1}{\omega R} \tag{2.26}$$

Taking the logarithm, this is equivalent to:

$$\log(-\epsilon'') = \log(\frac{1}{\omega R}) = -\log(\omega R) = -\log(\omega) - \log(R) \tag{2.27}$$

As such the logarithm of the loss of energy in the capacitor will consist of a frequency-dependent part as well as a constant term. Considering $\log(-\epsilon'')$ a function of the logarithm of ω, the function has a slope of -1. So for conduction phenomena we would expect to see a linear decrease in $\log(-\epsilon'')$ for increasing frequency [12].

In our case, we use a cylindrical capacitor, where the geometry makes the calculation a bit different. But since the separation between the 2 plates, inner and outer shell is so small, it is a reasonable assumption to consider it as a simple parallel plate capacitor.

Chapter 3

Dynamics of liquids

In this chapter, we will introduce to some basics about the dynamics of liquids [13–17]. First we start talking about hydrogen bonded liquids, more precisely mono alcohols and then about the glass transition. In the following part, we will present some concepts about elastic models and more specifically about the shoving model, and about the isomorph theory and its prediction about what is called "R-simple" liquids.

There are three main relaxation types we will talk about in this work, the α, β and Debye relaxation. The α relaxation is understood as the main relaxation of a system, one which is correlated to macroscopic values like viscosity. In some systems, like in polymers, side groups can exhibit a faster process which is called β. In strong directional multi molecular structures, a mode slower than the α relaxation can be seen in dielectric spectroscopy with strong intensity and a Debye shape, a symmetrical peak with slopes of 1 in log-log plots.

We will present in this chapter an introduction to the glass transition followed by a model and a theory about the dynamics of liquids, namely the shoving model and the isomorph theory. We will start by introducing molecular van der Waals liquids as weakly interacting liquids then the more complex hydrogen bonded liquids with their directional bonds that can make macrostructures.

3.1 Hydrogen bonded liquids

In this section, we will introduce the dynamics of hydrogen bonded liquids and more specifically about mono and poly alcohols, based mostly on Böhmer et al. [18], a long review from 2014.

Hydrogen bonded liquids possess a unique feature from which many interesting properties follow that other liquids do not share. It is the fact that they have the ability to break and reform bonds, either with another molecule or another hydrogen bonding section of the same molecule. This property allows then these liquids to form supramolecular structures. The hydrogen bonding unit, most commonly $N-H$ or $O-H$ can form more than one bond. The hydrogen can bond with a free electron pair from another atom. The oxygen has two free electron pairs, while nitrogen has one, that can bond with another hydrogen. These different possibilities allow then for many structures of different complexities to exist.

The functional groups that permit hydrogen bonding do also have quite a unique particularity. The bond between the hydrogen acceptor and the hydrogen can sometimes break and the free hydrogen can then rebind itself to another molecule's hydrogen acceptor. This property has been shown like in Hine and Thomas [10] where they looked in the exchange of H^+ and D^+ in alcohols and amines.

Due to their high polarization in their bonds, alcohols do possess strong dielectric signal that is easily measured by broadband dielectric spectroscopy, a technique that will be explained further in section 2.2.

One big question with the different dynamic modes that hydrogen bonded liquids have is what is actually contributing, at the local level, to the α, β or even Debye relaxation modes.

Davidson and Cole [19] showed that while the Debye model fitted well the main process of the data of monohydroxy alcohols, it failed for the poly alcohols. We do know now that the main process is not the α but an additional slow one.

3.1.1 1-propanol

Monohydroxy alcohols are a group of molecules that do possess as their main or only functional group an alcohol (O-H). The presence of only one

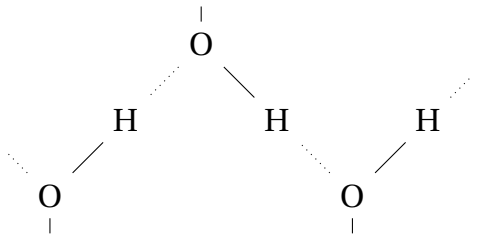

Figure 3.1: Schematic of hydrogen bonds $(\cdots)$ in chain. It is these bonds that can break and rearrange. The vertical lines from the (O) represent the chemical bonds between oxygen and the rest of the molecules.

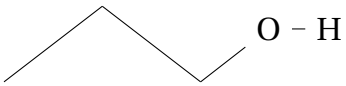

Figure 3.2: Propanol

group that is by itself polar makes these molecules strongly polar. This makes these molecules very easily studied by dielectric methods and thus studied for at least a century [20]. In early works, it was found that primary alcohols [21] do present a much higher dielectric constant than their tertiary counterparts, pointing to the possibility that they must make complex associations which possess strong polarizability. X-ray scattering [22] at the time also showed different structural length and other analysis pointed to the alcohol groups linking to form chains.

1-propanol is a monohydroxy alcohol with its alcohol group as a primary alcohol, as shown in figure 3.2. It was chosen for this project as it is a well studied alcohol by dielectrics, like in figure 3.3 with 3 fitted relaxation modes, and other methods [19, 23–32] in its neat form and there are still some open questions about which part of the molecule contribute to which dynamical mode.

1-propanol, like other mono alcohols, is thought to make macro structures that can resemble chains or rings. We show in figure 3.4 some schema of how they could look like. It is important to remember that since the hydrogen bonds can easily break that those structures are not static and chain length can vary through time, disassembling and reforming with other molecules or bunch of molecules from the neighboring.

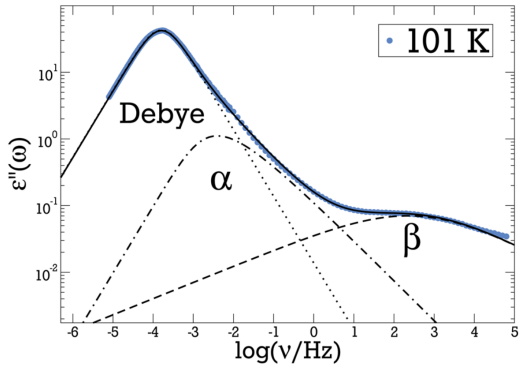

Figure 3.3: 1-propanol dielectric spectroscopy. Data (left) and figure (right) from Gabriel et al. [30]

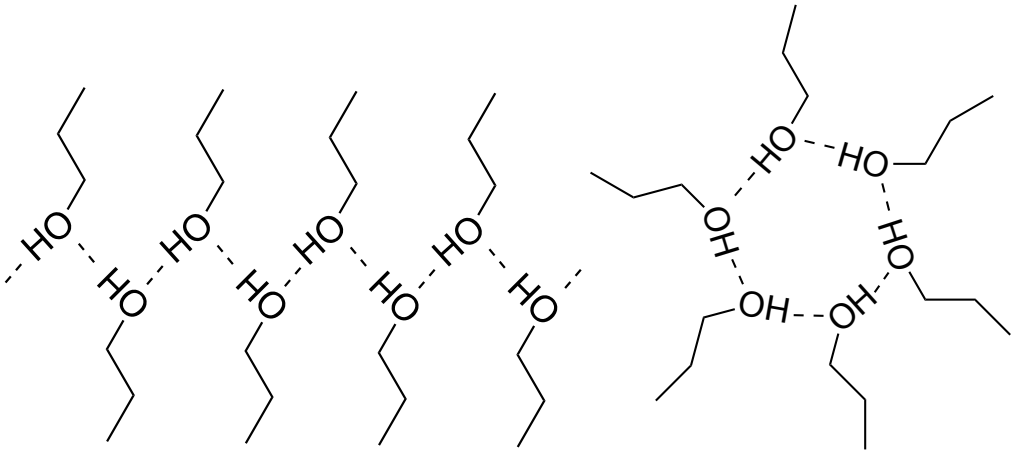

Figure 3.4: Schematic example of macro structure for 1-propanol. Left, chain like; right, ring like.

3.1.2 Glycerol

Poly alcohols are as the name implies molecules possessing more than one alcohol group. Glycerol is a poly alcohol with one alcohol group on each of its three carbons, so two primary alcohol groups and one secondary alcohol group, as shown in figure 3.5.

Glycerol-water mixtures were also studied in the glycerol rich region of the eutectic mixture (above 28 % molar ratio) via rheology [33]. It was shown that an additional slow mode is seen as a shoulder on the slow side of the maximum of the frequency dependent shear modulus G'' in rheology that is not present in dielectric spectroscopy. This shoulder is very present at high glycerol content, and disappears nearly at a concentration of 55 % and lower molar glycerol, with a sharp decline at that point. To make clear,

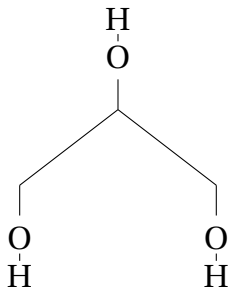

Figure 3.5: Glycerol

the addition of water, above a certain threshold, does inhibit an extra slow mode. The decoupling between the 2 modes can be seen in figure 3.6. The authors propose that the slow mode is linked to the rearrangement on the branched hydrogen network, which the water dampens at first then mostly destroys from a certain concentration.

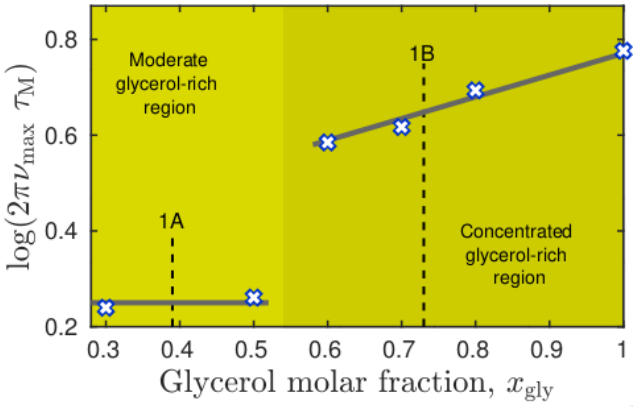

Figure 3.6: Decoupling index between the main relaxation and a slower mode at a frequency of 10 Hz in glycerol water mixtures, from Jensen et al. [33]

A few years prior, Puzenko et al. [34], Hayashi et al. [35] and Towey et al. [36] have already talked about the behavior difference at that threshold. That instinctively would have been at 40 % molar glycerol, the point at which there is the same amount of H-bonds offered by water as by glycerol. The schematic model proposed is that under 55 % molar glycerol, we start to see some water-water interaction.

3.2 The glass transition

The glass transition is a very loosely defined term, as it is not considered a phase transition. It is mostly describing a transformation where some physical properties of a sample change rather quickly over a short temperature, called the glass transition temperature (T_g). Liquids, as they cool down past their melting temperature, can either crystallize or become supercooled, meaning staying fluid under the melting temperature. When a liquid crystallizes, its atoms or molecules go through a transition that will lock into place their position in an orderly fashion (unit cell) that repeats itself in a 2D or mostly 3D arrangement. Its structure is dependent on the temperature and pressure at which it transforms and its physico-chemical properties. For supercooled liquids, the molecules slowly lose their translational energy/motion, seen in the α relaxation moving to longer timescale. To the extreme, this makes then once at or below the glass transition rearrangement into a crystal impossible and nearly locks into place the molecules. This makes the glass, unlike the supercooled liquid, stable out of equilibrium instead of a metastable equilibrium. There are some clear differences between crystallization and the glass transition. Crystallization involves a discontinuity in the density or specific volume, while the glass transition does not. The change in heat capacity or thermal expressivity in glasses shows a smooth step in lieu of a sharp one for crystallization, as is seen in figure 3.7. Still, for glasses some parameters even if smooth still change drastically, like viscosity or dielectric loss' timescale that changes many orders of magnitude.

All liquids can form glasses, with the caveat that for some, the rate of cooling needed to lock in place everything to inhibit the formation of a crystal needs to be too high to be practical in any sense for the ones we commonly not see as glasses. For example in some metals, the cooling rate necessary is in the order of hundreds of thousands of kelvin per second [37]. The glass transition is not a transition between states of thermodynamic equilibrium. The glass transition is history dependent, meaning that depending on what temperature/pressure, cooling rate the glass was formed, its thermodynamic properties are different, and the glass transition temperature T_g is different, as we show in the figure 3.7. The limits by which the glass transition is defined in physical terms is not standard across all of science. For rheological studies, it can be defined as a viscosity of 10^{12} Pa·s, for dielectric studies, like in this study, it is when the maximum of the di-

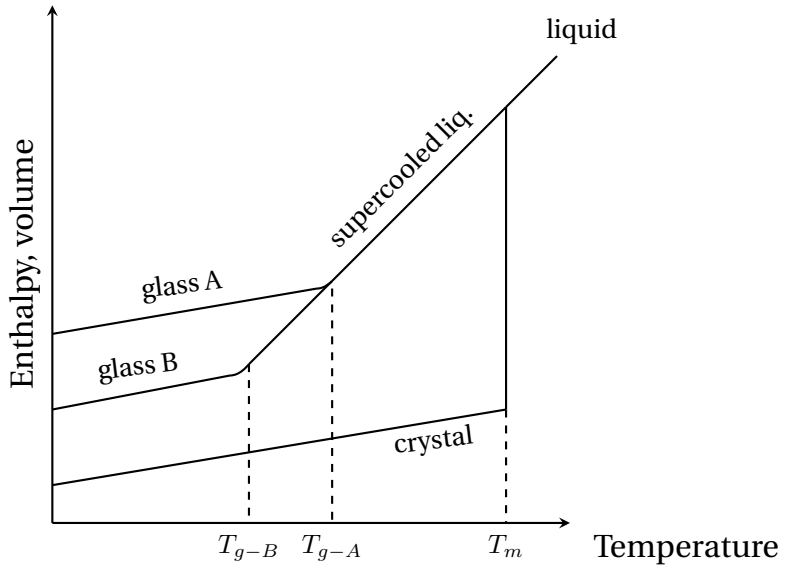

Figure 3.7: Schematic of two glass transitions and crystallization in temperature vs enthalpy/volume

electric loss is at a timescale of 100 s or for calorimetry, it is the intersection of the linear expansion of the curve before and the curve during the heat capacity increase, the increase can be seen in the insert of figure 3.8.

The relaxation process in liquids is thought to be governed by a potential energy barrier that is defined by an activation that the thermal energy can help overcome. The timescale of their average relaxation time is defined by [39, 40].

$$\tau(T) = \tau_0 \exp(\frac{\Delta E(T)}{k_B T}) \tag{3.1}$$

This process is similar to what happens in chemistry for the rearrangement of bonds and that follows an Arrhenius law. What has been seen is that glass formers do not follow as well an Arrhenius law, and Angell classified them with the concept of fragility. To find the fragility m of a system, we need to plot the log of the viscosity, or timescale of dielectric process versus T_g/T. The slope of the curve when $T_g/T \to 1$ is the fragility, see equation 3.2. We can see as the diagonal in figure 3.8 showing how a pure Arrhenius liquid would behave. The further a curve is from the diagonal, the less Arrhenius like it is and the more fragile it is called.

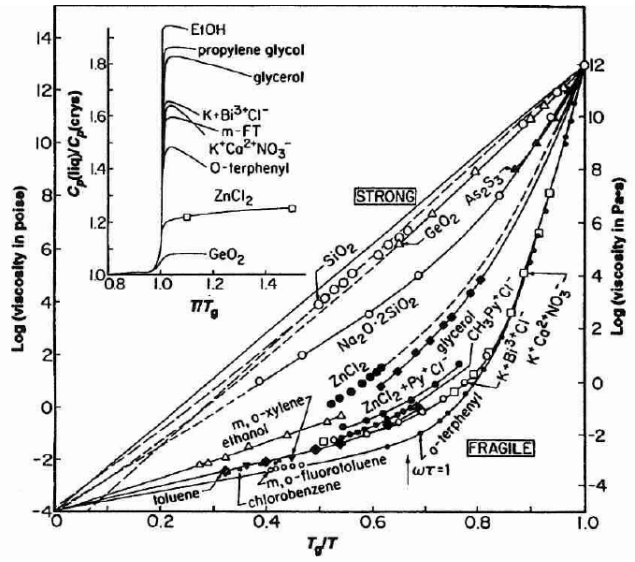

Figure 3.8: Angell plots: logarithm of viscosity vs. reduced temperature (T_g/T) plot for some glass forming liquids. Insert: heat capacity change at the glass transition for some liquids [38].

$$m = \frac{d \log_{10} \tau(T)}{d(T_g/T)} \tag{3.2}$$

3.3 Shoving model

What governs at the base relaxation time in liquids is still a very much open question. Some elastic models are trying to link fast and slow dynamics in liquids. We chose to concentrate on one of them, the shoving model.

As said before, one of the properties of glass forming liquids is that they can be supercooled, where the viscosity increases by orders of magnitude. In this state, van der Waals liquids flow events require a lot of molecules to rearrange themselves as they are densely packed. As the molecules this packed and of their strong repulsion forces, it requires a high amount of energy for them to rearrange. The idea about the shoving model [41, 42], is that in these cases, molecules can shove aside some molecules, creating a local increase in volume to rearrange themselves. The assumptions we need for the shoving model to work is that [43]: (1) The main contribution to the activation energy is elastic, (2) the elastic energy is only in the surroundings of the rearranging molecules and (3) the elastic energy is shear

energy, which is not related to any density change.

The work that needs to be done for the local rearrangement of the surrounding molecules creates an energy barrier. This barrier has 2 components contributing to it. First, the need for shoving the molecules aside and second for rearranging themselves. As these events are fast, it can be considered that the molecules surrounding this shell is solid. The shoving work depends then on the instantaneous shear modulus G_∞:

$$\Delta E(T) = G_\infty(T) V_c \tag{3.3}$$

V_c is the characteristic volume, which assumed to be temperature independent. For small changes in volume, it is

$$V_c = \frac{2}{3}\frac{(\Delta V)^2}{V}. \tag{3.4}$$

To know the potential energy, the harmonic oscillator parabola is assumed.

$$U = U_0 + \left(\frac{\Lambda}{2}\right) x^2 \tag{3.5}$$

Λ is a spring constant of our harmonic oscillator system. x is the distance from the minimum. Statistical mechanics gives us that $\langle u^2 \rangle = k_B T/\Lambda$. Here,$\langle u^2 \rangle$ is the configuration space average, and in the case of single atom, it is equivalent to the mean squared displacement. If we consider 2 parabolas for 2 local minima, then with the intersection of the 2 parabolas at a distance b from the minimum, the estimated lower barrier is given by

$$\Delta E(T) = \frac{\lambda}{2} b^2 = \frac{k_B T}{\langle x^2 \rangle}\frac{b^2}{2}. \tag{3.6}$$

We can then say about the energy barrier the following.

$$\Delta E(T) \propto \frac{k_B T}{\langle u^2 \rangle} \tag{3.7}$$

Since the energy barrier is inversely proportional to the mean squared displacement, it is possible to test it experimentally, as is then continued

further in section 3.4.2. We know also that the activation energy changes logarithmically with temperature and decreases with an increase in temperature. We can then define a temperature index:

$$I_{\Delta E} = -\frac{d\ln \Delta E(T)}{d\ln T} \tag{3.8}$$

The next following step is straightforward to go to the fragility (m), as shown in equation 3.2. A normal Arrhenius behavior gives an m value of 16, more explanation for that is shown in section 3.4.2. Merging the last 2 equations, we can then get a value for the fragility that becomes:

$$m = 16[1 + I_{\Delta E}(T_g)] \tag{3.9}$$

This last equation gives us a way to test this model . We will come back further for the experimental way how it was done.

3.3.1 The isomorph theory

Developed over the last years [44–47], its fundamental prediction is the existence of isomorphs. They are curved lines in the phase diagram along which all dynamical processes and structure are invariant, coming from the experimental results showing density scaling and isochronal superposition. This would imply that the α relaxation as well as the Debye mode and others would behave in an identical way along the isomorph line.

The limitation for this system to work was defined as having a correlation value R higher than 0.9, and these liquids are called "R-simple" liquids. The R value is given by

$$R = \frac{\langle \Delta U \Delta W \rangle}{\sqrt{\langle (\Delta U)^2 \rangle \langle (\Delta W)^2 \rangle}}. \tag{3.10}$$

U is the potential energy and W is the virial, coming from the intermolecular interactions. Systems that are expected to be strongly correlating are as examples, small van der Waals liquids [48] or polymers [49]. In this theory, these liquids can be approximated to obey a power law density scaling over small density variations, meaning that the relaxation times are a function of $\Gamma = \rho^\gamma/T$, γ is the density scaling exponent.

Along an isomorph, with particle coordinates vector $\boldsymbol{R} \equiv (r_1, ..., r_n)$, the reduced coordinates become $\tilde{\boldsymbol{R}} \equiv \rho^{1/3}\boldsymbol{R}$, if 2 state points (1,2) have the same reduced units, this applies:

$$\exp \frac{-U(\boldsymbol{R}_1)}{k_B T_1} \cong C_{12} \exp \frac{-U(\boldsymbol{R}_2)}{k_B T_2} \tag{3.11}$$

The constant C_{12} does not depend on the configurations. Then if two different configurations along an isomorph have the same reduced units, they have the same structure and dynamics in reduced units. This works then only for systems with perfect inverse power law potentials. For the other systems, as for hydrogen bonded systems, it is only an approximation.

Coming again to something that can be observed in experiments, isochronal superposition is the superposition of relaxation spectra for points along an isochrone, a line of constant relaxation time. Meaning that the shape of it for both state points is in all points identical. It is said that complex intermolecular bonding systems are lacking it[50–52]. For density scaling, γ is often linked to intermolecular potential and for liquids with a pure inverse power law approximation for their interaction, r^{-n}, $\gamma = n/3$. Scaling for the structural relaxation of hydrogen bonded liquids have been shown to not work[53, 54].

In dipropylene glycerol which is a di alcohol, one in both terminal positions, a study [55] has shown that the isochronal superposition still exists and isomorph theory does still hold quite well for intermolecular interactions. The techniques they used were both neutron backscattering and dielectric spectroscopy and the two predictions worked quite well over this wide timescale.

3.4 Fitting models

We will present here the different models we will use to analyze the experimental data, both for dielectric spectroscopy and neutron scattering.

3.4.1 Dielectric spectroscopy

For dielectric spectroscopy, two methods are used to analyze the data. The two analyses are phenomenological in nature. To convert the frequency

in the time domain, the simple transformation $\tau = 1/2\pi f$ is done with f being the measured frequency.

First, to find relaxation times, a 4^{th} polynomial fit was done from roughly $\pm$ 1 decade from the approximate maximum. This gives us for hydrogen bonded liquids most often a Debye like macrostructure relaxation time and not what would be considered as standard to characterize values like the the glass transition T_g, the α relaxation.

For the glycerol-water under pressure project, a simple half width at half a decade under maximum dielectric loss was determined. Only the right half is measured as it is, in the case of this study the only clearly visible change that occurred, as shown underneath in figure 3.9.

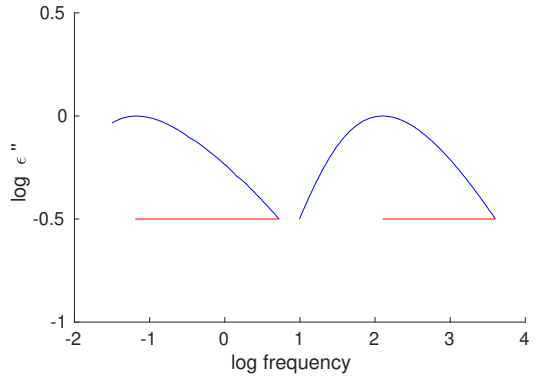

Figure 3.9: Half width at half decade under the max example. 2 spectra shown of glycerol-water 40 %. In red is the HWHD value.

3.4.2 Neutron scattering

Quantitative fits of the neutron spectra were done only for the 1-propanol/glycerol project in chapter 5.

For neutron scattering, implementation of fitting functions depend on the domain on which the data is. For IN16B FWS, we have a temperature dependent signal at a fixed energy transfer. For IN16B full window and IN5, we have an energy transfer/frequency dependent signal, while WASP and the Fourier transformed IN16B full window and IN5 data I(Q,t) is a timescale dependent signal.

The model that we chose to fit with required two processes to be in-

cluded. The first process was modeled as a Lorentzian function and the other one as a KohlrauschWilliamsWatts (KWW) function, which is the Fourier transformation of a stretched exponential relaxation. If the β stretching factor of the stretched exponential goes to 1, we find the simple exponential.

For the I(Q,t) analysis, since we are in the time domain, we add a stretched exponential to a simple exponential, giving us

$$F(Q,t) = A_\kappa(Q) * \exp - \left(\frac{t}{\tau_\kappa(Q)}\right)^\beta + A_\mathcal{L}(Q) * \exp\left(-\frac{t}{\tau_\mathcal{L}(Q)}\right) + B. \quad (3.12)$$

With τ being the timescale of either process a or b, A the amplitude and β the stretching factor. B is a flat background. This model was used to fit Neutron spin echo data and to fit the merged data of IN16B BATS and IN5, I(Q,t) transformed by the Mantid software.

For the $S(Q,\omega)$ data, we used a Fourier transform representation of this model. This is a Lorentzian for a simple exponential. An Arrhenius law was used to fit the data that was recorded as a function of temperature.

The Lorentzian function ($\mathcal{L}$) is

$$\mathcal{L}(Q,\omega,T) = (1-N)\frac{1}{1+(\frac{E_{tr}}{\Gamma(Q)})^2}, \quad (3.13)$$

N is a normalization parameter, dependent of the elastic incoherent structure factor and the resolution convolution factor. E_{tr} is the energy transfer to the neutron and Γ is the FWHM, more info can be read in Frick et al. [7]. We have the assumption that the behavior of Γ with temperature follows an Arrhenius law:

$$\Gamma(Q) = \Gamma_0(Q) \cdot e^{\left(\frac{-E_a}{k_B T}\right)} \quad (3.14)$$

Since there is no analytical transformation of a stretched exponential, a numerical transformation, presented by Wuttke [56] was used.

As we are interested in the real part, the scattering law becomes

$$S(Q,\omega) = \frac{1}{\pi}\mathrm{Re}\, F_Q(\omega). \quad (3.15)$$

From here. the integration is done from 0, time of the event, to ∞ and not from $-\infty$ to ∞ as causality tells us that what comes before the perturbation is not relevant to the behavior after it. The KWW function (κ) is then

$$\kappa = \int_0^\infty dt \cos(\omega t) \exp(-t^\beta). \tag{3.16}$$

With the addition of a flat background B, our model is then:

$$S_{model}(Q,\omega,T) = B(Q) + \frac{A_\mathcal{L}(Q)}{\pi} \cdot \frac{\mathcal{L}}{\Gamma_\mathcal{L}(Q)} + \frac{A_\kappa(Q)}{\pi} \cdot \frac{\kappa}{\Gamma_\kappa(Q)}. \tag{3.17}$$

Where B, a flat background; A, the amplitudes and Γ the FWHM for $\mathcal{L}$ and κ function respectively. The parameters are Q dependent.

For the FWS spectra, we take directly $S_{model}(Q,\omega)$ as we work on a discrete energy but for the BATS spectra, equation 3.17 is convoluted with a resolution, Res, taken at 15 K of each sample and becomes:

$$S_{BATS}(Q,\omega) = S_{model}(Q,\omega) \otimes Res(\omega, Q) \tag{3.18}$$

Mean-squared displacement

Using the Gaussian approximation to model the vibration of the molecules that we got from the derivation above (eq. 2.15) that we will rewrite here, we can find the mean-squared displacement (MSD) using the Q-dependence of the elastic incoherent intermediate scattering function versus temperature in the time limit of the instrument.

$$I_{inc} = e^{-\frac{Q^2\langle u^2\rangle}{3}} \tag{3.19}$$

The timescale of the MSD we get using this method is the resolution of the instrument used. In this case, IN16B in standard mode has a resolution of 0.7 μeV. Using IN5, with an energy resolution of roughly 100 μeV, the timescale would be in the 10s of picoseconds.

To extract then $\langle u^2\rangle$, we do a temperature dependent linear fit of the logarithm of the intensity versus Q^2. At high temperature, meaning above 1.2-1.4 times the glass transition temperature, this approximation can not be

considered viable anymore as we start to see the α relaxation come into the timescale of the instrument.

From the mean squared displacement, if we take equation 3.2 about fragility and make it isobaric, with τ_0 of 10^{-14} and τ_g of 10^2 s, we get the equation that gives us the prediction the shoving model for the fragility, which is valid only when the MSD's validity holds so in the 1-1.2 T/T_g:

$$m_p = \log_{10}\left(\frac{\tau_g}{\tau_0}\right)\left.\frac{d\log\langle u^2\rangle}{d\log T}\right|_p \tag{3.20}$$

in our case, when numbers are set in, it gives;

$$\log\tau(T) = 16\frac{\langle u^2\rangle_{T_g}}{\langle u^2\rangle(T)} - 14 \tag{3.21}$$

3.5 Density measurements

To do density scaling, the temperature-pressure dependent densities of glywa04 and glywa07 were done with a piston-cylinder with the travel of the piston precisely measured in the temperature range 245 - 315 K and 0.1 to 400 MPa, then extrapolated to other temperatures by fitting with a Tait equation.

Chapter 4

Methodology

This chapter will present the experimental instruments, tools, samples and settings used for this work.

The sample environment for both dielectric spectroscopy and neutron scattering is either an ILL orange cryostat, with a maximum operating temperature of 320 K, or cryofurnace, with a maximum operating temperature of 500 K. Mixing of samples with 1-propanol was done in a glove bag. Mixing and preparation of cells for samples with water, and preparation of cells for samples with 1-propanol was done in a container under continuous flow of nitrogen.

4.1 Samples

For the projects on the mixtures of glycerol with water, we worked on a 40 % and 70 % mol ratio glycerol in water. For the propanol project, we worked with neat propanol and a 10 % mol ratio glycerol in 1-propanol. The deuteration of the samples are, for glycerol-water, the water and the alcohol groups of glycerol; for 1-propanol-glycerol, the alcohol of 1-propanol and glycerol fully deuterated.

Origin of chemicals

1-propanol	Purity, $\geqslant 99.9\%$. From Sigma.
1-propanol(OD)	From Cambrige Isotope Laboratories.
glycerol	Purity, $\geqslant 99.5\%$. Water $\leqslant 0.1\%$. From Sigma.
glycerol$(OD)_3$	Purity, $\geqslant 98\%$. Water $\leqslant 0.75\%$. From Cambridge Isotope

	Laboratories.
glycerol-D8	From Sigma, $\geqslant 99.5\%$ deuterated.
D_2O	From Sigma, $\geqslant 99.9\%$ deuterated.
H_2O	Milli-Q system

Samples used

glywa04	40 % mol ratio glycerol in H_2O.
glywa04D	40 % mol ratio glycerol$(OD)_3$ in D_2O.
glywa07	70 % mol ratio glycerol in H_2O.
glywa07D	70 % mol ratio glycerol$(OD)_3$ in D_2O.
Prop	neat 1-propanol.
PropD	neat 1-propanol(OD).
Mix	10 % mol ratio glycerol in 1-propanol.
MixD	10 % mol ratio glycerol-D8 in 1-propanol(OD).

4.2 Sample cells

4.2.1 Pressure cell

The sample cell used for the pressure experiments is an aluminium cell with a cylindrical capacitor insert with a length of 24 mm, an outer diameter of 11.7 mm and 150 μm space between the inner and outer electrode and another 150 μm between the outer electrode and the pressure cell. Due mechanical stress the pressure cells need to sustain and the low incoherent cross section background needed for QENS, aluminium was chosen. The thickness of the cell does have a non negligible effect on the neutrons. This makes the empty cell have a transmittance of roughly 53%. The details about the cell can be read in [57]. The general aim in neutron scattering experiment is to keep the sample studied around a 90 % transmittance. This amount is chosen as to minimize the probability of neutrons scattering more than once in the sample. Only having neutrons that have only one scattering event makes scattering vector Q directly linked to the measured angle, depending on the energy transfer. Secondly, 90 % transmittance still allows for a reasonable amount of scattering event to take place and have relatively good count rate in the instruments.

4.2.2 Ambient pressure cell

For the neutron experiments on the glycerol water ambient pressure project, standard IN16B cell of 22 mm with 100 μm thickness was used.

For the propanol project, a new simultaneous dielectric cell was designed and made between the ILL and RUC. Basing it on the standard model for IN16B BATS cell, modifications were done as to have the inner and outer shell of the cell become a capacitor to do simultaneous dielectric spectroscopy during neutron scattering. The schematic of the cell is shown in figure 4.1 and 4.2. The height of the cell is 63 mm and diameter of the outer cylinder is 14 mm. The spacing between the electrodes is 50 μm. The insulating separator and centering distance part are made from polyetheretherce-tone PEEK. The signal pin outer electrode is also insulated with PEEK and serves as axial alignment. The holes for screwing through the inner electrode are widener to avoid short circuit when the cell is closed with steel or aluminium screws and bolts.

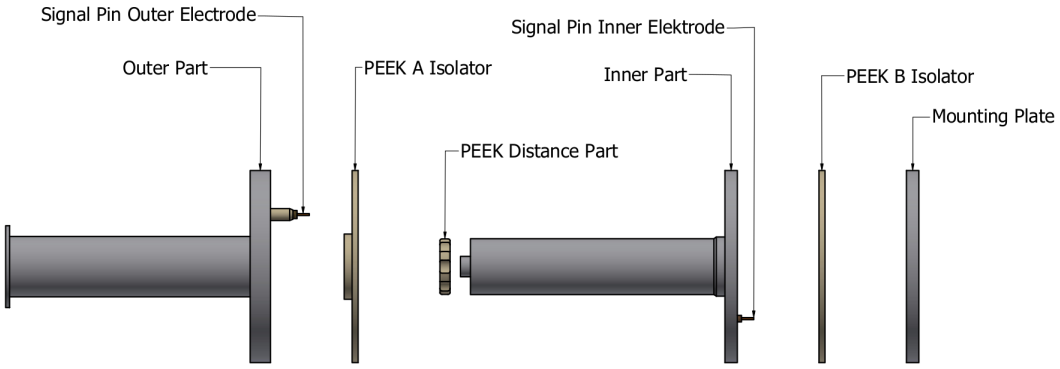

Figure 4.1: Schematic of the ambient pressure dielectric cell.

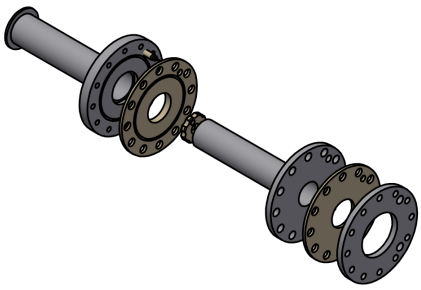

Figure 4.2: Schematic of the partially mounted ambient pressure dielectric cell. The circular grooves in the outer cell and PEEK A isolator are for indium seal.

For use in neutron scattering instruments, cadmium shielding is used to shield the PEEK parts and steel screws. This is done by circling and covering the bottom flat part. The small flange seen on the left side of the schematic is made to keep the shielding on place. For the top part, a cadmium disk is sided and taped to the top flange.

4.3 Dielectric spectroscopy

The equipment used is the alpha-analyzer by Novocontrol with a 4 wire test interface. The length of the cables from the interface to the cane cell holder is 10 cm. the length of the cane from the plug to the cell is about 105 cm, giving the capacitor located at about 1-1.5 m from the interface which gives some noise at high frequency at high temperature. This limits the measurable high frequency to about 10^6 Hz. During all neutron scattering experiments, except glycerol water at ambient pressure, simultaneous dielectric spectroscopy was performed. During cooling ramps, with 10 points per decade from 10^6 to 10^1 Hz and 5 points per decade from 10^1 to 10^{-1} Hz and during long scans 10 points per decade from 10^6 to 10^{-2} Hz.

4.4 Neutron scattering

Neutron scattering was done on 3 different instruments at the Institut Laue-Langevin. IN16B, in its Doppler mode and BATS settings, IN5 and WASP. A brief test on the SANS instrument D22 was performed for one experiment. For the pressure experiments, due to the low transmittance of the cell used and to still have a reasonable signal over noise ratio, a thicker than normal sample was used, with a transmittance of about 70 $\%$. This low transmittance makes multiple scattering very likely and thus Q dependent analysis for these experiments were not done. Simultaneous dielectric spectroscopy was done on all experiments except for glycerol-water samples at atmospheric pressure as the new cell was not produced at the time of the experiments.

For instrument IN16B in Doppler mode, backscattering, the incoming neutrons wavelength were 6.27 Å. Two types of measurements were performed. Full window scans, with acquisition time of 4 hours and fixed window scans, with a fixed offset energy of either 0, 3 or 6 μeV during a cooling ramp of 0.4 K/min from high temperature, 315 or 330 K, to the sample's glass transition temperature minus 10 K then fast to 10 K. The acquisition time

was respectively with the energy transfer 30 s for 0 μeV, 90 s for 3 and 6 μeV.

For instrument IN16B in BATS mode, mix of backscattering and time of flight, the mode used was with a rather broad resolution generated by the 14 deg slit in the pulse choppers. Two types of measurements were performed. Full window scans were done in two settings. At set temperature an pressure with acquisition time of 4 hours. Another setting was during a cooling ramp of 0.4 K/min from high temperature, 315 or 330 K, to the glass transition temperature minus 10 K then fast to 10 K, short acquisition time of 2 min were done to simulate later a Doppler mode fixed window scan.

For instrument IN5, the incoming neutrons wavelength is 6 Å. Measurements are done with an acquisition time of 30 min.

For instrument WASP, spin echo, the acquisition time per temperature is around 2.5 h. For the measurement of about half of the spectrum towards longer Fourier times, dielectric spectroscopy needed to be disabled due to the interaction of the magnetic field on the analyzer's electronics making measurements impossible.

Data analysis for neutron scattering was done in MANTID software, the intensities are normalized to vanadium for IN16B and IN5. Instrument background and empty cell measurement were recorded separately and subtracted from the data using standard routines on the instrument. Data analysis for dielectric spectroscopy was done in Matlab.

Chapter 5

1-propanol / glycerol

5.1 Introduction

In this chapter we will be looking into the effect of the addition of glycerol on 1-propanol. Neat 1-propanol has been quite extensively studied, from dielectric spectroscopy, mechanical spectroscopy, calorimetry, light scattering, near-infrared spectroscopy or neutron scattering to cite a few [19, 23–31, 58, 59]. 1-propanol, as many other mono alcohols, possesses in dielectric spectroscopy a strong main relaxation which follows a Debye shape.

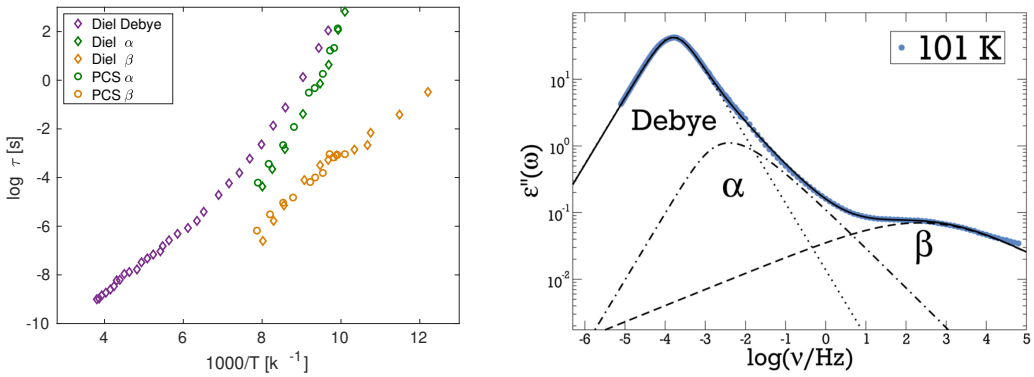

Figure 5.1: Left, relaxation time of the Debye (violet), α (green) and β (orange) process found using dielectric spectroscopy ($\diamond$) and photon correlation spectroscopy ($\circ$). Right, 1-propanol dielectric spectroscopy. Data (left) and figure (right) from Gabriel et al. [30]

The current understanding is that this process is linked to a chain like

or ring like macro structure of multiple molecules linked through the hydrogen bonds of their alcohol [27]. The different processes can be well separate for example in Gabriel et al. [30], where dielectric spectroscopy and photon correlation spectroscopy was used to separate the Debye, α and β processes, which can be seen in figure 5.1.

Comparatively, the mixture of 1-propanol and glycerol has been less studied but nonetheless for a long time. Coming as far as Kono et al. [23] in 1966 studied the dielectric and mechanical relaxations in mixtures of 1-propanol and glycerol. They found that around 25 $\%$ molar ratio glycerol a change in behavior was happening.

As can be seen in figure 5.2, with data from Kono et al. [23], the left part shows shear and compression moduli while the left part shows the width parameters for the fitting of the main relaxation of dielectric loss and rheology. The dielectric loss shape goes from a Debye like for propanol to a broader signal at around 30 $\%$ then stays quite stable up to neat glycerol. the same change in trend is also advanced by the authors for the rheology part. We know now, contrary at the time of the publication that the main relaxation of propanol in dielectric spectroscopy points to a mode which is thought to be due to the macro structure through the hydrogen bonds. We still think that the signal in rheology is mainly the α relaxation. It is interesting to see that with both techniques there seem to be a change from a propanol like behavior to a glycerol like around the same dilution.

Neutron scattering on 1-propanol has already been done on the fully deuterated version, showing mostly coherent scattering by Sillrén et al. [28]. The time scale of their experiment spanned 0.2 to 2000 ps at temperatures from around 300 to 10 K. They also used NMR, rheology. They found that the QENS results at the main peak coincides with the relaxation time estimated on the basis of the Maxwell relation from rheological data, i.e the α relaxation. They also found that the pre-peak region's time scale coincided with their NMR results for the dynamics of the O-H groups.

We aim in this project to use the benefice that inelastic neutron scattering gives using the tool of deuteration, which will give us the possibility to hide the contribution of part of the molecule. With this, we hope to see if the hydrogens in the O-H bonds are at the local level linked to the Debye process at high temperature and short time scale. The use of a small addi-

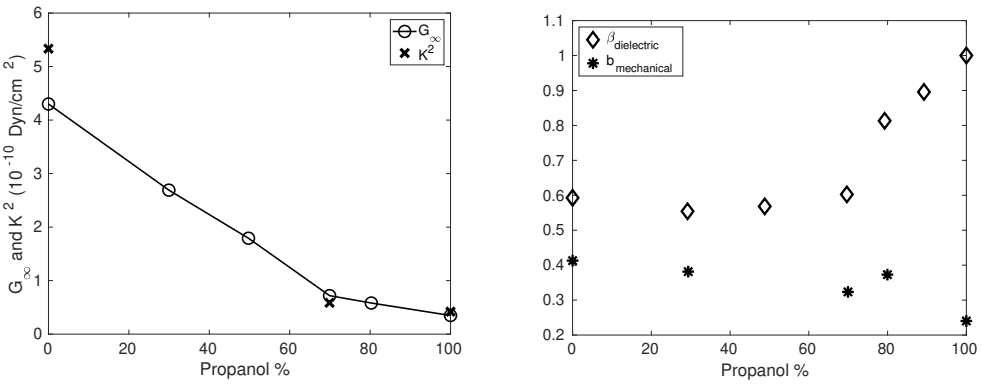

Figure 5.2: Shear and compressional moduli (left) and distribution of relaxation time parameters (right) in n-propanol-glycerol mixtures plotted against mole percent n-propanol at -60° C. β(dielectric) is the width parameter associated with Cole-Davidson model for the main relaxation; b(mechanical) is the width parameter associated with a Gaussian distribution function. Data from Kono et al. [23]

tion of poly alcohol, in our case glycerol, helps both to increase the signal of hydrogen bond ratio to aliphatic hydrogens, giving a better contrast and to possibly disrupt the hydrogen network by cross linking chains.

In the case of molecules with hydrogen bonds, partial deuteration does impose a limit due to the process of relatively fast exchange of protons between molecules or between different hydrogen bonds inside the same molecule. Small alcohols mixed with D_2O have a half-life of 4 hours [10]. This implies that in a mixture of liquids, it is not possible to have only one of them have its O-H hydrogen stay deuterated while the other one stays protonated as the neutron scattering experiments last hours.This influenced the choice for the deuterated version of the mixture of 1-propanol with glycerol. We then decided to deuterate the alcohol of 1-propanol and fully deuterate glycerol. The result is that in quasi elastic neutron scattering, the signal for what we see for the deuterated version of both 1-propanol and the mixture is the aliphatic hydrogens of 1-propanol, i.e. its carbon backbone.

The precise choice of the mixture was defined by doing dielectric spectroscopy on a range of dilutions and since one of the focus of this work is to study the dynamics of 1-propanol, a glycerol lean mixture was selected. As a result of these experiments, the choice of a 10% mixture of glycerol in

1-propanol was selected. So the 4 liquids that were studied are: 1-propanol **(Prop)**, 1-propanol(OD) **(PropD)**, 10 % glycerol in 1-propanol **(Mix)** and 10 % glycerol-d8 in 1-propanol(OD) **(MixD)**. The details of the chemicals are shown in section 4.1. The dielectric experiment is shown in section 5.3.

5.2 Experiment conditions

In this project, we took advantage of the panel of instruments that were possible to use from the ILL to have a broadband time scale through neutron quasi elastic spectroscopy. Using spin echo, WASP instrument, with its wide window covering nearly 3 orders of magnitude from about 8 ps to 6 ns. In parallel, QENS instruments of time of flight, IN5 with a time scale window of 1 ps to 50 ps, and mix of backscattering and time of flight, IN16B BATS mode 20 ps to 400 ps. Backscattering instrument IN16B in Doppler mode was used with fixed window scan at 0, 3 and 6 μeV energy transfer, referring to elastic scattering and a time scale of 1 and 0.5 ns. All experiments were done with simultaneous dielectric spectroscopy to monitor if the sample underwent crystallization or not while in supercooled state as we are interested in the liquid dynamics. The advantage of having the simultaneous measurement is that dielectric spectroscopy is a fast, known and reliable technique. This can then assure us that the data we collect during the long neutron scattering experiment is about our sample in the liquid state.

The details of the instruments and sample cell can be seen in section 4.4. The raw data can be found via the following digital object identifiers (DOI). 10.5291/ILL-DATA.6-05-1049 (WASP), 10.5291/ILL-DATA.6-05-1040 (IN5), 10.5291/ILL-DATA.INTER-531 (BATS). IN16B was done on internal buffer time and has thus not been given a DOI.

For the WASP experiment, which relies on spin interaction with the nucleus, the ratio of protons and deuterons and their respective scattering lengths can in some cases make the data much harder to read. Our wish to see the dynamics of the different parts of propanol and the mixture imposing some limitation in the choice of isotopic exchange made the deuterated mixture fall in the problematic window. This technical difficulty make then the deuterated mixture too complicated to analyze in the context of this thesis. During the WASP experiment, there was a hint that there could be some structure in our sample at very low Q. To check this, an internal SANS

measurement was done on instrument D22, see figure 5.3, which showed no structure.

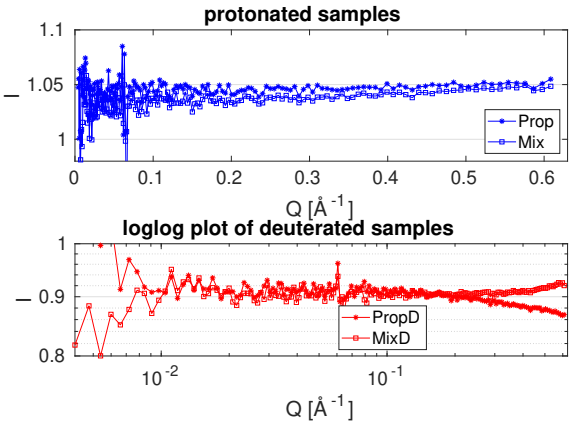

Figure 5.3: SANS data of, Top, the protonated samples and; bottom, a loglog plot of the deuterated samples. No structure is visible in the instrument range.

To gather information on the macroscopic time scale, dielectric spectroscopy was done also with stable temperature steps of 5 or 10 K with a frequency range of 0.01 or 0.1 to 10^6 Hz and 10 points per decade. The cell and sample environment was the same as for neutron scattering. Another technique used is thermalization calorimetry. This technique is a passive heating calorimeter measuring the rate of heating of a liquid in a small tube. The samples are first quenched in liquid nitrogen then quickly transferred in a polystyrene box and left to passively heat up to room temperature. The full detail about the instrument can be found in Jakobsen et al. [60].

5.3 Macroscopic dynamics

The choice of which precise mixture to study was decided by doing dielectric spectroscopy on a few dilutions, namely 2.8, 10, 20, 30, 80 % mol ratio glycerol, neat glycerol and neat 1-propanol. There is a gap in the dilutions studied between 30 and 80 % as we already knew that we wanted to study a propanol rich environment. From previous publication, we knew that it meant staying at a lower concentration than about 25 %. In figure 5.4 left we show a near isochrone of all the above mentioned liquids of the main dielectric loss peak around 200 Hz, which could be the α, Debye or a mix of them. From neat propanol up to 30 % glycerol, it is also an isotherm, at 136 K, where the maximum dielectric loss' position lowers quickly in fre-

quency then stabilizes and slightly increases. In figure 5.4 right, the low frequency slope and the maximum dielectric loss relative to 1-propanol is plotted against the glycerol ratio. The low frequency slope of the dielectric loss in a log-log plot changes from a relatively sharp Debye like peak for 1-propanol of 0.9 to reach a minimum near 0.35 for 20 % glycerol before increasing again and reaching a maximum near 1 for neat glycerol. The intensity of the dielectric loss of the different dilutions relative to neat 1-propanol also quickly lowers while hitting a minimum at 30 % glycerol. A first observation is that these two factors do not have a minimum at the same dilution. As we aim in our project to study the dynamics of propanol, we chose to keep a margin with the minima while still having a clear effect, a glycerol lean mixture of 10 % mol ratio was chosen.

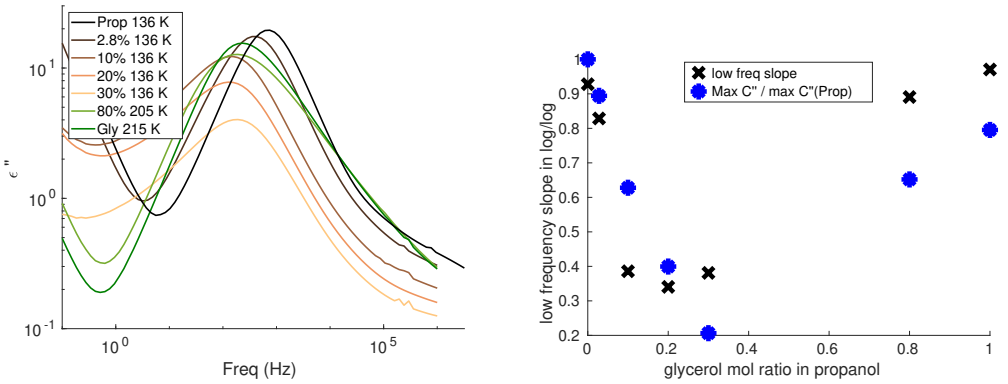

Figure 5.4: Dielectric loss of near isochrones of 1-propanol, glycerol and some of their mixture, 2.8, 10, 20, 30 and 80 % mol ratio. around a relaxation frequency of 200 Hz. And on the right, mixture dependent slope of the low frequency side of the peak and the peak's max dielectric loss ratio with neat propanol.

As said earlier in section 2.1.2, isotopic exchange between proton and deuteron can not be assumed to be without effect on the dynamics of the system. For this purpose, dielectric spectroscopy was done on all 4 samples, namely 1-propanol, 1-propanol(OD), 10 % glycerol in 1-propanol and 10 % glycerol-d8 in 1-propanol(OD). The relaxation map of the main peak is shown in figure 5.5, with protonated samples in blue, deuterated samples are in red and the black is data from Gabriel et al. [30]. For these samples, deuteration does not change the dynamics of the main process. We define a T_{Debye} as the temperature at which the main peak's relaxation time is 100

s. VFT fits were done to extrapolate the results to find a T_{Debye} for propanol and the mixture which is **103.85** K and **107.25** K respectively.

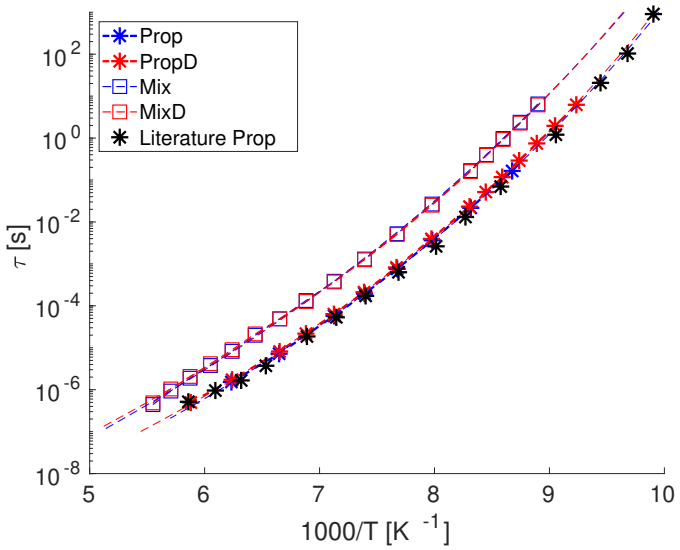

Figure 5.5: Relaxation map of Prop (∗), PropD (∗), Mix (□) and MixD (□). Deuteration does not change the relaxation time of the Debye process. In dashed line is the corresponding VFT fits. In black is data extracted from Gabriel et al. [30].

The shape change of the dielectric loss related to the deuteration of our sample can be seen in figure 5.6. Looking at the low frequency side of the peak, conduction is coming as the strong increase of the signal, seen around 1 Hz for both propanols and just slightly around 0.1 Hz for the mixtures. With this, no change is seen in the propanol while for the mixture, the signal is very slightly sharper for the deuterated version on the low frequency side.

Another interesting fact is the β relaxation does not change in frequency with the addition of glycerol. As can be seen in figure 5.7, where we see an isotherm of 1-propanol and mixtures up to 30 % glycerol at 95 K and the β relaxation loses a bit of intensity. This could be explained by the relative lowering of density of propanol molecules in the mixture.

As we are interested in the α relaxation too, thermalization calorimetry was performed to find the glass transition temperature. As dielectric spectroscopy showed no clear hint at a change in its dynamics with deuteration, calorimetry was done only on fully protonated version of propanol and the

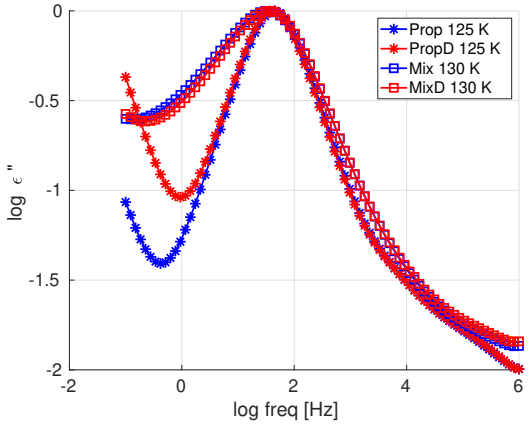

Figure 5.6: Dielectric loss of all samples, at 125 K for Prop (∗) and PropD (∗) and 130 K for Mix (□) and MixD (□) . Deuteration has only a small effect on the low frequency side of the mixture. the low frequency increase is due to conduction.

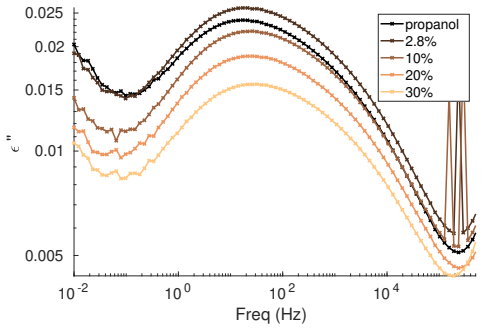

Figure 5.7: Dielectric loss of propanol rich mixture and propanol at 95 K. Showing the β relaxation.

mixture. The results can be seen in figure 5.8. To find T_g with this instrument, we look for the local minimum that is here around 100 K. T_g is then for propanol **101.5** K and for the mixture **106** K.

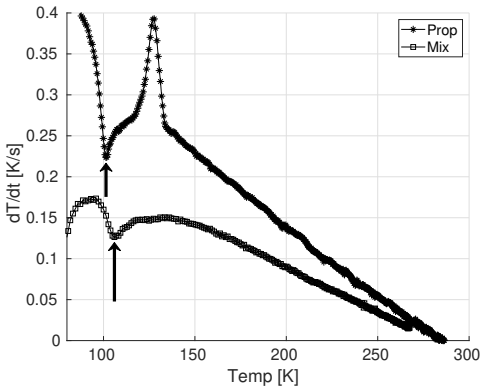

Figure 5.8: Thermalization calorimetry for Prop ($*$) and Mix ($\square$). The local minimums, pointed by arrows, corresponds to T_g, 101.5 K for propanol and 106 K for the mixture.

5.4 Elastic neutron scattering

Elastic neutron scattering data is obtained by elastic fixed window scan on ILL's instrument IN16B. In figure 5.9 is presented the elastic signal summed over all Q. The mixture has, as in dielectric spectroscopy, a slower dynamic than neat propanol. Deuteration has negligible effect on 1-propanol while intensity of the deuterated version of the mixture decays at a lower temperature than its fully protonated variant. This means that the elastically scattered intensity of the aliphatic carbons from 1-propanol in the mixture decays at a lower temperature than the average of the full mixture.

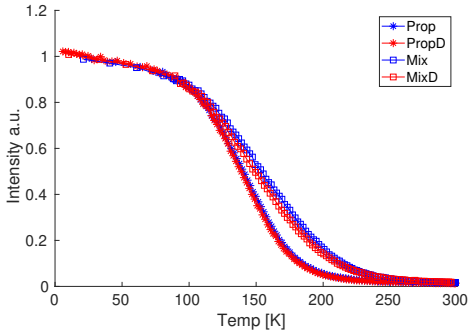

Figure 5.9: Elastic FWS summed over all Q. Deuteration does not change 1-propanol's signal while for the mixture it makes it a little faster.

Mean squared displacement was found using the Gaussian approximation on the Q dependent elastic signal. The results are shown in figure 5.10,

both versus temperature and versus temperature scaled to T_g. In those figures, we can see that for propanol, whether we look at the dynamics of the whole molecule or if we focus on its carbon backbone, the mean squared displacement is similar. In the case of the mixture, we see a clear change with the propanol's carbon backbone, shown as the deuterated mixture, being faster than the average mixture. Once we scale the temperature of both samples to their respective T_g, it seems that the carbon backbone of 1-propanol in the mixture moves roughly at the same pace as neat 1-propanol. This shows that the effect of the addition of glycerol mainly slows down 1-propanol's carbon backbone.

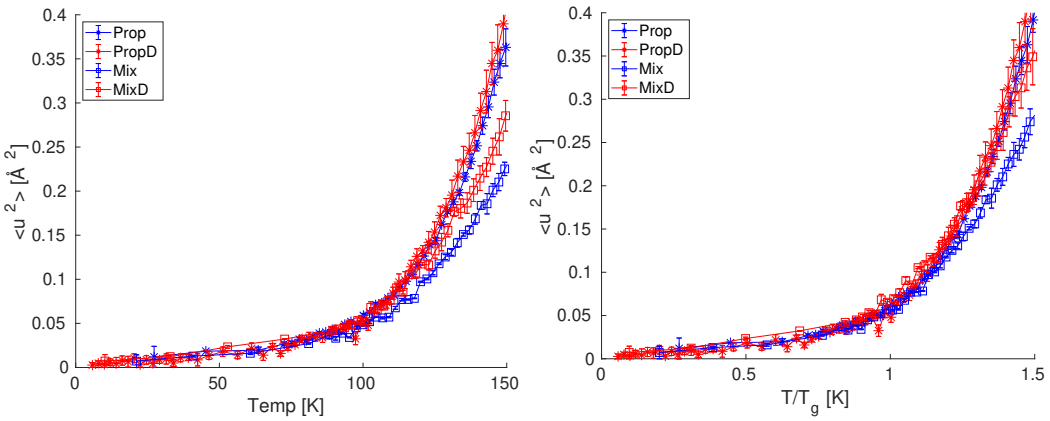

Figure 5.10: Mean squared displacement versus temperature (left) or T/T_g (right). There is very little difference in the MSD of propanol with deuteration while we see that there is a clear difference in the mixture. When scaled to T_g, the deuterated mixture does seem to follow quite well the neat propanol's dynamic.

To test the shoving model on these liquids, the fragility was obtain by extracting data from [30] to get the α relaxation. Since in the relaxation map, figure 5.5, it seems that deuteration does not change the main relaxation and that the relaxation of the mixture seems just like a translation of neat propanol, we assumed the following. Deuterated samples' α relaxation are the same as in the fully protonated samples and for the mixtures, the α relaxation follows the same way the Debye peak as in neat 1-propanol. Testing the shoving model on these liquids, we see that the prediction given from the liquid's fragility is not valid for both propanol and the mixture. If we plot $\langle u^2 \rangle$ scaled to $\langle u^2 \rangle_{T_g}$ against T/T_g, we can test the elastic model's prediction from the fragility, figure 5.11, shows this and the prediction fails.

A first telltale is showing at a T/T_g of about 0.8 where we already see a kink in the slope. A more simple liquid would posses a linearly increasing MSD from 0 to T_g, then a kink following the elastic model's prediction. In our case, there is a first change in slope at 0.8 then another one around T_g and a last one around 1.15. The intriguing part is that this behavior is common between all 4 samples, which means it can not be different dynamics of purely $C-H$ nature. One possibility could be that even though deuteration hides the hydrogen bonding chain from the signal, the rattling of it's motion is transmitted and shaking the aliphatic protons.

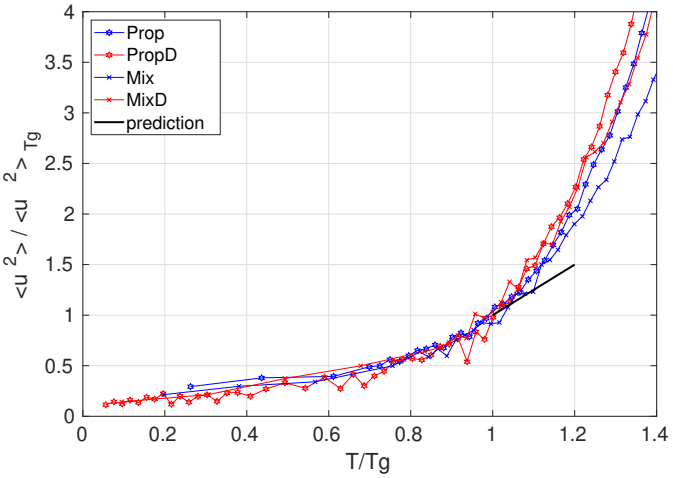

Figure 5.11: The measured $\langle u^2 \rangle$ scaled to $\langle u^2 \rangle_{T_g}$ for propanol ($*$) and its mixture ($\times$). The black straight line illustrate the prediction from fragility, using equation 3.2.

5.5 Inelastic neutron scattering

Inelastic neutron scattering data is obtained by fixed window scan, with an energy transfer of 3 and 6 μeV, on ILL's instrument IN16B in its Doppler mode. IN16B in BATS mode, WASP and IN5 scans were done at 4 different temperatures, 150, 180, 220 and 330 K. IN16B in BATS mode pseudo fixed window scans were between 20 and 340 K. It means short scans of 3 min were taken during a cooling rate similar to the Doppler mode one of 0.4 K/min then were rebinned and showed as a fixed window scan with 4 energy windows. IN5 and WASP data are treated in section 5.7.

The inelastic data from IN16B Doppler mode and summed over all Q can be seen in figure 5.12. For the mixture, it seems rather clear that there

is more than one process. A high temperature process is clearly losing intensity with deuteration. For propanol, deuteration also lowers signal on the high temperature side of the peak, but no explanation can be hypothesized about it without fitting it.

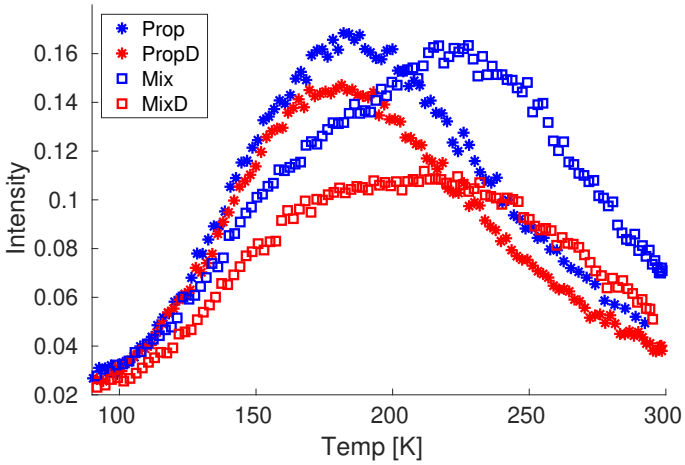

Figure 5.12: IN16B fixed window scan summed over all Q at 3 μeV of the 4 sample. For both samples, signal at the high temperature side lowers with deuteration which is much more visible in the mixture, with the peak at 225 K lowering considerably.

The data for the pseudo fixed window scans were done by binning in broad windows the short scans during a cooling ramp. The binning chosen is 5-20, 20-50, 50-80 and 80 to 100 μeV, which can be seen in figure 5.13. The low temperature of the lowest energy bin stays above 0 as there might still be some part of the elastic signal from the instrument's resolution. For both the Doppler mode FWS in figure 5.12 and the BATS pseudo FWS in figure 5.13, we can see that on the high temperature side of the peaks that deuteration lowers the signal. To discover what happens more in detail, we show how we fitted the in16B Doppler mode FWS and BATS spectrum.

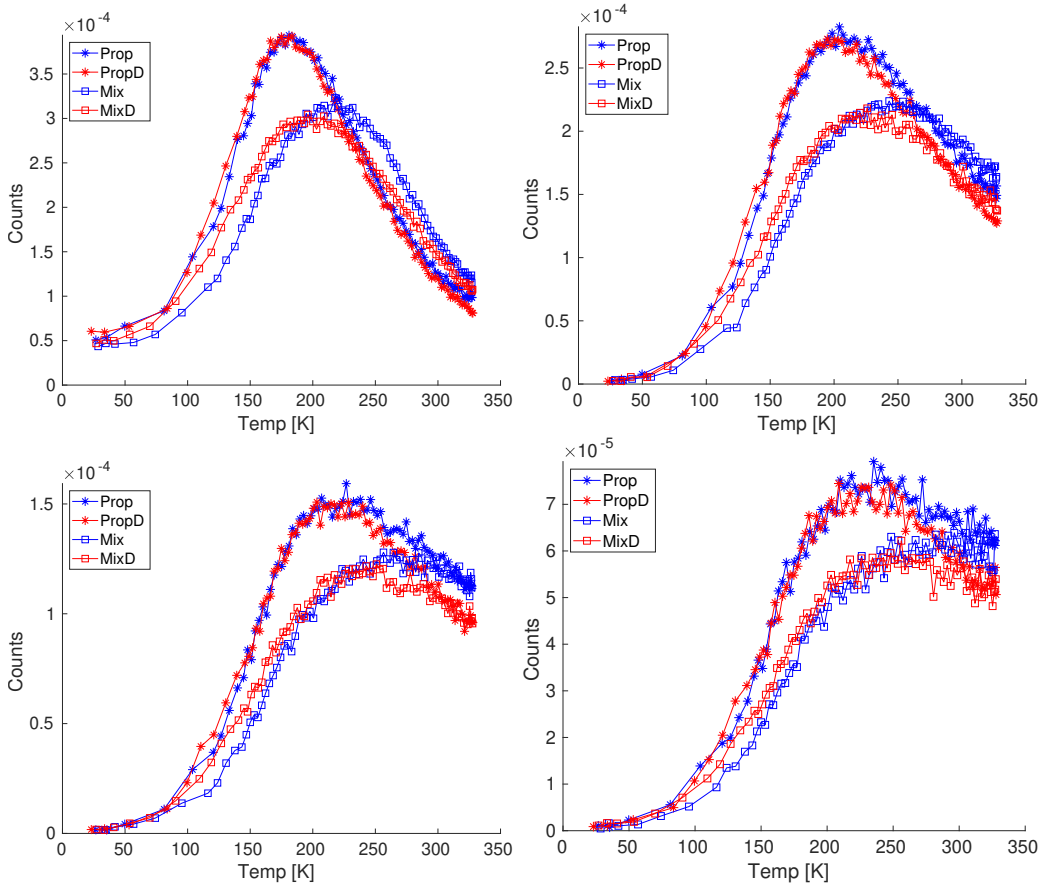

Figure 5.13: IN16B BATS mode, summed over all Q pseudo fixed window scans made from binning 4 different energy ranges; from left to right and top to bottom, 5-20, 20-50, 50-80 and 80 to 100 μeV.

5.6 Fitting of neutron scattering

To have some insight into what happens with deuteration and the processes involved in our mixture, we looked at the Q dependent difference between the protonated versus the deuterated version of 1-propanol. we then fitted this with the IFWS model of the Lorentzian talked previously, as can be seen for Q = 1.39 Å^{-1} in figure 5.14. The Lorentzian seemed to reasonably well fit the data over the whole Q range.

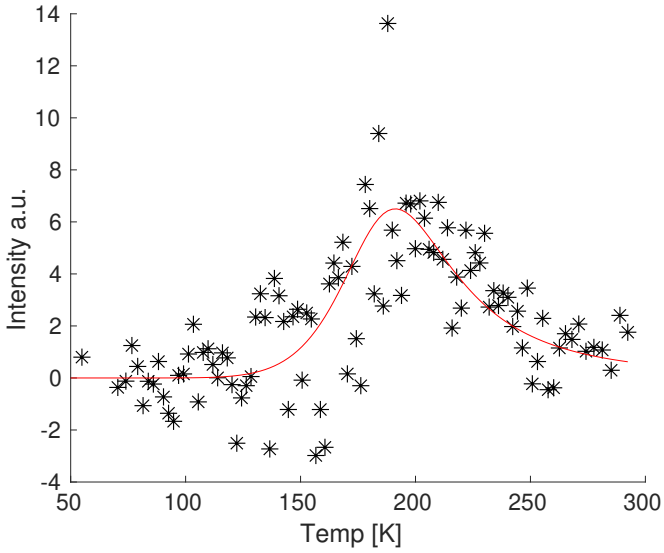

Figure 5.14: FWS, protonated minus deuterated, 1-propanol at Q = 1.39 Å^{-1} with a Lorentzian fit in red.

Looking in figure 5.12, the signal is still quite broad and would hardly be fitted only by a Lorentzian model. To count for this broad signal that was left, we chose to fit it to a KWW function. The model used to fit is then an IFWS model based on a Lorentzian and a KWW, as described in section 3.4.2. For the mixture, we chose to keep the same model. We do not assume that the KWW represents only one relaxation process.

The fitting was done in the MANTID software and the scripts are available through the BATS DOI. The neutron data was fitted simultaneously with the IN16B fixed window scans at 3 and 6 μeV (in the range $\approx$ 20 to 300 K) and IN16B BATS at 150, 180, 220 and 330 K (In the range $\approx$ -140 to 180 μeV) with 14 Q values from 0.59 to 1.84 Å^{-1}. For BATS data, the elastic region between $\pm$ 5 μeV were excluded from the spectra fits due to residual intensity from not fully subtracted sample cell background. We use the transforma-

tion done by Wuttke [56] which also made a python package to implement in our script.

The fitting procedure was done on the FWS (at 3 and 6 μeV) and the spectra of 4 BATS temperatures (150, 180, 220 and 330 K), at all 14 Q values, of the protonated and deuterated samples simultaneously in one batch for 1-propanol and another batch for the mixtures. The parameters that were globally fitted were: The activation energies for each mode to one value for propanol and one for the mixture and β for the KWW to one value for propanol and one for the mixture. Γ_0 is tied to one value per Q for each mode as each Q represent a different distance moved in the same time scale. The intensities of each mode and the background were free for each individual spectra. The following activation energies are expressed as E_a/k_B in kelvin.

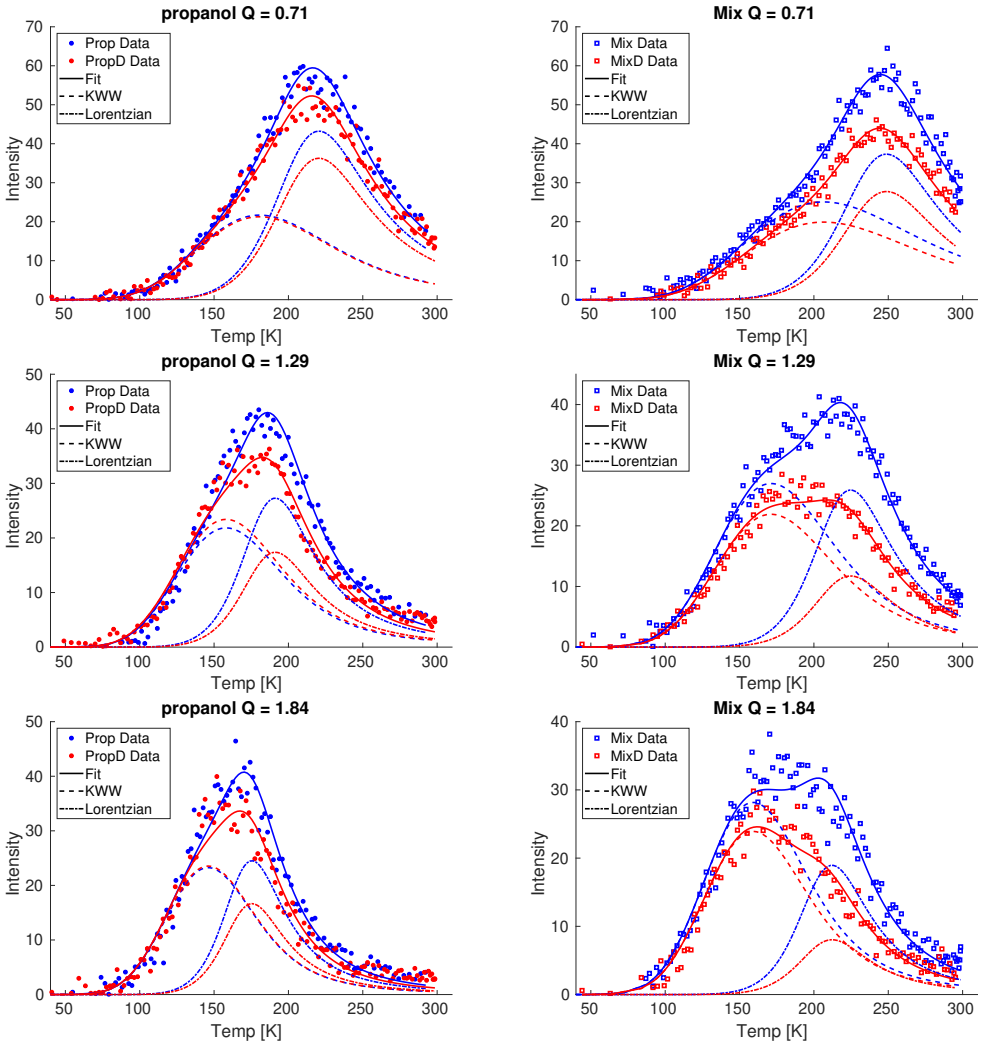

Figure 5.15: Fitting of FWS 3 μeV for propanol (left) and the mixture (right) with a KWW and a Lorentzian mode. showing the total fit (-) and each component, KWW (−−) and Lorentzian (−·). for a Q of 0.71 (top), 1.29 (middle) and 1.84 Å^{-1} (bottom). Protonated sample in blue and deuterated sample in red. For both neat propanol and the mixture, the Lorentzian mode clearly loses intensity, while the KWW mostly loses intensity only in the mixture upon deuteration.

In the fits of the FWS, seen in figure 5.15 showing 3 Q values per sample, the Lorentzian mode has its maximum intensity at a higher temperature than the KWW. The intensities are decreasing substantially with deuteration for both 1-propanol and the mixture for the Lorentzian. The KWW varies only a little with deuteration in 1-propanol, while systematically by about 20 $\%$ for the mixture. The Lorentzian losing intensity might point to a slow mode linked to the hydrogen bonds partly disappearing. For the fits of the BATS data, seen in figure 5.16 we show a selection of 3 temperatures at 1 selected Q per temperature. As opposed to the FWS, the stretched exponential is, for temperatures other than 330 K, at least an order of magnitude stronger than the Lorentzian. Because of this, the BATS data is mostly helpful in the global fitting to set the **stretching exponent** of the KWW, namely **0.445** for 1-propanol and **0.437** for the mixture. The fact that some signal of the Lorentzian is still present in the deuterated version of 1-propanol and the mixture shows that this slow motion is not only in the $O-H\cdot\cdot O$ but is propagated to the other protons.

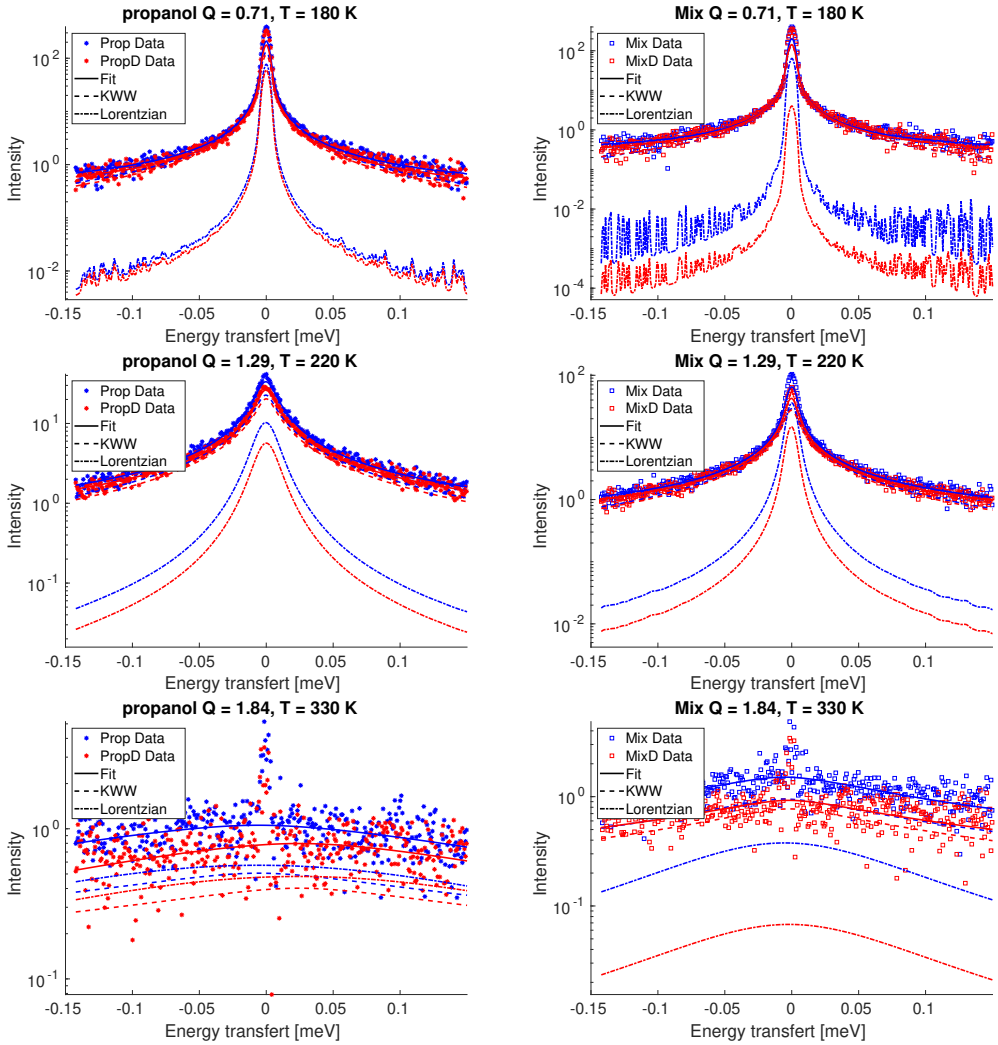

Figure 5.16: Fitting of BATS for propanol (left) and the mixture (right) with a KWW and a Lorentzian mode. showing the total fit (-) and each component, KWW (−−) and Lorentzian (−·). for a Q of 0.71 (top), 1.29 (middle) and 1.84 Å^{-1} (bottom). Protonated sample in blue and deuterated sample in red. For both neat propanol and the mixture, the Lorentzian mode clearly loses intensity, while the KWW mostly loses intensity only in the mixture upon deuteration.

We present further some figures showing the parameters given by the fits. In figure 5.17 is plotted the Q dependent intensities ratio for each mode between the protonated and deuterated version, on the left for propanol and on the right for the mixture. The change in intensities between the FWS and BATS for each mode do not correspond as well as expected. The KWW's intensity does not have any Q dependence, and it nearly does not

change in 1-propanol while it does lower in the mixture by about 20 %. The Lorentzian change is in contrast Q dependent and more pronounced in the mixture. We do not have an explanation for the Q dependence of it. The bigger change in the mixture was expected as the proportion of hydrogen in hydrogen bonds is higher than in 1-propanol, but is to an extent bigger than the molecular change, that went from 12.5 to 15 % of total hydrogens. As the last information from the fit, the **activation energies** for 1-propanol are **1645** K for the KWW and **1663** K for the Lorentzian, and for the mixture **1732** K for the KWW and **2094** K for the Lorentzian. We trust more the FWS intensities, as for the BATS data, the Lorentzian's intensity are very low to start with. Trying to fit the BATS data only with a KWW alone resulted in reasonable qualities of fitting by itself. Our understanding is that in the mixture, the glycerol participates in each mode. Since the deuterated version is fully deuterated, the loss of intensity should also be seen in the KWW.

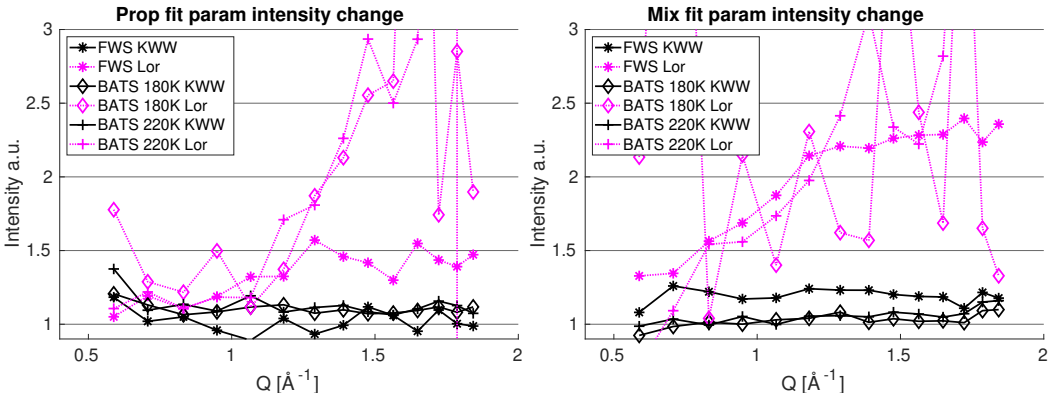

Figure 5.17: Q dependent ratio of intensities for the separate modes of the fits. Values are protonated sample divided by deuterated sample. KWW $(--)$ and Lorentzian $(-\cdot)$ for FWS $*$), BATS 180 K ($\diamond$) and BATS 220 K (+). For both samples, the Lorentzian mode has a Q dependence, with a stronger loss at higher Q with deuteration, while the KWW process is Q independent with deuteration.

In figure 5.18, we show the Q dependent Γ_0 parameter for propanol and the mixture. As a reference, in red is a purely diffusive model. Both modes for each samples follow a rather diffusive like behavior which seems a little more complex in the mixture than in neat propanol.

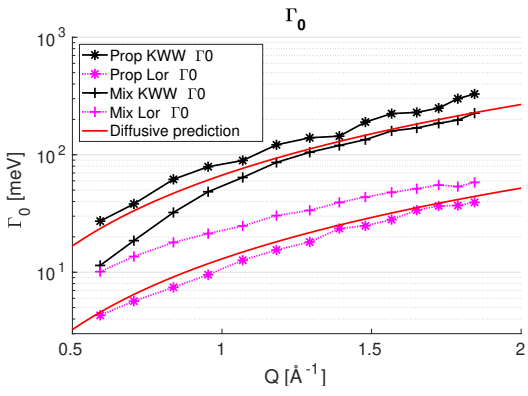

Figure 5.18: Γ_0 parameter for propanol $(*)$ and the mixture $(+)$ with in red a theoretical diffusive $D * Q^2$ process.

Looking at the Q dependent time scale of each mode in figure 5.19, the change over the Q window is about 1 order of magnitude and the difference between the KWW and the Lorentzian is also about 1 order of magnitude. For the highest temperature, the calculated values give a time scale faster than what the instruments can actually see.

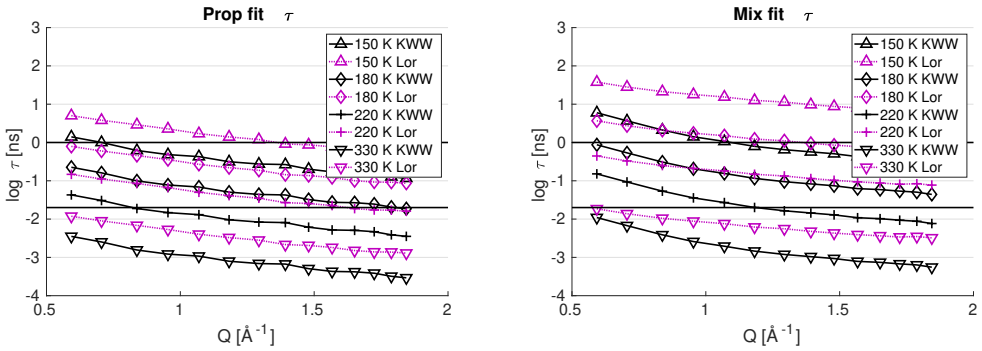

Figure 5.19: Time scale of the KWW and Lorentzian process from the fitting of previous data for propanol (left) and the mixture (right) at 4 temperatures, 150, 180, 220 and 330 K. The 2 horizontal lines show the limits of the instruments measuring time scale.

In figure 5.20, we present the time scales for each mode and both propanol and the mixture, associated to the highest and lowest Q. For comparison, data from photon correlation spectroscopy [30], dielectric spectroscopy [28, 30], NMR O^1H/O^2H [61], η/G_∞ [23] and coherent neutron scattering [28] is shown. All literature data is about 1-propanol, fully deuterated for QENS and fully protonated for the others.

We see that the time scales fitted from our I(Q,t) and WASP data sets give slower Lorentzian and faster KWW. As this instrument is showing us only a small window of time scales, we will look in the next section that these results hold for a wider time scale with data from IN5 and WASP.

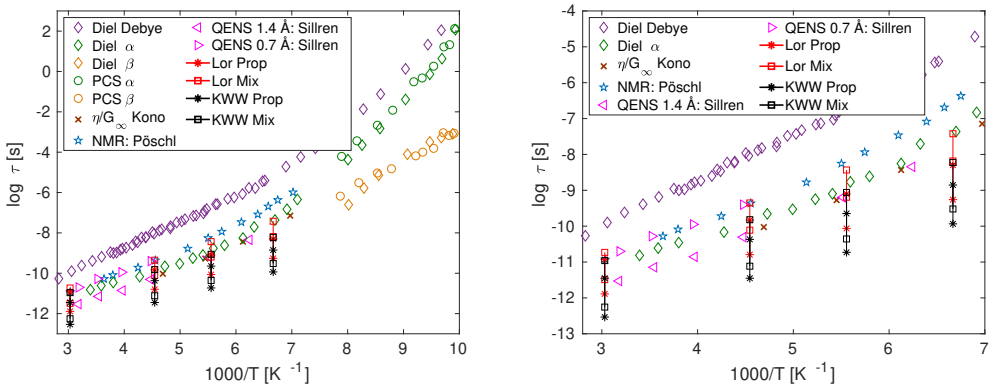

Figure 5.20: Arrhenius plot with PCS data [30], dielectric data [28, 30], NMR data [61], η/G_∞ [23] and coherent neutron scattering [28]. All literature data is for of 1-propanol . The time scale from this experiment for Prop ($*$) and mixture ($\square$) of KWW (black) and Lorentzian (red) with the lowest (0.59 Å^{-1}) and highest (1.84 Å^{-1}) fitted Q, with the lines showing the span between them. Right part is zoomed in from 3 to 7 1000/T.

5.7 Transformation to the time domain

To expand to a broader time scale, data from neutron time of flight (IN5) and spin echo (WASP) are looked into. WASP data is by default in the time domain, looking at the echo's signal. To bridge with the prior section, Both IN5 and IN16B BATS data, that are normally in counts versus energy transfer, are transformed to the time domain through a standard I(Q,t) transformation in MANTID software. Then, to merge the 2 instrument's data as they partially overlap in time scale, the intensities of the data from IN16B BATS were scaled to match the overlapping time scales.

Then, we tried to fit these data using the same KWW and Lorentzian model with the same τ and β values from the previous section. This method resulted in poor fits. We chosen then to fit the propanol data while fixing only the β of the KWW. There is no ties on the intensities and τ of each mode, which are then Q and sample independent.

The fits for the I(Q,T) transformation of IN16B BATS and IN5 can be seen for 1-propanol and the mixture in figure 5.21. For WASP, the fit for the protonated 1-propanol and mixture is shown in figure 5.22. What is clear is that the WASP data, even though spanning over a higher and partially slower time scale has much more noise, which reduced the quality of the fits.

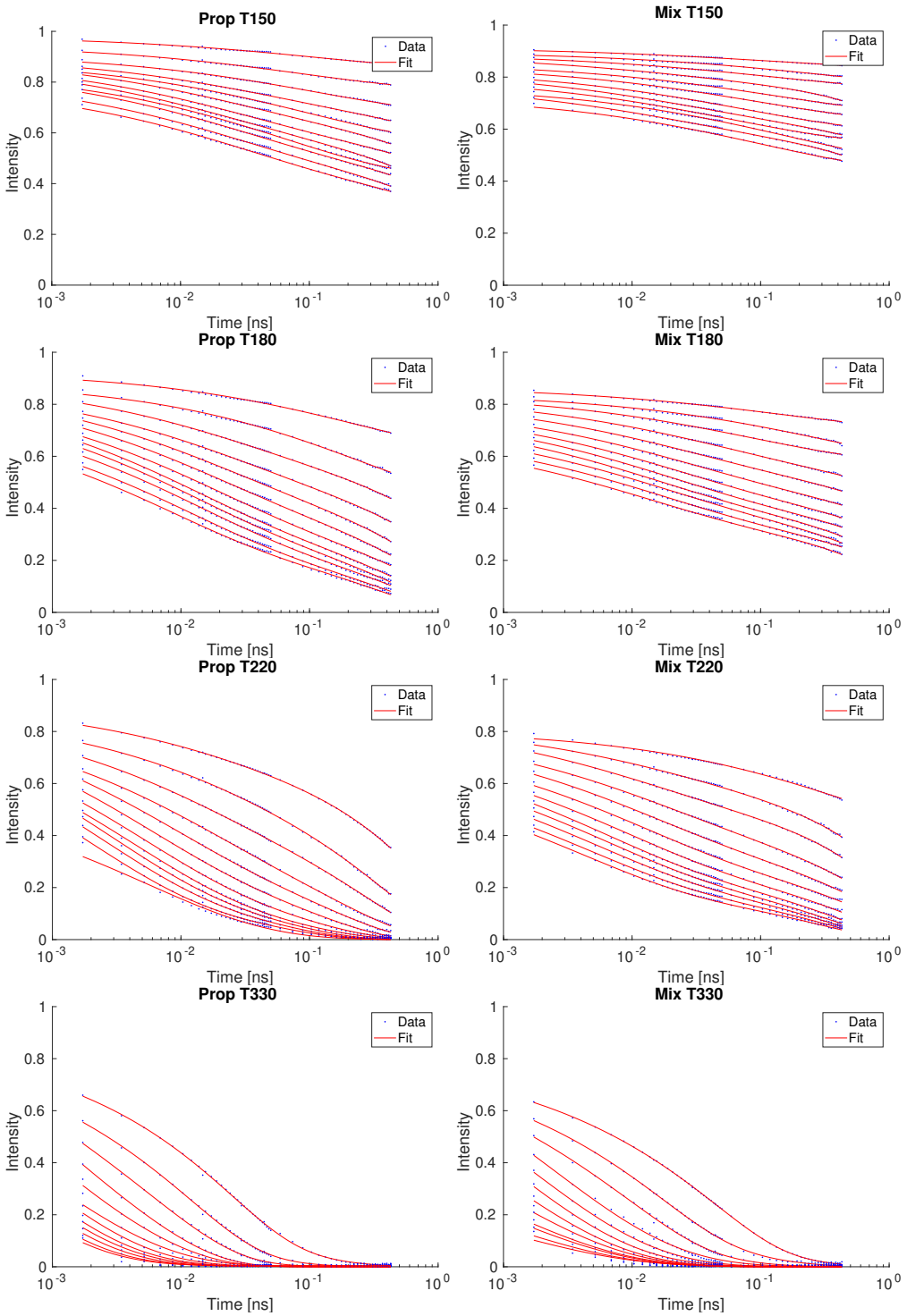

Figure 5.21: Fourier transformed data of IN5 and IN16B BATS merged for propanol (left) and mixture (right) at 150, 180, 220 and 330 K (top to bottom) with KWW + Lorentzian fit with previously extracted β parameter.

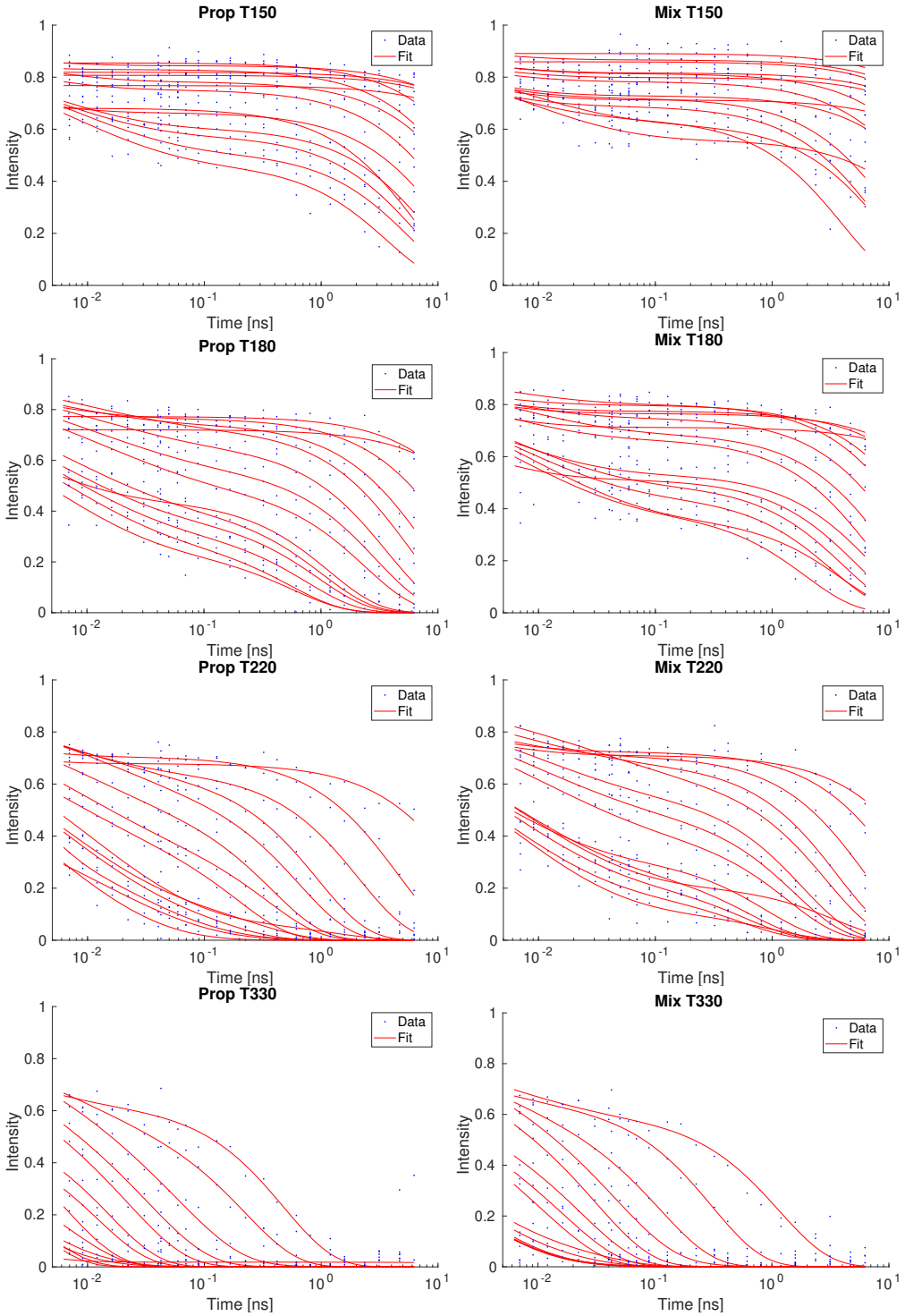

Figure 5.22: WASP for Prop (left) and Mix (right) at 150, 180, 220 and 330 K (top to bottom) with KWW + Lorentzian fit with β parameter 0.2.

We present then the τ parameters from these fits against the values shown in the last section, for 1-propanol in figure 5.23 and for the mixture in figure 5.24. Even as there were no ties between the protonated and deuterated version of our samples, the time scale of their different mode are roughly the same with deuteration. The main change that we see is that the separation between the 2 modes is bigger than the ones from last section, the KWW is faster and the Lorentzian is slower. The Q dependence of the time scale does still have the same behavior as before, and with the addition of WASP information, even expanded to lower Q values.

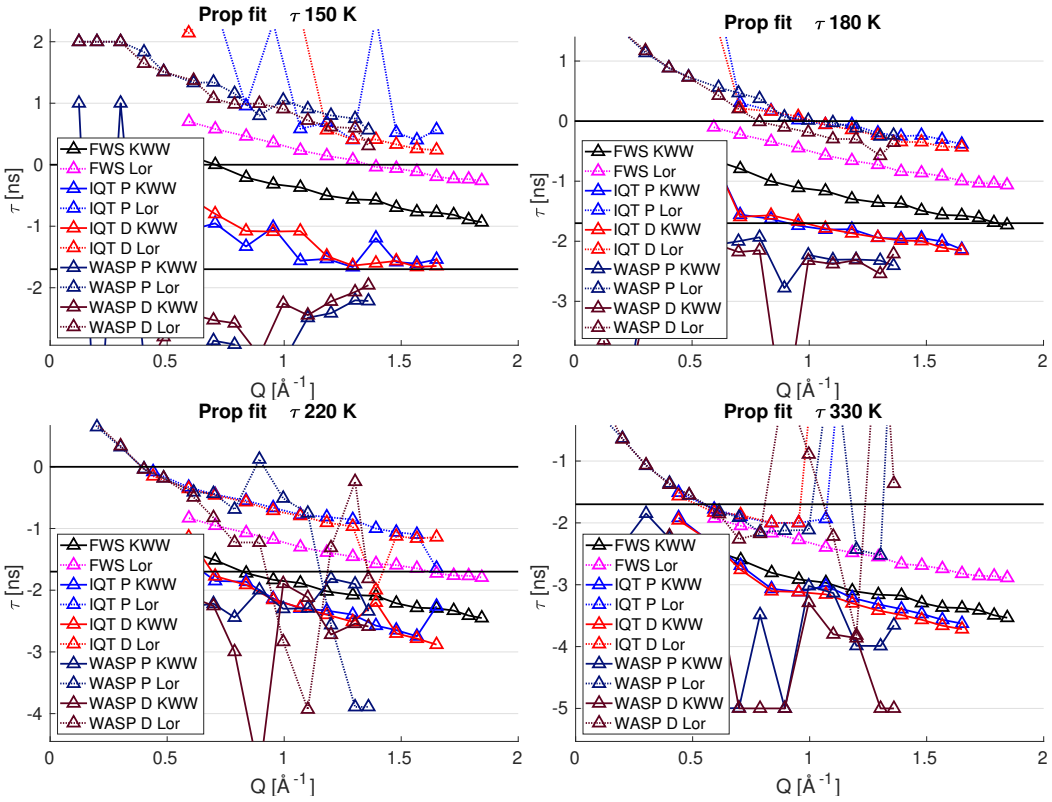

Figure 5.23: Temperature dependent time scale of the processes from the fits for Prop at 150, 180, 220 330 K (left to right, top to bottom). P means protonated and D deuterated sample.

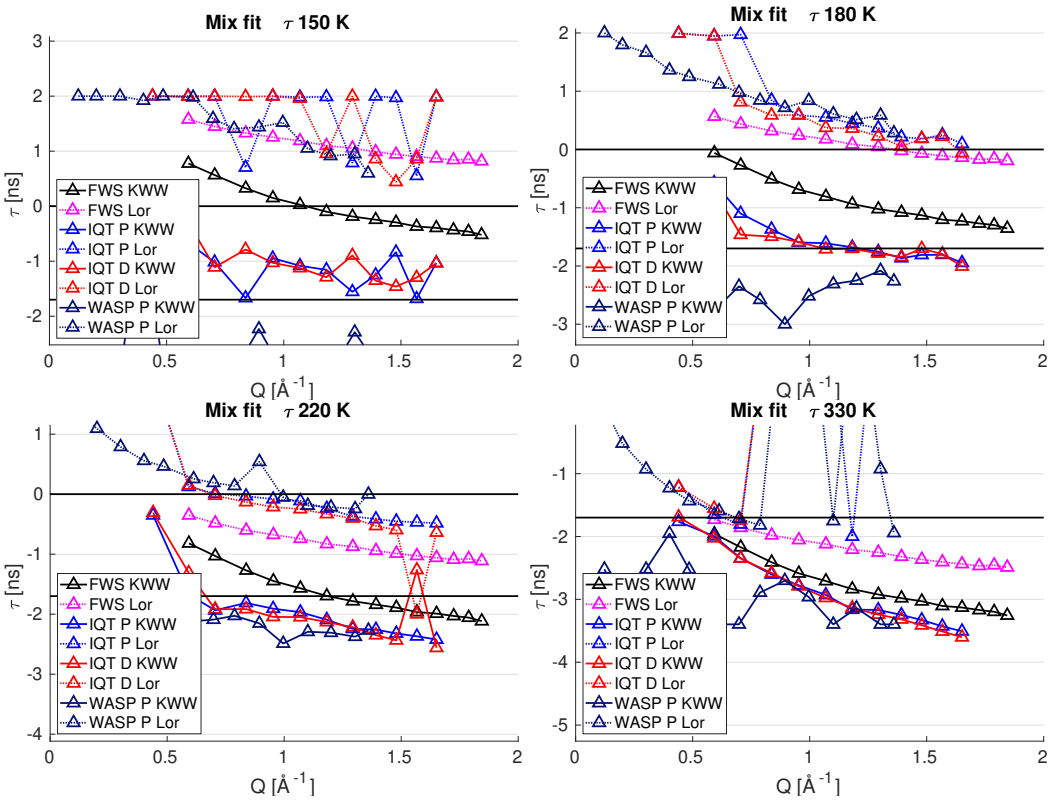

Figure 5.24: Temperature dependent time scale of the processes from the fits for Mix at 150, 180, 220 330 K (left to right, top to bottom). P means protonated and D deuterated sample.

The Arrhenius plot in figure 5.20 change slightly as can be seen in a new version in figure 5.25. We show there the difference of the time scales window in an Arrhenius plot between the time scales given from the FWS fits of last section and the I(Q,t) fits of this section. Cutting just the highest 3 Q values, which did not change substantially the fast limit of the time scale windows shown. For 150 K, the Lorentzian is too slow to be fitted in any reasonable way. The time scales are more separated in the data from this section compared to last section. First, the KWW does not change significantly time scale, while the Lorentzian does get systematically a little slower. For 330 K, the results do not substantially differ from what we saw in the FWS fits.

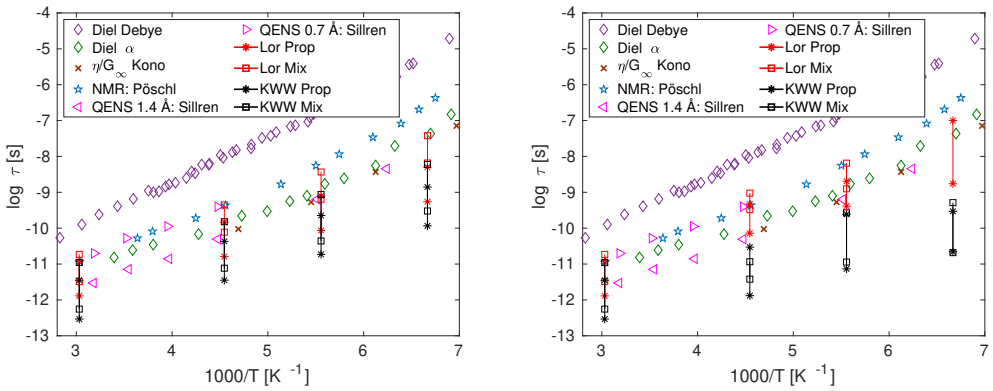

Figure 5.25: Arrhenius plot with PCS data [30], dielectric data [28, 30], NMR data [61], η/G_∞ [23] and coherent neutron scattering [28]. All literature data is for of 1 propanol . The time scale for Prop ($*$) and mixture ($\square$) of KWW (black) and Lorentzian (red) with the lowest (0.59 Å^{-1}) and highest (1.84 for FWS and 1.65 Å^{-1} for IN5) fitted Q, with the lines showing the span between them. Left is from FWS fits and right is from IN5 and IN16B BATS, I(Q,t) fits.

5.8 Summary

The use of quasi elastic neutron scattering in conjunction with partial deuteration showed us that the protons in the hydrogen bonding are clearly part of a separate and unique process. This mode seems quite clearly to fit in the time scale of the α relaxation that was found earlier in literature and the KWW lining with the β relaxation. A counter argument is that for most liquids, it is known that the α relaxation is not a Lorentzian and would much more push towards being the Debye relaxation. The KWW might be a composite of the α and β relaxation. For both neutron scattering, in figure 5.25, as well in dielectric spectroscopy, in figure 5.7, the addition of glycerol does not change the time scale of this process.

Chapter 6

Glycerol-water ambient pressure

6.1 Introduction

Glycerol is a very commonly used molecule. From additives in pharmaceuticals to personal care and food products, to protect skin from irritation and moisturizing, it is ubiquitous in modern day life. Glycerol is one of the most studied liquids in the supercooled state as it is very stable and hardly crystallizes, with techniques like dielectric spectroscopy, photon correlation spectroscopy and others [19, 61–71]. One of its major uses is its mixing with water. It has then multiples effects, one being the equilibrium between the glycerol-water ratio and humidity level [72]. Another big use is as a cryoprotectant. Glycerol is added to many systems, whether liquids or solution of proteins to lower the temperature or freezing and inhibit partially the formation of water crystals. Many studies have been done in dielectric spectroscopy and rheology, differential scanning calorimetry or other on this system [34, 35, 73–83], or with molecular dynamics [84–89].

Previous work by Jensen et al. [33] shows that, in the glycerol rich region (>30 % glycerol mol ratio), a threshold in rheology around 55 % glycerol is seen where a relaxation mode slower than the α appears. As seen in figure 6.1, we show data from their publication. The separation of dynamic between the main peak and the slower mode has a two regimes. In dielectric spectroscopy, this behavior has not been seen. Literature points to water preferring bonding with glycerol than other water molecules Towey et al. [36], and water clusters are present in the moderately enriched region while glycerol clusters are in the highly enriched region.

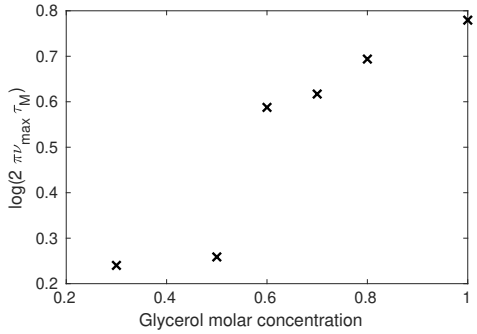

Figure 6.1: Glycerol concentration dependent separation of dynamics in rheology between main peak and slower mode. Data from Jensen et al. [33].

Our aim in this chapter is to test 2 things. First, with the help of inelastic neutron scattering and the tool of deuteration, verify if we can confirm the existence of either neat glycerol or neat water clusters in mixtures of glycerol-water as hypothesized in the previous paragraph. Second, it is to test some predictions of the Shoving model on a mixture more complex, meaning with a lot of hydrogen bonds and long distance structure, in the continuation of Hansen et al. [90] where they tested the shoving model on 3 van der Waals liquids with different fragility. We will study these liquids with broadband dielectric spectroscopy and quasi elastic neutron scattering to help resolve the question about if more complex liquids still follow this theory.

To test the neat glycerol or water clusters in the mixture, we then chose to study 2 mixtures, one on either side of this 55 % glycerol mol ratio in water, namely 40 % (glywa04) and 70 % (glywa07) glycerol mol ratio. We also have a deuterated variant for both mixtures where the water molecules and the alcohol group of glycerol have their hydrogens exchanged for deuteriums. The deuteration here allows us to segregate and see only the dynamics of the glycerol's aliphatic hydrogens in inelastic neutron scattering. So the fully protonated samples will show the dynamics of the whole liquid, while the deuterated version will give us the dynamics of glycerol's carbon backbone. This gives us our four samples with the added D for the deuterated version, namely **glywa04**, **glywa04D**, **glywa07**, **glywa07D**.

6.2 Experiment conditions

For dielectric spectroscopy, the data used for glywa04 and glywa04D is gathered during beam time 6-05-1008 (January 2020). Glywa07 and glywa07D were measured in November 2020 at ambient pressure using the pressure cell with 150 μm sample thickness with stabilized temperature steps. The temperature reading for glywa04 and glywa04D are the temperature of the start of the measurement, which was taken during a cooling ramp of 0.4 K/min. For glywa07 and glywa07D, done in November 2020, no temperature sensor for the sample was available to be in contact with the cell. The temperature used is then the cryostat regulation temperature, corrected by the amount calculated from previous experiments where the difference between regulation and sample sensor temperature was measured. Neutron scattering was done on IN16B during multiple beam times and during buffer days from 2019 to 2021.

6.3 Macroscopic dynamics

The assumption commonly used in many areas of neutron scattering, that replacing hydrogen atoms with deuterium does not change anything, might be wrong when looking at the dynamics of hydrogen-bonded liquids. Dielectric spectroscopy has been done to evaluate the difference, if any, between the protonated and deuterated mixtures of glycerol and water at 40 and 70 $\%$ mol ratio glycerol. In figure 6.2, we show the relaxation map of the main peak for our 4 samples with a fitted VFT function, see equation 6.1. In black is dielectric loss data from Puzenko et al. [34]. The deuterated liquids of both mixtures are slower than the fully protonated ones. Pure water does also exhibit a similar behavior. We used the VFT fit to find the glass transition temperature T_g, with its timescale = 100 s, for **glywa04** of **169 K**, **glywa04D** of **170.8 K**, **glywa07** of **181.6 K** and **glywa07D** of **185.2 K**.

$$\tau(T) = \tau_0 e^{\left(\frac{A}{T-T_0}\right)} \qquad (T_0 < T) \tag{6.1}$$

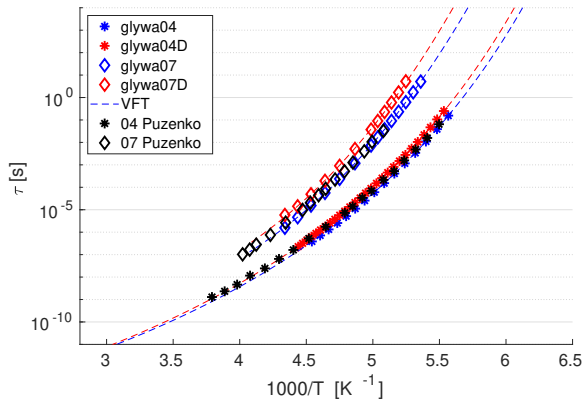

Figure 6.2: Relaxation map of glywa04 and glywa07 main peak with their respective VFT fits. In black is literature data [34]. We see a clear difference in dynamics due to the isotopic exchange of the hydrogens of the alcohols and water.

More than just offsetting the temperature at which the dynamics of our mixture are, the deuteration of the alcohols do have a time scale dependence of the effect. We show the same data in temperature versus frequency and the difference between the VFT fits of the protonated minus the deuterated version of each sample in figure 6.3. The faster the dynamics and the warmer the sample, the bigger the effect is due to the isotopic exchange. This shows a trend that we will confirm in the inelastic scattering section, where we look into nano second scale dynamics at higher temperature.

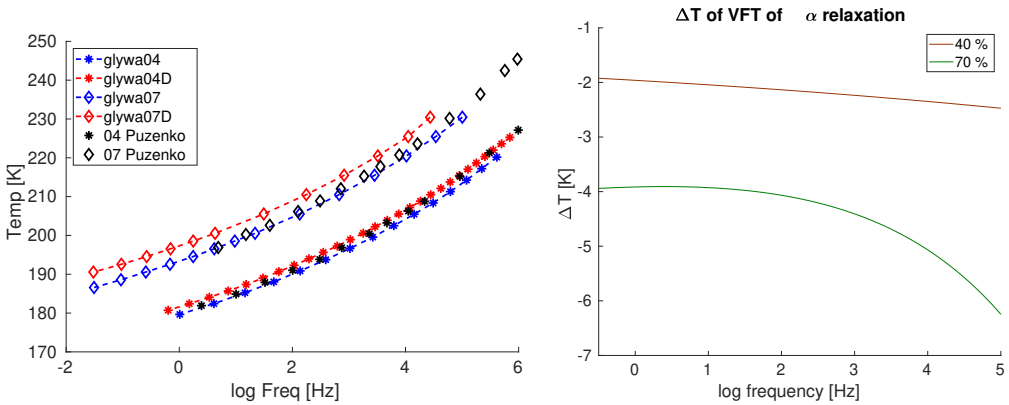

Figure 6.3: Left: relaxation map of all 4 samples in T VS log Frequency. Right: Frequency dependent difference in temperature of the VFT fit of the α-relaxation of the protonated minus the deuterated version of each mixtures.

Looking at the effect on the shape of the dielectric loss, shown in figure

6.4 with a superposition of the high frequency slope of all four samples, we see differences. Specifically, while the high frequency slope is similar, the low frequency slope lowers earlier and the maximum loss diminishes. For the 40 % mixture, the difference is very small, but clearly visible for the 70 %. The replacement of protons by deuterons in the alcohol groups do change the bonding strength and could then impact a macro structure, Debye like, dynamic.

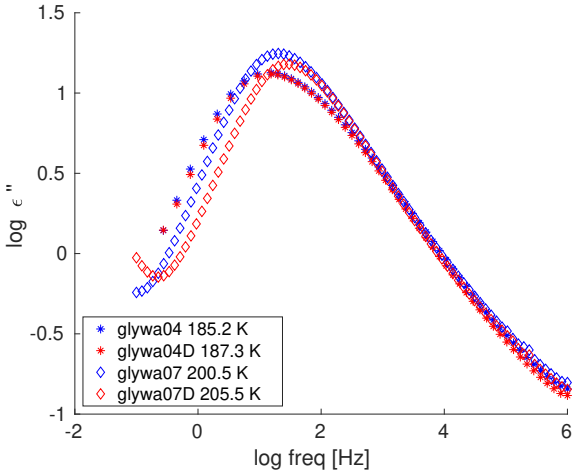

Figure 6.4: Dielectric loss of a rough isochrone of the 4 samples.

6.4 Shoving model test

Elastic neutron scattering data is measured by elastic fixed window scan on ILL's instrument IN16B. In figure 6.5, we present the elastic signal summed over all Q with the intensity at 10 K normalized to 1. The partial deuteration of our sample has, in our case, allowed to see only the dynamics of the glycerol's aliphatic hydrogens, i.e. the carbon backbone's dynamics. The deuterated version of both mixtures show a decrease in signal at higher temperature compared to their fully protonated variant. This shows that, like what was seen in dielectrics at lower temperature, the deuterated version show a slower relaxation.

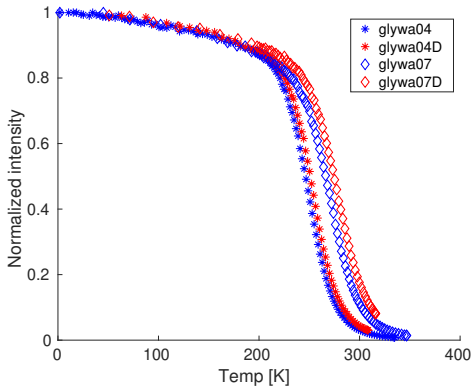

Figure 6.5: IN16B elastic FWS of all 4 samples. Intensity is normalized at 1 for 10 K.

From the Q dependent data, we extracted the mean squared displacement. In figure 6.6 we show both the MSD versus temperature and versus the temperature scaled to T_g. As was seen in the elastic data previously, the MSD shows also a difference in temperature with deuteration. Once the temperature is scaled with T_g, as seen in the right figure, the MSD is similar between all 4 samples. This means that once taking into account the dynamical isotopic effect, through their different T_g, the glycerol backbone has the same dynamics as the full mixture. There is then no separation of dynamics between glycerol and the water. Another point from this T_g scaled version is that both mixtures have the same shape once scaling is taken into account.

We then test a prediction that follows from the shoving model. It is the link between a liquid's fragility, found here using dielectric spectroscopy (the slope approaching 1 of T_g/T vs timescale of the α relaxation a 100 s),

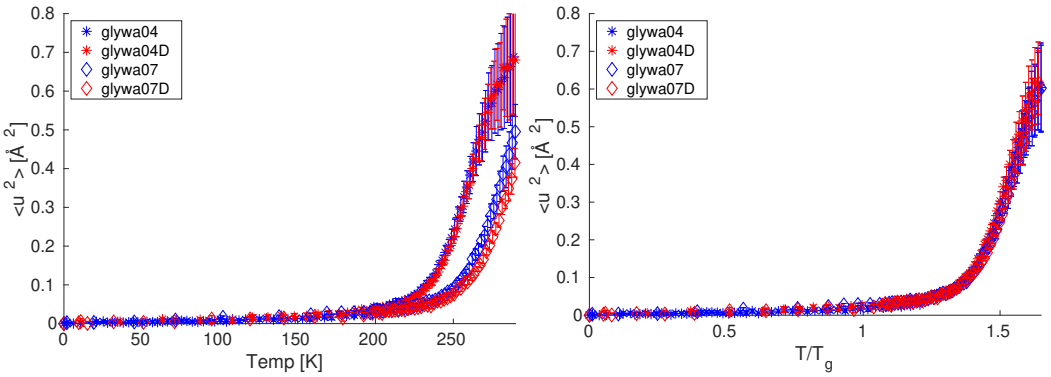

Figure 6.6: Mean-squared displacement of all 4 samples. On the left, the temperature axis is scaled to T_g.

and the mean squared displacement via the equation 3.20. In figure 6.7, the mean squared displacement is scaled by its value at T_g and the temperature by T_g. In black dashed line is a linear increase from 0 at 0 K to 1 at T_g and in full line is the prediction calculated from the previous equation. The MSD being very noisy, the only conclusion we have is that this data does not contradict the shoving model's prediction from fragility.

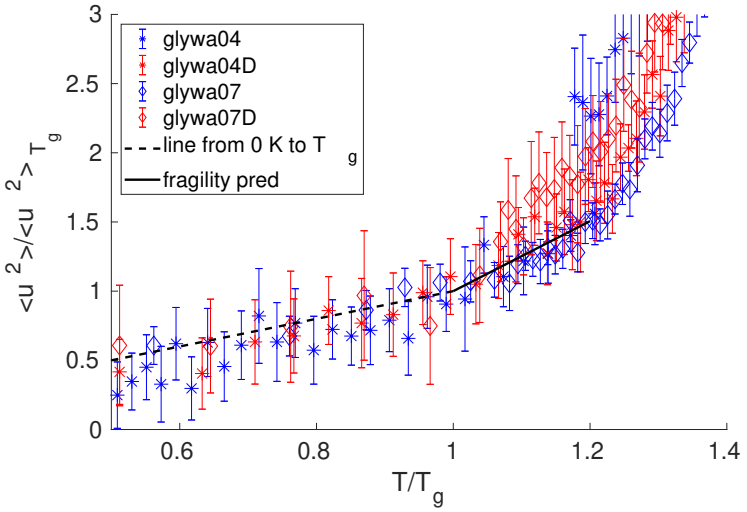

Figure 6.7: MSD scaled to it's T_g value versus T/T_g. In dashed black is a linear increase from 0 at 0 K to 1 at T_g and in full line black is the shoving model prediction from the fragility.

To test the shoving model, that was explained before in section 3.3, we show both the neutron and the dielectric data. For the dielectric data, it is the same as an Angell fragility plot. For the mean squared displacement, we use equation 3.21.

The shoving plot for our 4 samples is shown in figure 6.8. Showing glywa04 ($*$) and glywa07 ($\diamond$), the MSD (blue and red), the dielectric spectroscopy (navy and Bordeaux) and the temperature of the peak at IFWS max intensity (cyan and orange) for protonated and deuterated version respectively. The dielectric data is the α relaxation time τ plotted against T_g/T. We have a clear superposition of all 4 samples and its slope approaching T_g gives us the fragility. The data from neutron scattering is scaled by MSD at temperature T_g. Here we show that the noise in the data is rather big, which lessens our confidence in our conclusion. One thing we can say is that in general, it does still follow in general the shoving prediction, which is the black straight line. And if we concentrate on the deuterated sample, where we see only the carbon backbone, which is less influenced by long distance structure, it seems to follow a bit better. With the noise in the original data, it is still possible that all 4 samples behave the same.

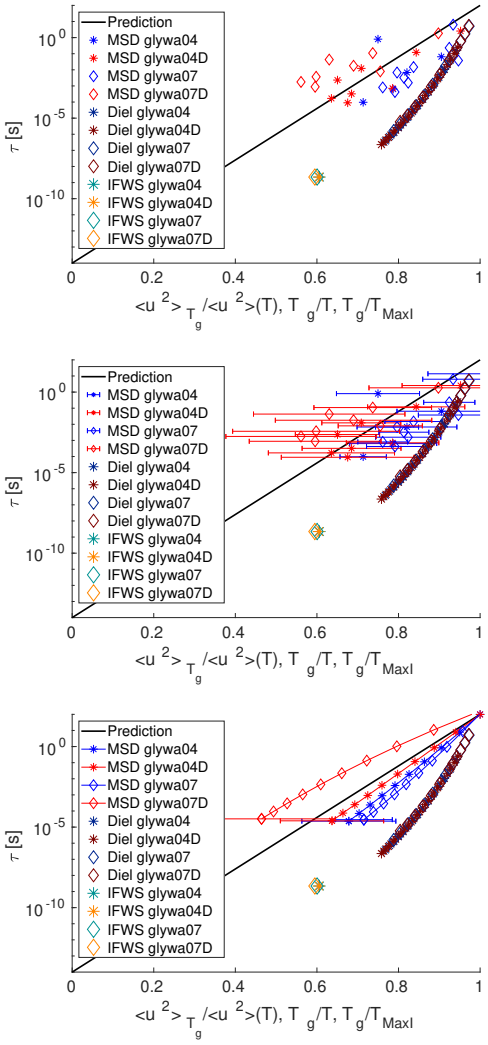

Figure 6.8: Shoving plot of the 4 samples. showing the timescale dependence $< u^2 >_{T_g} / < u^2 > (T)$ (top, just data, middle data with error bars and bottom linear regression of fig 6.7 between 1-1.2 T_g/T and average error bar shown at the fastest point) and the typical Angell fragility plot of dielectric T_g/T versus α relaxation time, and the FWS's T_g/T_{MaxI} versus it's 3 μeV energy transfer time scale.

6.5 Inelastic scattering

The neutron scattering experiment on IN16B were done with two techniques, fixed window scans and standard full energy transfer window. We will start first with the fixed window scans.

6.5.1 Inelastic fixed window scan

In this section, we will focus on the dynamical shape of glycerol in the two different glycerol-water mixtures with neutron backscattering instrument IN16B in an inelastic fixed window scan. It is a 3 μeV energy transfer window taken during a cooling ramp of 0.4 K/min. As in previous section, the partial deuteration of our sample shows only the dynamics of the glycerol's aliphatic hydrogens, i.e. the carbon backbone's dynamics.

In figure 6.9 we show the inelastic fixed window scans of both protonated and deuterated of both mixtures of glycerol and water. Deuteration does shift the temperature of the peak's position to a higher temperature and the mixture with higher glycerol content has also its peak shifted to higher temperature. This could potentially be explained by the isotopic exchange effect.

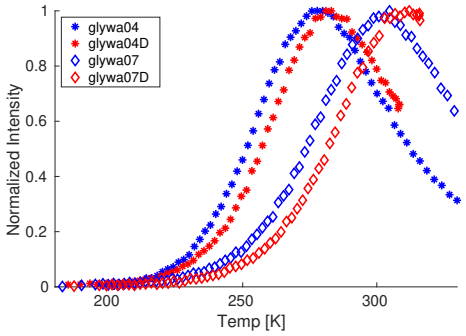

Figure 6.9: IN16B FWS at 3 μeV of all 4 samples. Maximum temperature was limited to the experimental setup.

As mentioned previously in the macroscopic dynamics section 6.3, the isotopic exchange of hydrogens by deuterons in the hydrogen bonding of these mixture do influence their dynamics. This effect makes a direct comparison between the protonated and deuterated version of a specific mixture, as we did in the previous chapter, not suitable. A correction has then to be applied to account for the isotopic exchange effect. As we showed in figure 6.3, as the macroscopic dynamics goes faster, the difference be-

tween the protonated and deuterated sample increases. Thus we chose to scale the temperature for the IFWS to the temperature of it's maximum's intensity. The figure representing this can be seen in fig 6.10, where the maximum intensities were also normalized to 1 to better see shape differences.

We see two things. First, carbon backbone's dynamics, seen with deuteration, has no separable effect from the total mixtures' dynamics. Second, it is clear that once we do scale to this temperature, both the concentrated glycerol rich mixture, at 70 % and the moderately glycerol rich mixture, at 40 % glycerol mol ratio behave the same. This leads us to believe that if nano sized clusters of either neat water, in glywa04, or neat glycerol, in glywa07 exist , they have no local and fast dynamics that are separable from the rest of the liquid.

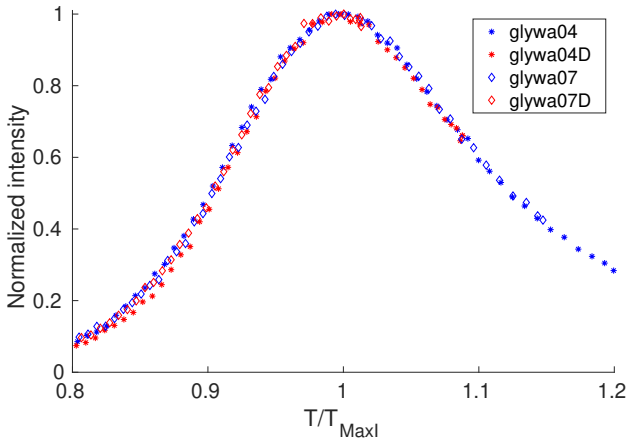

Figure 6.10: IN16B FWS at 3 μeV of all 4 samples. The temperature axis is scaled to the maximum's intensity temperature.

In figure 6.11, we show a surface plot of all four samples with the Q value in X, the temperature in Y and the color, from dark blue to yellow, the IFWS intensity. From a global view, there does not seem to be any different Q dependence of the signal between the different samples, just a translation in temperature. The fixed window scans show all in general no change once the samples are scaled in temperature with a corresponding time scale.

6.5.2 QENS

Quasi elastic spectra at 4 different temperatures (260, 280, 291 and 310 K) and a low temperature resolution, seen in figure 6.12 summed over all Q, were done to have a point of comparison with low cell noise for next chap-

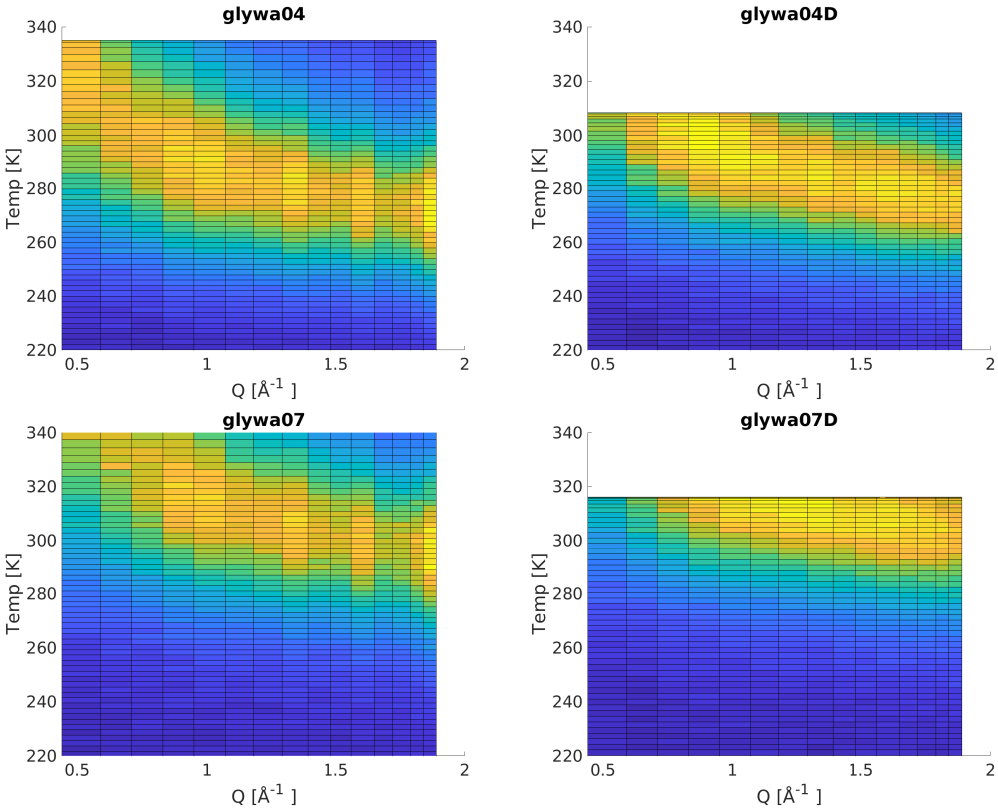

Figure 6.11: Surface map of the Q and temperature dependent intensity of the IFWS at 3 μeV of the four samples. Color are relative to each plot, from lowest intensities in dark blue to highest in yellow.

ter. Since isotopic exchange does affect the dynamics of the mixtures, we are not sure with the data we have that the shift talked about in the previous section is timescale independent, thus, direct comparison between fully protonated and partially deuterated sample is not possible.

By chance, we find between glywa04 at 260 K, glywa04D at 280 K, glywa07 at 291 K and glywa07D at 310 K, two cases where the data nearly fully overlaps, which can be seen in figure 6.13. The vertical black line represents the energy of the fixed window scans we show, 3 μeV. We see that in the energy window of roughly 1 order of magnitude, the behavior of all 4 sample show no clear deviations.

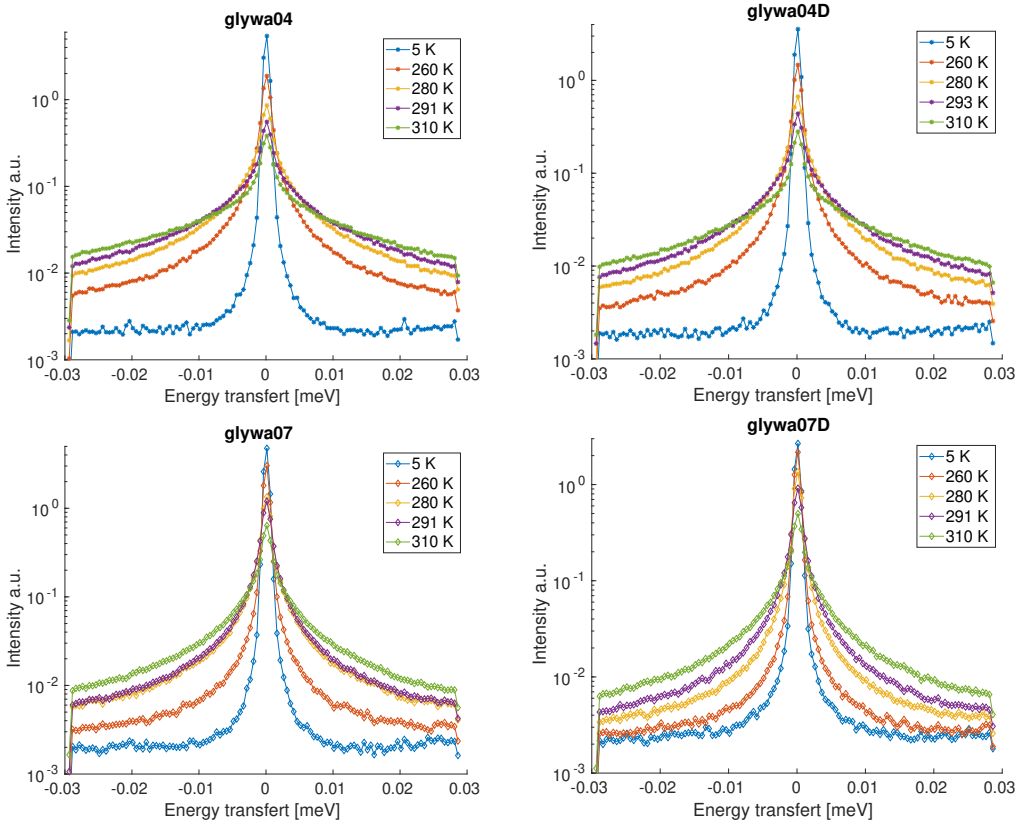

Figure 6.12: Full QENS of glywa04 (top) and glywa07 (bottom), protonated (left) and deuterated (right) at 5, 260, 280, 291-293 and 310 K.

6.6 Summary

The first point to keep in mind to summarize this chapter is that deuteration is a tool that in this case has its drawback and makes us have a bit more assumptions. Mainly, the deuteration effect is temperature and timescale dependent.

With this in mind then, once we scale our sample to their respective time scale, corresponding to the temperature, whether T_g for dielectric spectroscopy or the temperature of the maximum intensity for the inelastic fixed window scan, we see no difference in the dynamics of all 4 samples. Both deuteration, giving the dynamics of the glycerol backbone, and the difference in water content do not change the behavior of our liquids once scaled.

From here, we conclude that for the existence of neat water or neat glycerol clusters, their dynamics on a short time scale and local effect has to

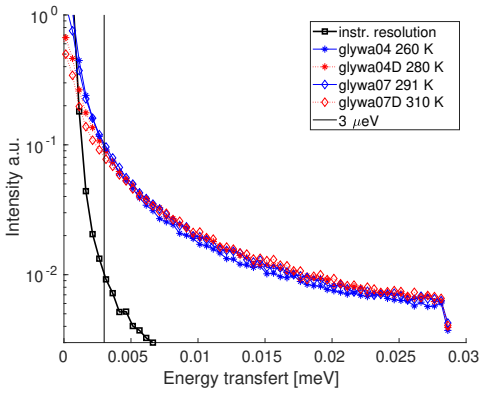

Figure 6.13: QENS near isochrone with glywa at 260 K, glywa04D at 280 K, glywa07 at 191 K and glywa07D at 310 K. The vertical black line is 3 μeV, where the FWS are taken at.

be indissociable from the bulk and not free. We would argue that one of the only clear change between the two mixture ratio is the strength of the macroscopic Debye peak in dielectric spectroscopy, where the more water rich mixture has a lower maximum dielectric loss and deuteration of the 70 % mixture also decreases it as seen in figure 6.4. About the Shoving model prediction, we would argue that for these liquids, the MSD version follows it rather well, taking into account the high noise of our data.

Chapter 7

Glycerol-water under pressure

7.1 Introduction

In this chapter, we continue our investigation of the two same glycerol water mixtures. This time, we look into their change in behavior when pressure is applied. A lot of liquids are known to obey density scaling and isochronal superposition, even some complex liquids, like the hydrogen bonding dipropylene glycol studied by Hansen et al. [55]. Simple liquids have been shown to exhibit isomorphs[44, 48, 91], which tried to offer an explanation of these phenomenons. What happens when we look at even more complex liquids is still unknown. We will try to look at isodynes, which are lines where different dynamical properties are invariant [92], or as he says it: "adiabats having the property of approximate dynamical invariance". It is a more simple and understandable concept than isomorphs, for which these complex system should not follow. We will test this property in a domains where isomorph theory is expected to not work.

In the figures 7.1 underneath, fixed window scans on IN16B at an energy transfer of 0 and 2 μeV, intensity is shown versus density scaled temperatures, do show signs of isochronal superposition. Some small amount of hydrogen bonds and its associated structural effect does seem to not strongly impede on the isomorph theory's prediction.

We wanted to build up on that finding and increase the complexity a little further by having a liquid with even more hydrogen bonds. In our case, we chose to investigate the same liquids as in the previous chapter, namely the mixture of glycerol and water with a mol ratio of 40 and 70 $\%$ glycerol.

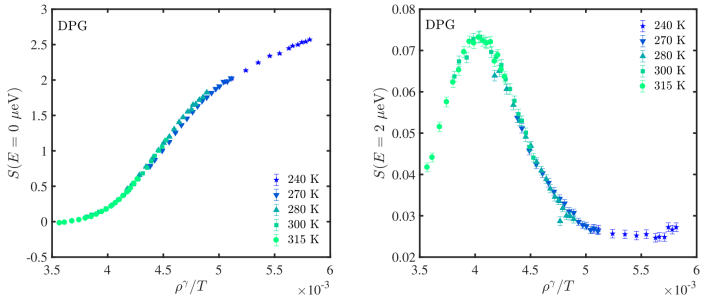

Figure 7.1: QENS fixed window scan, elastic (left) and inelastic 2 μeV (right), of dipropylene glycol versus scaled density over temperature. From [55].

The increase of hydrogen bonds in the liquid is present by both having a molecule with multiple alcohol groups, which provide multiple points of hydrogen bonds, and with the addition of water which is well known as a very complex liquid when looking into its dynamics. Glycerol under pressure has already been well studied, mostly in the supercooled regime, by dielectric spectroscopy, calorimetry, viscosity or simulations [44, 49, 58, 76, 93–104]. These studies show that glycerol dielectric loss peak widens, its fragility increases and appearance of a secondary relaxation with increased pressure in pressure ranges of GPa.

7.2 Experiment conditions

For dielectric spectroscopy, the data used for glycerol water mixtures, with 40 % glycerol mol ratio (glywa04) and 70 % glycerol mol ratio (glywa07), were taken in discrete pressure and temperature steps, in range of 0.1 - 300 MPa and 174 - 235 K, in an orange cryostat over a week for each sample. Neutron scattering was done on IN16B Doppler monochromator mode during multiple beam times in 2020 and 2021. The cell used for all experiments is the pressure cell with a capacitor of 150 μm thickness and total sample thickness of 300 μm.

7.3 Dielectric spectroscopy

We will show in this section the effect that pressure has on the dielectric loss spectrum with an increase in pressure from atmospheric pressure up to 300 MPa. We concentrate on the fully protonated 40 % (glywa04) and 70 % (glywa07) glycerol mol ratio mixtures.

7.3.1 Measurements

The measurements follow the ones done in the previous chapter at atmospheric pressure. In figure 7.2, we present the different pressure and temperature state points that were measured and add in red the position of 3 different near isochrones that will be shown further in this section. Since we organized our experiment on a temperature grid with spacing of 2 and 5 K and 50 MPa, true isochrones were not possible. We then chose to show what we call near isochrones, where measurements that had relatively close timescale were scaled to superimpose, as is shown in figure 7.4. This protocol makes the measurements over the whole temperature range, in which the dielectric loss peak is visible, fast but does not allow us to have precise isochrones. For higher temperature, the temperature step was 5 K until the main relaxation peak was around 10 Hz. For these steps, the frequency range measured is 10^{-1} to 10^{6} Hz, while for lower temperature, where steps were 2 K, the range measured is 10^{-2} to 10^{6} Hz.

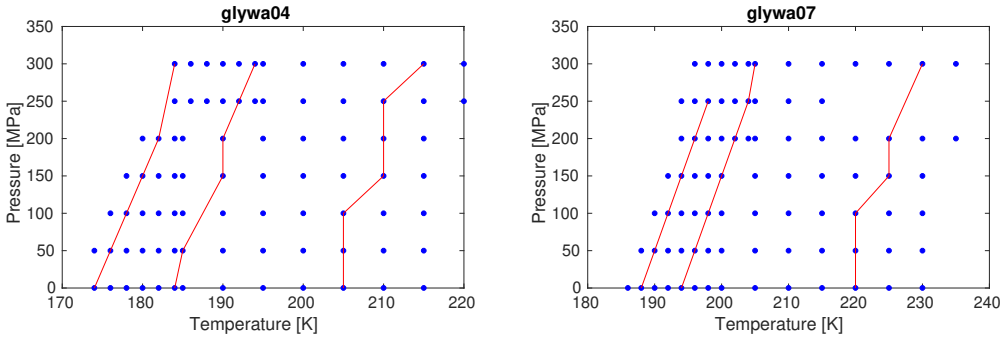

Figure 7.2: State points for dielectric spectroscopy for each sample. In blue are the measured state points with 50 MPa steps and either 2 or 5 K. In red we show the 3 near isochrones that are compared in figure 7.4.

In figure 7.3, a relaxation map of the main peak is shown, on the left for glywa04 and right for glywa07. In the pressure range studied, the increase in pressure causes a shift to slower relaxation time.

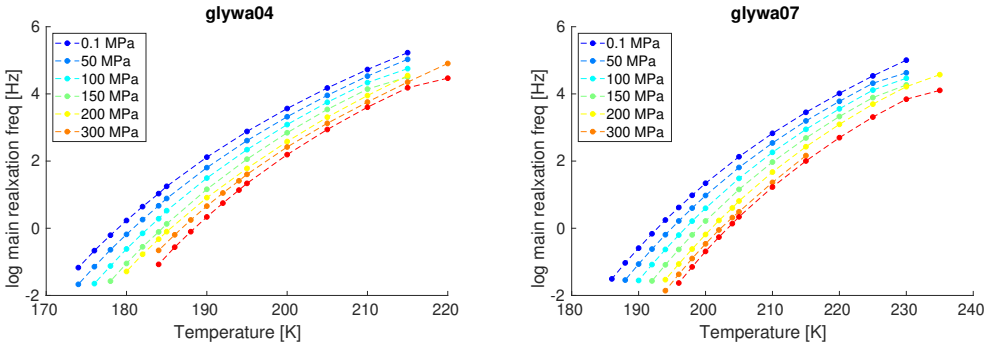

Figure 7.3: Relaxation map of glywa04 (left) and glywa07 (right).

7.3.2 Dielectric loss shape

The shape of the dielectric loss with pressure is shown in figure 7.4. 3 near isochrones are shown for glywa04, left, and glywa07, right. Each spectra is normalized in intensity and since they are only near isochrones, they are normalized in frequency too. We see a clear difference between glywa04 and glywa07. For glywa04, a strong high frequency shoulder is present at about two orders of magnitude from the maximum. This can be interpreted as an additional mode and it broadens with increased pressure. For glywa07, on the high frequency side we see a small shoulder only around three to four orders of magnitude from the maximum, which also increases with increased pressure. From a first glance, we can see that low frequency isochrones are more affected by pressure than high frequency ones. Second, for glywa04, the extra mode appears much closer in frequency from the maximum dielectric loss compared to the other mixture. For glywa07, the change seems more like a wing with a slightly shallower slope.

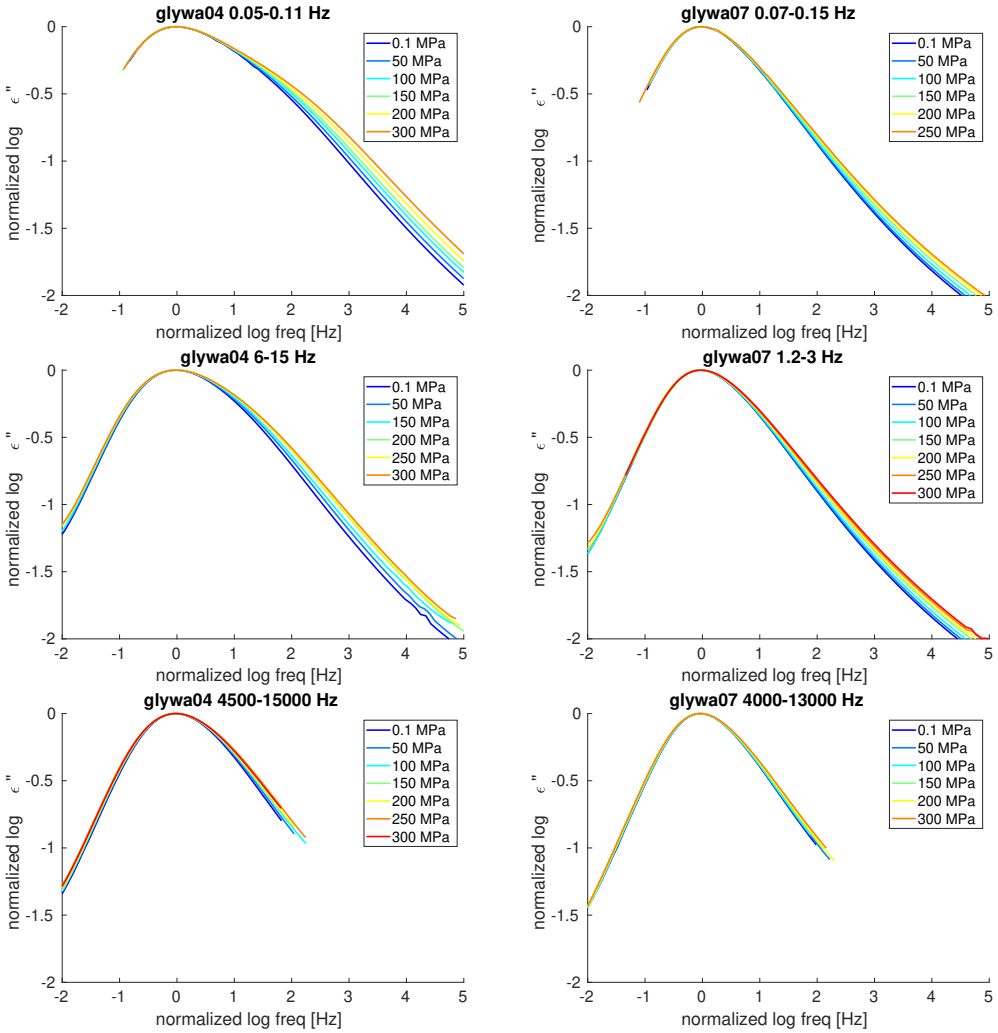

Figure 7.4: Dielectric loss of near isochrones of glywa04 (left) and glywa07 (right).

We see in figure 7.5 density scaling on the relaxation time versus ρ^γ/T where γ is the density-scaling factor. For glywa04, we have superposition with a γ of 1 and for glywa07, we have superposition with a γ of 1.4. Literature gives us a γ for glycerol of 1.8[105] which seems in line with our results, where the addition of water lowers γ.

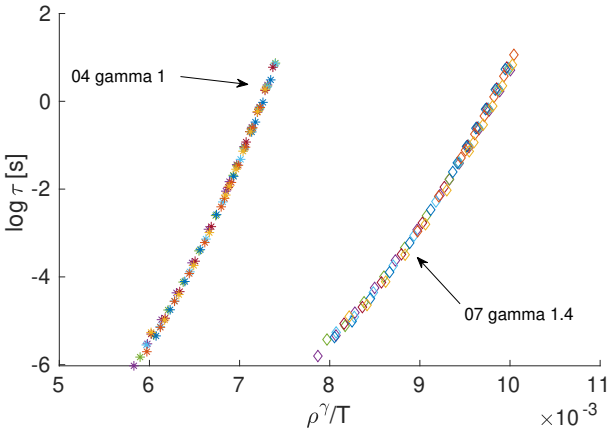

Figure 7.5: Relaxation map of glywa04 (left) and glywa07 (right) with inverse temperature scaled by density ρ^γ/T. For glywa04, γ = 1 while for glywa07 γ = 1.4.

To quantify better the change of the shape through the temperature-pressure domain, we extracted the high frequency side half width at half a decade (HWHD) under maximum dielectric loss. In figure 7.6 we show this parameter for glywa04 on top and glywa07 on bottom versus the frequency of the maximum dielectric loss on the left and versus the temperature on the right. On the left figures, the vertical lines represents isochrones while the vertical line on the figure on the right represents isotherms. There is a clear difference in the temperature dependence of the effect of pressure.Glywa04 shows that at higher temperature the effect of pressure is much less present than at lower temperature, while for glywa07, there does not seem to be much temperature dependence for the effect of pressure.

If we try to measure the change of HWHD for each isochrone along the isochrone, we come with the problem of quantifying a distance along an isochrone where we change both temperature and pressure, where each can have very different values and units, like a few K and a few millions of Pa. We use the method presented by Roed et al. [106] that quantifies the change of an observable along an isochrone by a factor L:

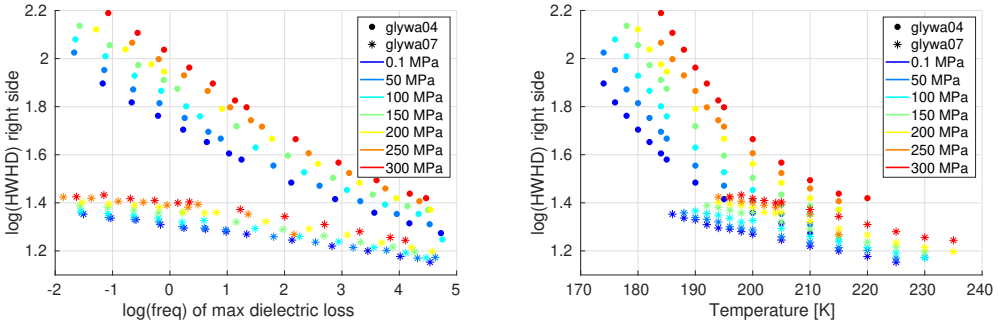

Figure 7.6: Dielectric loss main-relaxation frequency dependence (left) and temperature dependence (right) of the high frequency half width at half a decade lower than maximum.

$$L(X) = \frac{\delta X}{\delta s} \tag{7.1}$$

where X is the observable and s is the distance along the isochrone shown underneath with T the temperature and ρ the density.

$$\delta s^2 = (\delta \log T)^2 + (\delta \log \rho)^2 \tag{7.2}$$

We see now, in figure 7.7, that the amount of change of the HWHD along the isochrone is clearly smaller for glywa04 and that it changes only slightly for glywa07.

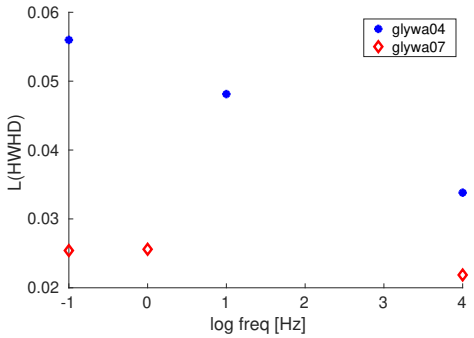

Figure 7.7: Rate of change of HWHD for a set distance along an isochrone.

7.4 Neutron scattering

In the last chapter, we showed that in neutron scattering once corrected for relative timescale due to both deuteration and the 2 dilutions, the samples looked similar at ambient pressure. In the last chapter, we have shown that the two dilutions exhibit in dielectric spectroscopy two different behaviors with the change in pressure. Knowing this, we investigated these samples on IN16B with both fixed window scans and full energy transfer spectra at fixed temperatures.

Contrary to the two previous chapters, we can not easily analyze the Q dependence of our data due to the technical limitation. The QENS technique made us choose aluminium for the the best mechanical strength to scattering background, which has limited mechanical strength to constrain liquids under pressure. Thus, the thickness and mass of metal used implies a lot of scattering from the cell itself. This made us select a thick sample as to have a signal over noise acceptable. Our sample thickness of the annulus of 300 μm gives us a transmittance of the sample only of around 0.7. This makes multiple scattering more than likely and bias the angular, i.e. Q, distribution of the scattered neutrons. For this reason, we will present for the neutron scattering experiments only data summed over all Q.

The pressure cell did not permit us reliable pressure cycling. This limits us into comparing somewhat reliably only data from the same beam time.

7.4.1 Inelastic fixed window scans

Inelastic fixed window scans at an energy transfer of 3 μeV of glywa04 and glywa07 at 0.1 and 400 MPa are shown in figure 7.8. For glywa07, we see that the high pressure data shows just the increase in intensity of the signal which corresponds to the left flank of the peak. Due to the experimental setting, we were limited to a highest temperature of 315 K. The lack of a peak at 400 MPa makes it hard to do any analysis at this pressure as the maximum intensity of a peak could be different.

To better compare the peak shape of the IFWS curves at different pressures, we scaled the temperature by the temperature of the maximum intensity. We can see in figure 7.9 that the increase in pressure does not change the shape of the IFWS, once scaled to its max temperature, neither does it change its intensity. The increase in pressure induces a uniform scaling of

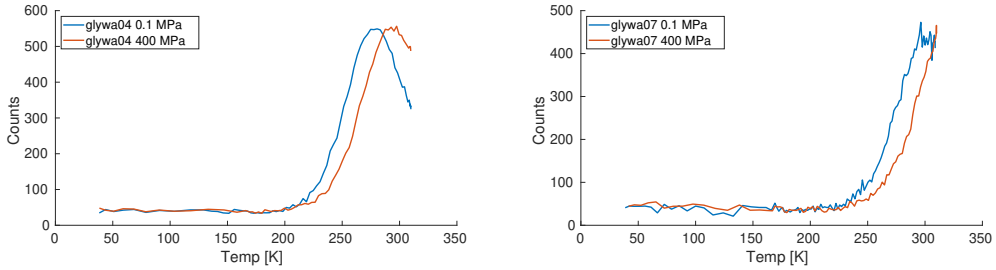

Figure 7.8: Inelastic FWS at 3 μeV of glywa04 (left) and glywa07 (right) at 0.1 (blue) and 400 MPa (red).

the observed dynamics by a factor of 1.06, which corresponds to a shift of 17 K in the temperature of the IFWS peak. The overlap is in line with the lack of difference we saw in previous chapter with the overlapping data when scaled between protonated and deuterated samples. It could be hypothesized that if water had separate dynamics, that was not seen to be independent at ambient pressure, it could be seen with increased pressure due to a possibly different pressure dependence.

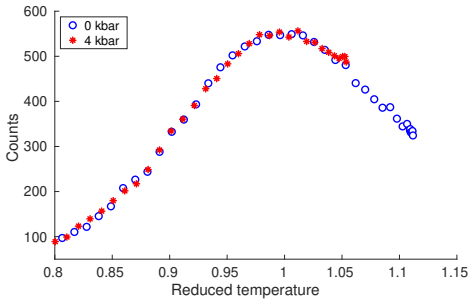

Figure 7.9: Inelastic FWS at 3 μeV of glywa04 at 0.1 and 400 MPa. Temperature is scaled to the maximum intensity's temperature.

7.4.2 Isochronal superposition

With quasielastic full window measurements in conjunction with simultaneous dielectric spectroscopy, we test the concepts of isodynes into further complex liquids. As said earlier, with the highly hydrogen bonded mixture we have with water and the 3 alcohol groups of glycerol, we are already quite outside the concept of weakly interacting liquids, that can roughly be simplified by interaction with only the first coordination shell and no long distance structure. We started the measurements with an atmospheric

pressure isobar fixed window scan then made a 310 K a full window scan at atmospheric pressure. Then continuing a 310 K isotherm from atmospheric pressure up to 2.5 or 4 kbar, depending on specific beam time. Then finishing with a high pressure 310 K full window scan. Subsequently, we matched the dielectric loss signal measured at high pressure 310 K to the closest match of the measurements during the atmospheric pressure isobar to find the isochrone temperature. We then measured full window scan of that temperature at atmospheric pressure and high pressure. State point figures of these point can be seen in figure 7.10 with the dashed line showing the isochrone state points.

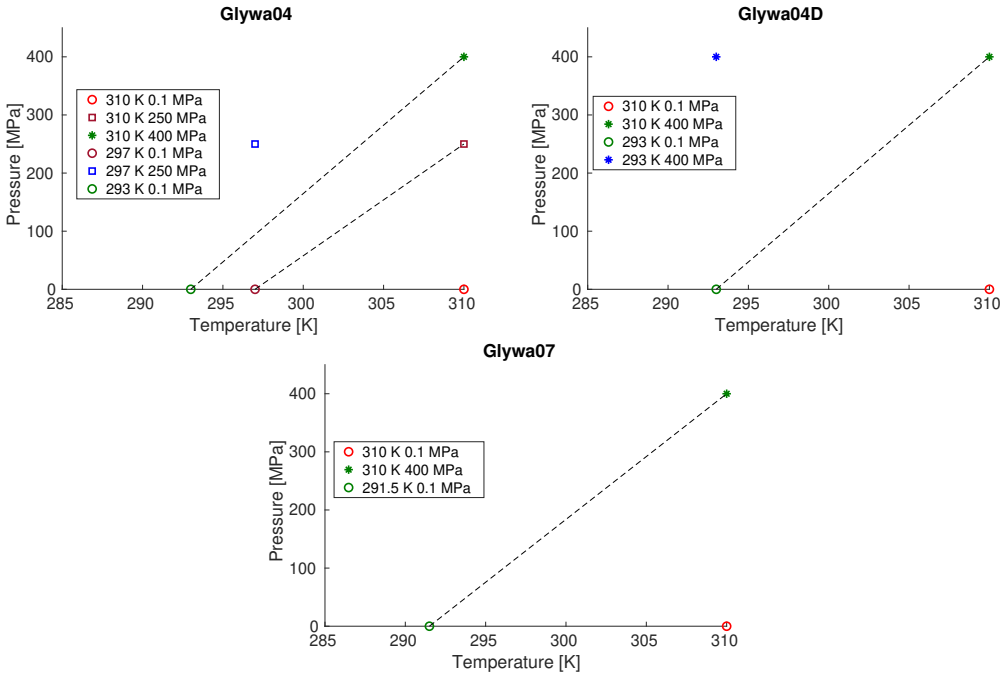

Figure 7.10: State points in the phase diagram that were investigated for the three samples. The isodynes for the 3 samples are connected by dashed lines.

Being at high temperature for the mixtures, the dielectric loss peak is already at much higher frequency than what can be seen in our setup that measures up to 1 MHz. What we measure then is the conduction band. The conduction seen in dielectric spectroscopy is internally consistent but not reproducible between samples. It is possible that low levels of contaminant change slightly the conduction of the measured liquids in amounts that are not easily controllable. We show in figure 7.11 the dielectric loss conduction signal of the four state points for each pair. The high temper-

ature high pressure data overlaps with the low temperature low pressure. In blue, we have the low temperature high pressure and in red, the high temperature low pressure. The overlap of the signal from taken simultaneously with the QENS is no surprise as the low temperature was chosen to overlap while looking at the data during the prior isobar measurement. We see the high temperature-atmospheric pressure at higher intensity and the low temperature-high pressure at lower intensity as we expected them as the increase in pressure act partially on the dynamics as a cooling down of the system.

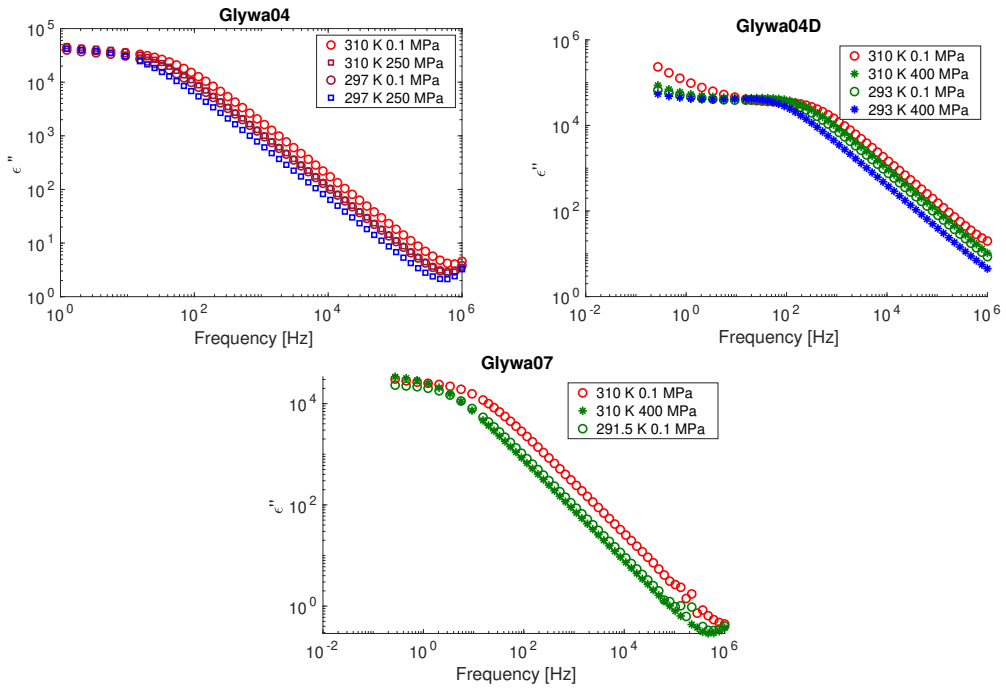

Figure 7.11: Dielectric loss of the isochrones for the 3 samples. The green isoconductivity for glywa04 is from another beam time and thus not comparable in absolute intensity with the other point in the figure. this is a visualization of the non replication of isoconductivity between experiments.

Now looking at the QENS spectra, we can see that the isochrone selected from dielectric spectroscopy results here, seen in figure 7.12, in excellent overlap over the whole energy spectrum. In this figure, we do not show the 310 K 400 MPa isochrone of glywa04 for clarity but the degree of overlap is similar to that the 310 K 250 MPa isochrone. Whether we look in at the intensity on a linear or logarithmic scale, no difference between the isochrones can be observed within the present experimental errors. It seems that at high temperature, the isoconductivity, even though it is not a very well understood phenomenon, is a good indicator to find isochrones at other timescale. This is in line with some of isomorph theory's prediction. Even though we did not correct the intensity for density, we expect little change in our conclusion as the difference is just a few percent, which is smaller than the noise of the data.

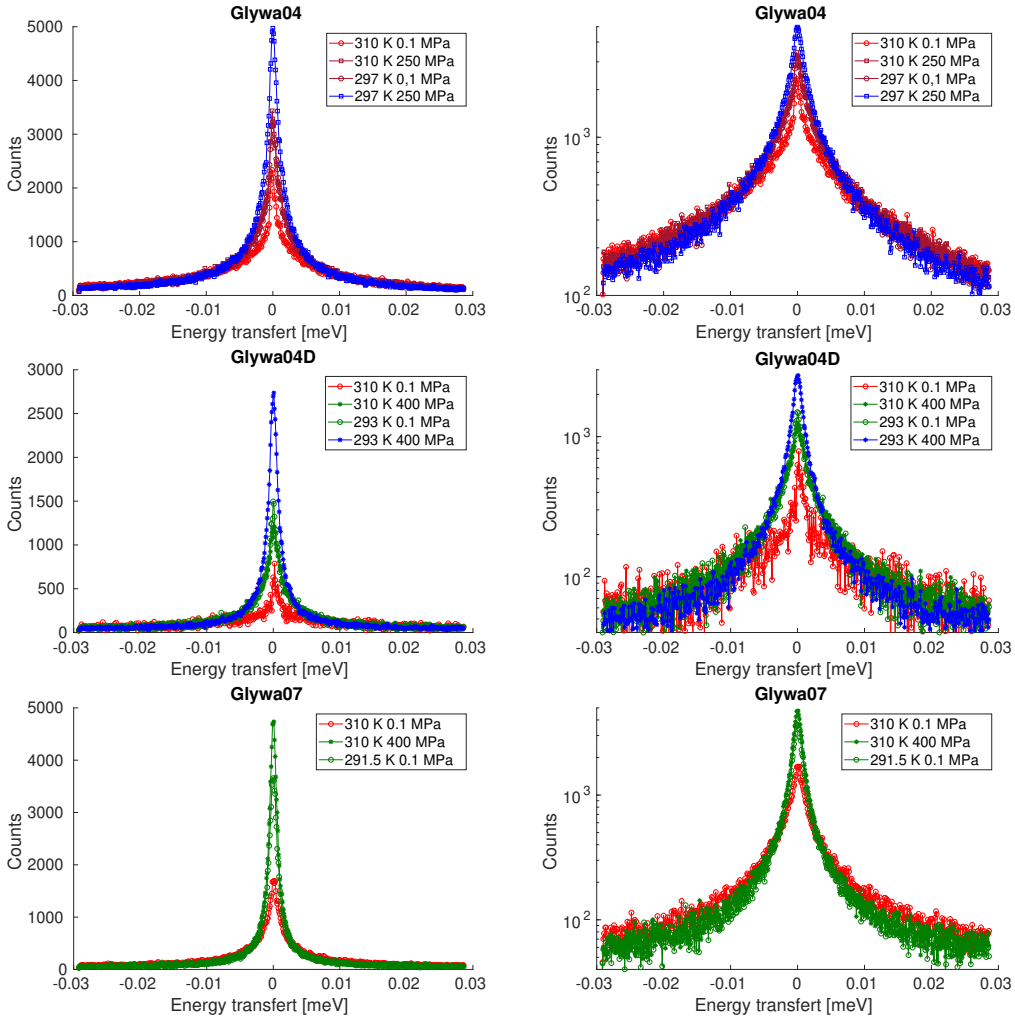

Figure 7.12: QENS spectra of isochrones for the 3 samples with surrounding P-T state points. The count numbers are in lin scale (left) and log scale (right).

7.5 Summary

A first conclusion of these experiments is that even though in the previous chapter, we could neither find clearly different behavior between the liquids and some hypothesized neat water nor glycerol clusters having their own dynamics, dielectric spectroscopy shows us there is a pressure dependent separate effect. There is something in these mixtures that makes the shape of the dielectric loss of the 70 % mixture pressure effect nearly temperature independent in the temperature range measured while for the 40 % there is a clear relation between the temperature and the amplitude of the effect of pressure. Secondly, we can see that the pressure effect on the dielectric spectra is less pronounced at higher temperatures. We hypothesise that this is due to the fact that at high energy-short timescale, all the relaxation modes tend to merge. Lastly, even though we are clearly outside the bounds of weakly interacting liquids, dielectric spectroscopy and even its conduction signal at high temperature can be a very good first approximation to find isochrones at other timescales and local effects. This shows that even outside of the theory's boundary of "simple" liquids, some more complex liquids, like our mixtures that do possess long distance structure, can still have properties well approximated by it.

The dielectric spectroscopic data point to some other fundamental difference between the two mixtures as was shown in the literature in rheology [33]. Prior assumption, like in previous chapter, that neat water or glycerol clusters are present could be viable in limited circumstance. If we consider that at a local and fast timescale, the confinement makes them always have the same dynamics. But a different compressing behavior between the neat clusters and the bulk would inhibit partially some fast rearrangement from the bulk's long distance structure. Another assumption could be that for glywa04, it is the appearance of water-water bonds in the bulk that makes the long distance structure change and behave much differently with regards to pressure.

Chapter 8

Concluding discussion

To summarize, extensive neutron scattering and dielectric spectroscopy was done on mixtures of glycerol with water and 1-propanol, neat or with 10 % glycerol.

For glycerol water mixtures, it looks like neither mixture shows any clear evidence of micro separation where either neat glycerol clusters in the most glycerol rich mixture or neat water clusters in the most glycerol lean mixture exist with separate dynamics. We show also that with this many possibilities of cross linking due to poly alcohol groups, the hydrogen bond network does not have a separate dynamics from the rest of the liquid. We also show that on either side of the 55 % molar ratio threshold, both mixtures exhibit the same dynamics in neutron scattering once we scale to their respective maximum intermediate scattering function. Under pressure change, neutron scattering showed no difference in the inelastic fixed window scan shape, while the dielectric loss showed clearly different shape with a broadening on the fast side of the peak and much more prevalent in 40 % glycerol mixture. The temperature, or isochronal dependence of that broadening is also different between the 2 samples, but they both still show a reduction of that effect at high temperature which could be explained with the general merging of dynamics that happens at high temperature.

For Propanol and its mixture, we show that the hydrogens in the hydrogen bonding network do definitively have a separate dynamic mode from the rest of the molecule. We show that the shape this relaxation mode in QENS follows a simple Lorentzian distribution. The rest of the dynamics

was modeled via a stretched exponential, but this can still be refined further as it might just be a placeholder for more than one relaxation mode. It is still not as clear to which dielectric relaxation mode, Debye like, alpha or beta relaxation, the hydrogen bond relates to. As the Lorentzian is the slower of the modes and the α relaxation is nearly never Lorentzian, it is hypothesized that it is related to the Debye. with the caveat that in QENS, we see the self correlation while in dielectric spectroscopy, the Debye is a macroscopic effect.

On the propanol topic, more will be done, through a new PhD student.

To conclude this work, I will first say that the use of simultaneous broadband dielectric spectroscopy and neutron scattering is a simple add-on with multiple facets that many experiments could benefit. From the quick on site following of liquid versus crystal state of supercooled liquids or when looking for a quick clue on isochrones between different temperature-pressure state points, whether in supercooled regime or at high temperature. With the different cells that were designed during this thesis or prior to it, there are already a wide variety of instruments in neutron spectroscopy that can benefit from it. This was extensively used for the project on glycerol-water under pressure, where isoconductivity in dielectric spectroscopy gave very good indication for isochrones in neutron scattering.

The selective deuteration is also a tool that has proven very useful, but not a panacea. It allows to sort the signal of some parts of the liquids and how they, like propanol and its mixture with 10 $\%$ molar ratio glycerol, are contributing to the total macroscopic dynamics of it. This comes also at a time with its own complication, like for glycerol water, where the isotopic exchange does have an ostensible effect on the dynamics of the system, giving isochrones between the 2 isotopes' system with a change in temperature from 1.8 to 3.6 K at T_g. This made us decide on scaling the temperature of the neutron scattering results by their relative maximum. This can be up to debate as it is not known, like via dielectric spectroscopy, how much the change in dynamics from isotopic substitution is temperature dependent.

The shoving model was tested on 2 hydrogen bonded liquids and for the glycerol-water mixtures, it is not disproven. It seems though that when a liquid has a rather strong long distance structure or interaction, like with propanol and its mixture, the shoving model prediction falls off. The pre-

diction, coming from the fragility measured via dielectric spectroscopy, takes into account the chain-like macroscopic dynamics. The mean squared displacement measured via neutron scattering was clearly faster than predicted. I do hypothesis that this result might be explained as with QENS incoherent scattering, we probe the local fast dynamics of molecules that can quickly break and reform the hydrogen bonds between neighboring chains, giving faster dynamics than the big macrostructure that contributes to the prediction.

Bibliography

[1] Henriette W. Hansen. *Dynamics of glass-forming liquids: Will theory and experiment ever meet?* PhD thesis, University of Roskilde, 2018.

[2] Mikkel H.n Jensen. *Structure and Dynamics of Hydrogen-Bonded Liquids. A Study of Supra-Molecular Structures and Crystallisation.* PhD thesis, University of Roskilde, 2018.

[3] G L Squires. *Introduction to the theory of thermal neutron scattering.* Cambridge University Press, Cambridge, England, 3 edition, March 2012.

[4] D S Sivia. *Elementary scattering theory.* Oxford University Press, London, England, January 2011.

[5] M Bée. *Quasielastic neutron scattering, principles and applications in solid state chemistry, biology and materials science.* CRC Press, London, England, January 1988.

[6] Bernhard Frick, Dan A Neumann, et al. Neutron backscattering. *Neutrons in Soft Matter*, pages 183–202, 2011.

[7] B. Frick, J. Combet, and L. van Eijck. New possibilities with inelastic fixed window scans and linear motor doppler drives on high resolution neutron backscattering spectrometers. *Nuclear Instruments and Methods in Physics Research Section A: Accelerators, Spectrometers, Detectors and Associated Equipment*, 669:7–13, March 2012. doi: 10.1016/j.nima.2011.11.090.

[8] Markus Appel, Bernhard Frick, and Andreas Magerl. A flexible high speed pulse chopper system for an inverted neutron time-of-flight option on backscattering spectrometers. *Sci. Rep.*, 8(1):13580, 2018. ISSN 2045-2322. doi: 10.1038/s41598-018-31774-y.

[9] Markus Appel, Bernhard Frick, and Andreas Magerl. First results with the neutron backscattering and tof spectrometer option bats on in16b. *Physica B: Condensed Matter*, 562:6 – 8, 2019. ISSN 0921-4526. doi: https://doi.org/10.1016/j.physb.2018.11.062.

[10] Jack Hine and Cyrus H. Thomas. Rate of deuterium exchange of certain amines and alcohols - 1, 2. *Journal of the American Chemical Society*, 76(2):612–612, January 1954. doi: 10.1021/ja01631a090.

[11] Boualem Hammouda. *The SANS Toolbox*. National Institute of Standards and Technology, Center for Neutron Research Gaithersburg, MD 20899-6102, 2016.

[12] Friedrich Kremer and Andreas Schönhals. *Broadband Dielectric Spectroscopy*. Springer, 2012.

[13] Ioannis M. Kalogeras and Haley Hagg Lobland. The nature of the glassy state: Structure and glass transitions. *Journal of Materials Education*, 34:69–94, 08 2012.

[14] L.-M. Martinez and C. A. Angell. A thermodynamic connection to the fragility of glass-forming liquids. *Nature*, 410(6829):663–667, April 2001. doi: 10.1038/35070517.

[15] Thomas B H Schroeder, Srikanth Sastry, Jeppe C. Dyre, and Sharon C. Glotzer. Crossover to potential energy landscape dominated dynamics in a model glass-forming liquid. *Journal of Chemical Physics*, 112: 9834–9840, 1999.

[16] David Chandler, John D. Weeks, and Hans C. Andersen. Van der waals picture of liquids, solids, and phase transformations. *Science*, 220 (4599):787–794, May 1983. doi: 10.1126/science.220.4599.787.

[17] L D Landau, L P Pitaevskii, A M Kosevich, and E M Lifshitz. *Theory of elasticity*. Course of Theoretical Physics. Butterworth-Heinemann, Woburn, MA, 3 edition, January 1986.

[18] Roland Böhmer, Catalin Gainaru, and Ranko Richert. Structure and dynamics of monohydroxy alcohols—milestones towards their microscopic understanding, 100 years after debye. *Physics Reports*, 545 (4):125–195, December 2014. doi: 10.1016/j.physrep.2014.07.005.

[19] D. W. Davidson and R. H. Cole. Dielectric relaxation in glycerol, propylene glycol, andn-propanol. *The Journal of Chemical Physics*, 19(12):1484–1490, December 1951. doi: 10.1063/1.1748105.

[20] G. Potapenko. Die elektrischen absorptions- und dispersionsspektren von methyl- und athylalkohol im bereiche von 30 bis 90 cm wellenlunge. *Zeitschrift fur Physik*, 20(1):21–35, December 1923. doi: 10.1007/bf01327916.

[21] Pierre Girard. Dipole association in pure liquids. *Transactions of the Faraday Society*, 30:763–772, 1934.

[22] George Walter Stewart and Roger M. Morrow. X-ray diffraction in liquids: Primary normal alcohols. *Physical Review*, 30:232–244, 1927.

[23] R. Kono, T. A. Litovitz, and G. E. McDuffie. Comparison of dielectric and mechanical relaxation processes in glycerol—n-propanol mixtures. *The Journal of Chemical Physics*, 45(5):1790–1796, September 1966. doi: 10.1063/1.1727831.

[24] B. Schiener and R. Böhmer. Dielectric relaxation in supercooled 1-propanol. *Journal of Non-Crystalline Solids*, 182(1-2):180–185, March 1995. doi: 10.1016/0022-3093(94)00581-8.

[25] C. Talón, G.J. Cuello, M.A. González, F.J. Bermejo, C. Cabrillo, and R. Connatser. A comparative study of the low-frequency dynamics of the two isomers of propanol. *Chemical Physics*, 292(2-3):263–271, August 2003. doi: 10.1016/s0301-0104(03)00053-3.

[26] S. Sudo. Broadband dielectric study on glass transition of 1-propanol-water mixture. In *AIP Conference Proceedings*. AIP, 2006. doi: 10.1063/1.2204477.

[27] A. Sahoo, S. Sarkar, V. Bhagat, and R. N. Joarder. The probable molecular association in liquid d-1-propanol through neutron diffraction. *The Journal of Physical Chemistry A*, 113(17):5160–5162, April 2009. doi: 10.1021/jp8107717.

[28] P. Sillrén, A. Matic, M. Karlsson, M. Koza, M. Maccarini, P. Fouquet, M. Götz, Th. Bauer, R. Gulich, P. Lunkenheimer, A. Loidl, J. Mattsson, C. Gainaru, E. Vynokur, S. Schildmann, S. Bauer, and R. Böhmer. Liquid 1-propanol studied by neutron scattering, near-infrared, and

dielectric spectroscopy. *The Journal of Chemical Physics*, 140(12): 124501, March 2014. doi: 10.1063/1.4868556.

[29] Th. Bauer, M. Michl, P. Lunkenheimer, and A. Loidl. Nonlinear dielectric response of debye, α , and β relaxation in 1-propanol. *Journal of Non-Crystalline Solids*, 407:66–71, January 2015. doi: 10.1016/j.jnoncrysol.2014.07.024.

[30] Jan Gabriel, Florian Pabst, and Thomas Blochowicz. Debye process and β-relaxation in 1-propanol probed by dielectric spectroscopy and depolarized dynamic light scattering. *The Journal of Physical Chemistry B*, 121(37):8847–8853, September 2017. doi: 10.1021/acs.jpcb.7b06134.

[31] Peter Weigl, Daniel Koestel, Florian Pabst, Jan Philipp Gabriel, Thomas Walther, and Thomas Blochowicz. Local dielectric response in 1-propanol: α-relaxation versus relaxation of mesoscale structures. *Physical Chemistry Chemical Physics*, 21(44):24778–24786, 2019. doi: 10.1039/c9cp05035c.

[32] Antonela Ananiadou, George Papamokos, Martin Steinhart, and George Floudas. Effect of confinement on the dynamics of 1-propanol and other monohydroxy alcohols. *The Journal of Chemical Physics*, 155(18):184504, November 2021. doi: 10.1063/5.0063967.

[33] M. H. Jensen, C. Gainaru, C. Alba-Simionesco, T. Hecksher, and K. Niss. Slow rheological mode in glycerol and glycerol–water mixtures. *Physical Chemistry Chemical Physics*, 20(3):1716–1723, 2018. doi: 10.1039/c7cp06482a.

[34] Alexander Puzenko, Yoshihito Hayashi, Yaroslav E. Ryabov, Igal Balin, Yuri Feldman, Udo Kaatze, and Ralph Behrends. Relaxation dynamics in glycerol-water mixtures: i. glycerol-rich mixtures. *The Journal of Physical Chemistry B*, 109(12):6031–6035, March 2005. doi: 10.1021/jp0445122.

[35] Yoshihito Hayashi, Alexander Puzenko, and Yuri Feldman. Slow and fast dynamics in glycerol–water mixtures. *Journal of non-crystalline solids*, 352(42-49):4696–4703, 2006.

[36] J. J. Towey, A. K. Soper, and L. Dougan. Preference for isolated water molecules in a concentrated glycerol–water mixture. *The Journal of Physical Chemistry B*, 115(24):7799–7807, June 2011. doi: 10.1021/jp203140b.

[37] Nobuyuki Nishiyama and Akihisa Inoue. Supercooling investigation and critical cooling rate for glass formation in pd–cu–ni–p alloy. *Acta Materialia*, 47(5):1487–1495, March 1999. doi: 10.1016/s1359-6454(99)00030-0.

[38] C. A. Angell. Strong and fragile liquids. In Kia L. Ngai and George B. Wright, editors, *Relaxations in Complex Systems*, pages 3–11, 1984.

[39] Jeppe C Dyre. Energy master equation: A low-temperature approximation to bässlers random-walk model. *Physical Review B*, 51(18):12276, 1995.

[40] Daniel Kivelson, Gilles Tarjus, Xiaolin Zhao, and Steven A Kivelson. Fitting of viscosity: Distinguishing the temperature dependences predicted by various models of supercooled liquids. *Physical Review E*, 53(1):751, 1996.

[41] Jeppe C. Dyre, Niels Boye Olsen, and Tage Christensen. Local elastic expansion model for viscous-flow activation energies of glass-forming molecular liquids. *Physical Review B*, 53(5):2171–2174, February 1996. doi: 10.1103/physrevb.53.2171.

[42] Jeppe C. Dyre and Niels Boye Olsen. Landscape equivalent of the shoving model. *Physical Review E*, 69(4), April 2004. doi: 10.1103/physreve.69.042501.

[43] Jeppe C. Dyre. Source of non-arrhenius average relaxation time in glass-forming liquids. *Journal of Non-Crystalline Solids*, 235-237:142–149, August 1998. doi: 10.1016/s0022-3093(98)00502-x.

[44] Nicoletta Gnan, Thomas B Schroder, Ulf R Pedersen, Nicholas P Bailey, and Jeppe C Dyre. Pressure-energy correlations in liquids. iv.isomorphs in liquid phase diagrams. *The Journal of chemical physics*, 131(23):234504, 2009.

[45] Thomas B. Schrøder and Jeppe C. Dyre. Simplicity of condensed matter at its core: Generic definition of a roskilde-simple system. *The*

Journal of Chemical Physics, 141(20):204502, November 2014. doi: 10.1063/1.4901215.

[46] Jeppe C. Dyre. Isomorph theory of physical aging. *The Journal of Chemical Physics*, 148(15):154502, April 2018. doi: 10.1063/1.5022999.

[47] Jeppe C. Dyre. Isomorph theory beyond thermal equilibrium. *The Journal of Chemical Physics*, 153(13):134502, October 2020. doi: 10.1063/5.0024212.

[48] Trond S Ingebrigtsen, Thomas B Schrøder, and Jeppe C Dyre. Isomorphs in model molecular liquids. *The Journal of Physical Chemistry B*, 116(3):1018–1034, 2012.

[49] Nicholas P Bailey, Ulf R Pedersen, Nicoletta Gnan, Thomas B Schrøder, and Jeppe C Dyre. Pressure-energy correlations in liquids. i. results from computer simulations. *The Journal of chemical physics*, 129(18):184507, 2008.

[50] K. L. Ngai, R. Casalini, S. Capaccioli, M. Paluch, and C. M. Roland. Do theories of the glass transition, in which the structural relaxation time does not define the dispersion of the structural relaxation, need revision? *The Journal of Physical Chemistry B*, 109(37):17356–17360, September 2005. doi: 10.1021/jp053439s.

[51] KL Ngai. *Relaxation and diffusion in complex systems*. Springer Science & Business Media, 2011.

[52] K. Adrjanowicz, J. Pionteck, and M. Paluch. Isochronal superposition and density scaling of the intermolecular dynamics in glass-forming liquids with varying hydrogen bonding propensity. *RSC Advances*, 6 (55):49370–49375, 2016. doi: 10.1039/c6ra08406k.

[53] CM Roland, S Hensel-Bielowka, M Paluch, and R Casalini. Supercooled dynamics of glass-forming liquids and polymers under hydrostatic pressure. *Reports on Progress in Physics*, 68(6):1405, 2005.

[54] CM Roland, R Casalini, Rikard Bergman, and Johan Mattsson. Role of hydrogen bonds in the supercooled dynamics of glass-forming liquids at high pressures. *Physical Review B*, 77(1):012201, 2008.

[55] Henriette Wase Hansen, Bernhard Frick, Simone Capaccioli, Alejandro Sanz, and Kristine Niss. Isochronal superposition and density scaling of the α-relaxation from pico- to millisecond. *The Journal of Chemical Physics*, 149(21):214503, December 2018. doi: 10.1063/1.5055665.

[56] Joachim Wuttke. Laplacefourier transform of the stretched exponential function: Analytic error bounds, double exponential transform, and open-source implementation libkww. *Algorithms*, 5(4):604–628, 2012. doi: 10.3390/a5040604.

[57] Alejandro Sanz, Henriette Wase Hansen, Bo Jakobsen, Ib H. Pedersen, Simone Capaccioli, Karolina Adrjanowicz, Marian Paluch, Julien Gonthier, Bernhard Frick, Eddy Lelièvre-Berna, Judith Peters, and Kristine Niss. High-pressure cell for simultaneous dielectric and neutron spectroscopy. *Review of Scientific Instruments*, 89(2):023904, February 2018. doi: 10.1063/1.5007021.

[58] A. Gilchrist, J. E. Earley, and R. H. Cole. Effect of pressure on dielectric properties and volume of 1-propanol and glycerol. *The Journal of Chemical Physics*, 26(1):196–200, January 1957. doi: 10.1063/1.1743249.

[59] Osamu Yamamuro, Kouji Harabe, Takasuke Matsuo, Kiyoshi Takeda, Itaru Tsukushi, and Toshiji Kanaya. Boson peaks of glassy mono- and polyalcohols studied by inelastic neutron scattering. *Journal of Physics: Condensed Matter*, 12(24):5143–5154, May 2000. doi: 10.1088/0953-8984/12/24/306. propanol.

[60] Bo Jakobsen, Alejandro Sanz, Kristine Niss, Tina Hecksher, Ib H. Pedersen, Torben Rasmussen, Tage Christensen, Niels Boye Olsen, and Jeppe C. Dyre. Thermalization calorimetry: A simple method for investigating glass transition and crystallization of supercooled liquids. *AIP Advances*, 6(5):055019, May 2016. doi: 10.1063/1.4952404.

[61] M. Poeschl and H. G. Hertz. Intramolecular thermal motions in liquid n-propanol + glycerol), a proton magnetic relaxation study. 2. *The Journal of Physical Chemistry*, 98(33):8195–8208, August 1994. doi: 10.1021/j100084a043.

[62] N Menon, Kevin P O'Brien, Paul K Dixon, Lei Wu, Sidney R Nagel, Bruce D Williams, and John P Carini. Wide-frequency dielectric susceptibility measurements in glycerol. *Journal of non-crystalline solids*, 141:61–65, 1992.

[63] J. Wuttke, J. Hernandez, G. Li, G. Coddens, H. Z. Cummins, F. Fujara, W. Petry, and H. Sillescu. Neutron and light scattering study of supercooled glycerol. *Physical Review Letters*, 72(19):3052–3055, May 1994. doi: 10.1103/physrevlett.72.3052.

[64] Peter Lunkenheimer, Andrei Pimenov, Martin Dressel, Yu G Goncharov, R Böhmer, and Alois Loidl. Fast dynamics of glass-forming glycerol studied by dielectric spectroscopy. *Physical review letters*, 77 (2):318, 1996.

[65] Elena Cornicchi, Stefania Cinelli, Francesca Natali, Giuseppe Onori, and Alessandro Paciaroni. Elastic neutron scattering study of proton dynamics in glycerol. *Physica B: Condensed Matter*, 350(1-3):E951–E954, July 2004. doi: 10.1016/j.physb.2004.03.245.

[66] S. Gupta, E. Mamontov, N. Jalarvo, L. Stingaciu, and M. Ohl. Characteristic length scales of the secondary relaxations in glass-forming glycerol. *The European Physical Journal E*, 39(3), March 2016. doi: 10.1140/epje/i2016-16040-7.

[67] Salman Seyedi, Daniel R. Martin, and Dmitry V. Matyushov. Dynamical and orientational structural crossovers in low-temperature glycerol. *Physical Review E*, 94(1), July 2016. doi: 10.1103/physreve.94.012616.

[68] J. Bartoš and H. Švajdlenková. On the mutual relationships between spin probe mobility, free volume and relaxation dynamics in organic glass-formers: Glycerol. *Chemical Physics Letters*, 670:58–63, February 2017. doi: 10.1016/j.cplett.2016.12.064.

[69] Alejandro Sanz and Kristine Niss. Liquid dynamics in partially crystalline glycerol. *The Journal of Chemical Physics*, 146(4):044502, January 2017. doi: 10.1063/1.4974831.

[70] Lisa Anita Roed, Tina Hecksher, Jeppe C. Dyre, and Kristine Niss. Generalized single-parameter aging tests and their application to

glycerol. *The Journal of Chemical Physics*, 150(4):044501, January 2019. doi: 10.1063/1.5066387.

[71] Jan Philipp Gabriel, Parvaneh Zourchang, Florian Pabst, Andreas Helbling, Peter Weigl, Till Böhmer, and Thomas Blochowicz. Intermolecular cross-correlations in the dielectric response of glycerol. *Physical Chemistry Chemical Physics*, 22(20):11644–11651, 2020. doi: 10.1039/c9cp06344g.

[72] Charles F. Forney and David G. Brandl. Control of humidity in small controlled-environment chambers using glycerol-water solutions. *HortTechnology*, 2(1):52–54, January 1992. doi: 10.21273/horttech.2.1.52.

[73] J. B. Segur and Helen E. Oberstar. Viscosity of glycerol and its aqueous solutions. *Industrial & Engineering Chemistry*, 43(9):2117–2120, September 1951. doi: 10.1021/ie50501a040.

[74] G. E. McDuffie, R. G. Quinn, and T. A. Litovitz. Dielectric properties of glycerol—water mixtures. *The Journal of Chemical Physics*, 37(2):239–242, July 1962. doi: 10.1063/1.1701311.

[75] G. P. Johari and E. Whalley. Dielectric properties of glycerol in the range 0.1–105hz, 218–357 k, 0–53 kb. *Faraday Symp. Chem. Soc.*, 6(0):23–41, 1972. doi: 10.1039/fs9720600023.

[76] Hans Forsman, Per Andersson, and Gunnar Bäckström. Dielectric relaxation of glycerol and n-propyl alcohol at high pressure. *Journal of the Chemical Society, Faraday Transactions 2: Molecular and Chemical Physics*, 82(5):857–868, 1986.

[77] JR Huck, GA Noyel, and LJ Jorat. Dielectric properties of supercooled glycerol-water solutions. *IEEE Transactions on Electrical Insulation*, 23(4):627–638, 1988.

[78] Murthy. Experimental study of the dynamics of water and the phase behavior of the supercooled aqueous solutions of propylene glycol, glycerol, poly(ethylene glycol)s, and poly(vinylpyrrolidone). *The Journal of Physical Chemistry B*, 104(29):69556962, Jul 2000. doi: 10.1021/jp9931915.

[79] Seiichi Sudo, Mayumi Shimomura, Naoki Shinyashiki, and Shin Yagihara. Broadband dielectric study of a-b separation for supercooled glycerol-water mixtures. *Journal of Non-Crystalline Solids*, 307-310: 356–363, September 2002. doi: 10.1016/s0022-3093(02)01496-5.

[80] Yoshihito Hayashi, Alexander Puzenko, Igal Balin, Yaroslav E. Ryabov, and Yuri Feldman. Relaxation dynamics in glycerol-water mixtures. 2. mesoscopic feature in water rich mixtures. *The Journal of Physical Chemistry B*, 109(18):9174–9177, May 2005. doi: 10.1021/jp050425d.

[81] Yoshihito Hayashi, Alexander Puzenko, and Yuri Feldman. Ice nanocrystals in glycerol-water mixtures. *The Journal of Physical Chemistry B*, 109(35):16979–16981, September 2005. doi: 10.1021/jp052512b.

[82] Alexander Puzenko, Yoshihito Hayashi, and Yuri Feldman. Space and time scaling in glycerol–water mixtures. *Journal of Non-Crystalline Solids*, 353(47-51):4518–4522, 2007.

[83] Debamalya Banerjee and S.V. Bhat. Vitrification, relaxation and free volume in glycerolwater binary liquid mixture: Spin probe esr studies. *Journal of Non-Crystalline Solids*, 355(5051):24332438, Dec 2009. doi: 10.1016/j.jnoncrysol.2009.08.045.

[84] Jennifer L. Dashnau, Nathaniel V. Nucci, Kim A. Sharp, and Jane M. Vanderkooi. Hydrogen bonding and the cryoprotective properties of glycerol/water mixtures. *The Journal of Physical Chemistry B*, 110 (27):13670–13677, July 2006. doi: 10.1021/jp0618680.

[85] Dai-Xi Li, Bao-Lin Liu, Yi shu Liu, and Cheng lung Chen. Predict the glass transition temperature of glycerol–water binary cryoprotectant by molecular dynamic simulation. *Cryobiology*, 56(2):114–119, April 2008. doi: 10.1016/j.cryobiol.2007.11.003.

[86] Cong Chen, Wei Zhong Li, Yong Chen Song, and Jian Yang. Hydrogen bonding analysis of glycerol aqueous solutions: A molecular dynamics simulation study. *Journal of Molecular Liquids*, 146(12):2328, May 2009. doi: 10.1016/j.molliq.2009.01.009.

[87] Cong Chen, Wei Zhong Li, Yong Chen Song, Lin Dong Weng, and Ning Zhang. The effect of geometrical criteria on hydrogen bonds anal-

ysis in aqueous glycerol solutions. *Journal of Molecular Imaging & Dynamics*, 1(1), 2011. doi: 10.4172/2155-9937.1000101.

[88] Andrei V. Egorov, Alexander P. Lyubartsev, and Aatto Laaksonen. Molecular dynamics simulation study of glycerolwater liquid mixtures. *The Journal of Physical Chemistry B*, 115(49):1457214581, Dec 2011. doi: 10.1021/jp208758r.

[89] Pavan K GhattyVenkataKrishna and Edward C Uberbacher. Effect of temperature and glycerol on the hydrogen-bond dynamics of water. *CryoLetters*, 34(2):166–173, 2013.

[90] Henriette W. Hansen, Bernhard Frick, Tina Hecksher, Jeppe C. Dyre, and Kristine Niss. Connection between fragility, mean-squared displacement, and shear modulus in two van der waals bonded glass-forming liquids. *Physical Review B*, 95(10), March 2017. doi: 10.1103/physrevb.95.104202.

[91] Wence Xiao, Jon Tofteskov, Troels V. Christensen, Jeppe C. Dyre, and Kristine Niss. Isomorph theory prediction for the dielectric loss variation along an isochrone. *Journal of Non-Crystalline Solids*, 407:190–195, January 2015. doi: 10.1016/j.jnoncrysol.2014.08.041.

[92] Peter A. Knudsen, Kristine Niss, and Nicholas P. Bailey. Quantifying dynamical and structural invariance in a simple molten salt model. *The Journal of Chemical Physics*, 155(5):054506, August 2021. doi: 10.1063/5.0055794.

[93] Richard L. Cook, H. E. King, Chris A. Herbst, and Dudley R. Herschbach. Pressure and temperature dependent viscosity of two glass forming liquids: Glycerol and dibutyl phthalate. *The Journal of Chemical Physics*, 100(7):5178–5189, April 1994. doi: 10.1063/1.467276.

[94] M Paluch, SJ Rzoska, P Habdas, and J Ziolo. Isothermal and high-pressure studies of dielectric relaxation in supercooled glycerol. *Journal of physics: Condensed matter*, 8(50):10885, 1996.

[95] M Paluch, SJ Rzoska, P Habdas, and J Ziolo. On the isothermal pressure behaviour of the relaxation times for supercooled glass-forming liquids. *Journal of Physics: Condensed Matter*, 10(19):4131, 1998.

[96] A. Tölle, H. Schober, J. Wuttke, O. G. Randl, and F. Fujara. Fast relaxation in a fragile liquid under pressure. *Physical Review Letters*, 80 (11):2374–2377, March 1998. doi: 10.1103/physrevlett.80.2374.

[97] M. Paluch, R. Casalini, S. Hensel-Bielowka, and C. M. Roland. Effect of pressure on the α relaxation in glycerol and xylitol. *The Journal of Chemical Physics*, 116(22):9839–9844, June 2002. doi: 10.1063/1.1473652.

[98] Christiane Alba-Simionesco, Daniel Kivelson, and Gilles Tarjus. Temperature, density, and pressure dependence of relaxation times in supercooled liquids. *The Journal of Chemical Physics*, 116(12):5033, 2002. doi: 10.1063/1.1452724.

[99] Andreas Reiser, Gernot Kasper, and Siegfried Hunklinger. Pressure-induced isothermal glass transition of small organic molecules. *Physical Review B*, 72(9), September 2005. doi: 10.1103/physrevb.72.094204.

[100] A. Drozd-Rzoska, S. J. Rzoska, M. Paluch, A. R. Imre, and C. M. Roland. On the glass temperature under extreme pressures. *The Journal of Chemical Physics*, 126(16):164504, April 2007. doi: 10.1063/1.2721044.

[101] S Pawlus, M Paluch, J Ziolo, and C M Roland. On the pressure dependence of the fragility of glycerol. *Journal of Physics: Condensed Matter*, 21(33):332101, July 2009. doi: 10.1088/0953-8984/21/33/332101.

[102] A. A. Pronin, M. V. Kondrin, A. G. Lyapin, V. V. Brazhkin, A. A. Volkov, P. Lunkenheimer, and A. Loidl. Pressure-induced change in the relaxation dynamics of glycerol. *JETP Letters*, 92(7):479–483, October 2010. doi: 10.1134/s0021364010190100.

[103] A. G. Lyapin, E. L. Gromnitskaya, I. V. Danilov, and V. V. Brazhkin. Elastic properties of the hydrogen-bonded liquid and glassy glycerol under high pressure - comparison with propylene carbonate. *RSC Advances*, 7(53):33278–33284, 2017. doi: 10.1039/c7ra06165j.

[104] Sylwester J. Rzoska. New challenges for the pressure evolution of the glass temperature. *Frontiers in Materials*, 4, November 2017. doi: 10.3389/fmats.2017.00033.

[105] Abel G.M. Ferreira, Ana P.V. Egas, Isabel M.A. Fonseca, Ana C. Costa, Danielly C. Abreu, and Lélio Q. Lobo. The viscosity of glycerol. *The Journal of Chemical Thermodynamics*, 113:162–182, October 2017. doi: 10.1016/j.jct.2017.05.042.

[106] Lisa Anita Roed, Ditte Gundermann, Jeppe C. Dyre, and Kristine Niss. Communication: Two measures of isochronal superposition. *The Journal of Chemical Physics*, 139(10):101101, 2013. doi: 10.1063/1.4821163.

Appendix A

Publication

A sample holder for simultaneous neutron and dielectric spectroscopy -

dielectric tests with glycerol, glycerol-water, water and phosphoric acid

Bernhard Frick[1,*], *Margarita* Fomina[1,2,], *David* Noirat[1,3,], *Henriette W* Hansen[3,], *Markus* Appel[1,**], and *Kristine* Niss[3,***]

[1]Institut Laue-Langevin (ILL), CS 20156, F - 38042 Grenoble Cedex 9, France
[2]Jülich Centre for Neutron Science (JCNS) at Heinz Maier-Leibnitz Zentrum (MLZ), Forschungszentrum Jülich GmbH, Garching, Germany
[3]Glass and Time, IMFUFA, Department of Science and Environment, Roskilde University, Postbox 260, DK-4000 Roskilde, Denmark

Abstract. We report on dielectric test measurements of a rectangular flat sample holder which serves as capacitor and which is aimed for simultaneous neutron and dielectric (n-DE) spectroscopy of acidic liquid samples. We describe technical details of the sample holder assembly and the dielectric and neutron equipment as well as the sample preparation procedure of the air sensitive acidic samples. The sample holder was characterised off-line from the neutron spectrometer by dielectric spectroscopy, but using the standard IN16B cryofurnace with a dielectric sample stick with 4-wire connection and a Novocontrol - equipment, previously setup by a collaborative effort between ILL and Roskilde University. Temperature-dependent dielectric scans on standard samples (glycerol, glycerol-water, and Milli-Q water) were measured in the frequency range between 0.27 Hz and 1 MHz. Step-like temperature changes allowed to probe the temperature equilibrium conditions and continuous temperature changes were made to mimic typical IN16B backscattering neutron fixed window scans. Both type of scans were carried out in cooling and in heating. The standard samples show that our dielectric setup with flat sample holder is well suited for simultaneous n-DE-experiments. On the other hand, the dielectric scan on phosphoric acid reveals the limitations of our setup in case of high sample conductivities, but also shows that the DC-conductivity can still be accessed in a sufficiently wide low temperature range where the onset of conductivity can be simultaneously probed with the change in proton dynamics as seen by neutron spectroscopy.

1 Introduction

Quasielastic neutron scattering (QENS) [1] and dielectric spectroscopy (DES) [2] are complementary techniques and the application of both is of interest for many areas of science. QENS offers both time and space resolution for characterising molecular motions, whereas DES probes the time- or frequency dependence of electrical dipoles. QENS thus has the potential to inform about the type and time scale of atomic or molecular motions, like e.g. on the diffusional behaviour of ionic or non-ionic species. Regarding the dynamics of ionic species it is known that the QENS signal is not always straightforward related to charge displacements. In contrast DES can probe at lower frequency the DC-conductivity and at higher frequency the transition to AC-conductivity arising from the motion of ionic species. Thus it is obvious that a combination of the two techniques does give deeper insight and this has been widely used by comparing results from dedicated experiments applying these complementary techniques.

Standard broad band DES covers an extremely wide frequency range of more than 9 orders of magnitude in a single experimental setup, like from the μHz to above-MHz region, whereas standard QENS offers typically only 2-3 decades between energy resolution and maximum energy transfer, thus requiring often a combination of different instruments or experimental setups. Even though these methods are probing different time scales, i.e. hundreds of seconds to 10^{-7}s for standard DES and 10^{-7}s to sub-picoseconds for QENS, it is in some cases of interest to carry out experiments simultaneously, in spite of evidence that dedicated individual experiments may deliver superior data quality. Scientific cases where simultaneous neutron and dielectric (n-DE) measurements are expected to give more information include i) non-equilibrium systems in general, ii) systems where a connection between low frequency dipole dynamics, probed by DES, and high frequency atomic motion, probed by QENS, is suspected, such as the hypothesis about a general connection between fast and slow dynamics [3], or more specific, iii) samples with crystallisation tendency or in metastable states which depend on the sample history, where it would be difficult to prepare the samples under exactly the same conditions in two separate experiments. Other more practical reasons could be parameter scans, like temperature or pressure scans, where kinetic delays between the measured

*e-mail: frick@ill.eu
**e-mail: appel@ill.eu
***e-mail: kniss@ruk.dk

parameter value and the actual intrinsic sample parameter value may differ and cause a non-equilibrium situation or samples with crystallisation tendency for which the interest is to measure with both methods exactly under the same conditions.

Simultaneous QENS and DES (called hereafter 'n-DE') experiments were started at the Institut Laue-Langevin some years ago by the group of K. Niss [4], mainly for n-DE experiments under pressure with a n-DE pressure cell allowing to access P=400MPa in a broad temperature range [5] and with Roskilde-owned DE-equipment (standard LCR meter 4284A from Agilent) from which emerged several publications (e.g. [6],[3],[7]). Recently, in continuation of this Roskilde-ILL collaboration, ILL has acquired a Novocontrol Alpha Analyser [8] which is now integrated into ILL's NOMAD data acquisition chain [9] and has built a sample stick with connectors for four-wire DES measurements fitting into the standard 50 mm diameter cryofurnaces and cryostats. Here we are reporting on tests of a flat sample holder, usable for ambient pressure experiments on acidic samples in a wide temperature range between T = 2 K and 340 K. We describe the sample holder assembly and off-line dielectric temperature scans, carried out under the same conditions and with the same equipment as found normally in fixed window scans [10] on IN16B [11]. As test samples we have chosen the well known (non-acidic) samples glycerol, glycerol-water and Milli-Q water, background reference samples as well as phosphoric acid water mixtures (PA-water) on which lies our main focus of future simultaneous n-DE experiments. We briefly describe the sample preparation procedure for the very air sensitive samples of PA and the practicality for user experiments. Dielectric scans were taken in a frequency range from 0.27 - 1 MHz and at temperatures between 2 and 340 K. Our tests show that our sample holder design is well suited for dielectric measurements at low temperatures as long as the sample conductivity and electrode polarisation is not too high. Both reduce the frequency and temperature range for measuring the conductivity with our dielectric setup. As our main interest of future work is to test at low temperatures for phosphoric acid - water mixtures a possible connection between the onset of conductivity (from the DC conductivity of DE spectra) and high frequency dynamics of proton displacement (from neutron fixed window scans, e.g. on IN16B or IN13), this restriction is acceptable.

2 Methods

2.1 Dielectric equipment and measured quantities

The dielectric equipment, which is available at ILL for simultaneous n-DE experiments [12], is based on a Novocontrol Alpha-AT Analyser, controlled by a PC running WINDETA software [8] and which can be triggered by the ILL instrument software NOMAD [9] to run simultaneous with the instrument data acquisition. With dedicated dielectric equipment the Novocontrol analyser covers a wide frequency range in the μHz- to above-MHz region. Our test measurements were carried out in a restricted frequency range from 0.27 Hz to 1 MHz. The DE-analyser is connected via a dispatch box to an ILL built sample stick, which is more than 1 m high and is usable with standard ILL top loading 'Orange cryostats' having a 50 mm diameter bore. For our tests we have used the standard IN16B cryofurnace. The length of the sample stick and the sample orientation is adjustable and serves for placing the sample in the centre of the neutron beam. The cables for 4-wire measurements are fed through the central tube of the sample stick and are at their end welded in pairs to two pin connectors. These can then be plugged onto the pins fixed on the electrodes of any type of sample holder. The sample holder is connected with an intermediate electrically insulating PEEK adapter via an M8 thread to the end of the sample stick and is thus located just below the place where the sample temperature is measured.

A detailed description of broad band dielectric spectroscopy can be found in the book by Kremer and Schönhals [2]. DES derives the electrical properties from a measurement of the complex impedance Z* of a sample placed between electrodes. From the measured impedance one can find the complex capacity C* which is related to the geometry of the sample cell by $C \propto \frac{A}{d}$, with A being the sample area and d the sample thickness. Thus for DES a large sample area A and a small sample thickness d result in a large measurable signal. From the complex capacity C* of the sample cell one can derive the sample permittivity $\epsilon^* = \frac{C^*}{C_0}$, where C_0 refers to the empty sample cell capacity, and the complex dielectric permittivity is given by $\epsilon^* = \epsilon' - i\epsilon''$. From the complex permittivity one can then calculate the complex conductivity $\sigma^* = \sigma' + i\sigma''$, which is related to the complex permittivity by $\sigma^* = i\omega\epsilon_0\epsilon^*$ (ϵ_0 is the dielectric permittivity of vacuum).

2.2 Sample holder and requirements for simultaneous n-DE experiments

For neutron scattering basics we refer to standard books, e.g. [13], [14] or [1] and discuss only the requirements for a neutron sample holder. For maximum intensity the projection of the sample holder area A should cover the incoming neutron beam area, which on the instruments used is typically about 10 -30 mm wide and 20 - 50 mm high. The sample thickness should be chosen thin enough to favour single over multiple scattering processes. For that reason a rule of thumb is to aim for a scattering probability of less than 10% , equal to a transmission larger than 90% if absorption is neglected. For protonated materials, due to the high incoherent cross section from Hydrogen, a sample thickness d for straight neutron transmission should therefore be in the order of 150 μm and can be thicker for other samples. Both, A and d required for n-scattering, are thus compatible with the requirements for DES described above.

Two major sample geometries are used for QENS, a flat sample holder which can be oriented with respect to the incident and scattered neutron beam and thus with respect to the scattering vector **Q** and a hollow cylinder geometry for which the neutrons pass twice through the an-

nular sample thickness. There are standard designs for both types at ILL (and similar design elsewhere), which allow to adapt easily to different sample thickness.

We limit ourselves to the flat sample holder design which we have modified to suit simultaneous n-DE-spectroscopy. A cylindrical sample holder for n-DE spectroscopy will be described elsewhere [15]. For completeness we should mention an earlier sample cell development which was aimed for simultaneous neutron diffraction (different requirements than for QENS) and dielectric spectroscopy [16].

For adjusting to different sample thickness, one part of the sample holder remains usually unchanged and the counter part is slightly changing its dimensions: for flat sample holders it is the base of the holder which remains unchanged and top cover plates of different depth are used which dive into the base plate sample holder (see Fig.1) and leave a gap defining the desired sample thickness between 0 - 3 mm. The standard flat sample holders are made from Aluminium (small scattering cross section for wavelength below the Bragg cut-off) and can be sealed with Indium wire, squeezed in between the outer more massive frames which are held together by Aluminium screws. For dielectric spectroscopy these two parts of the sample holder (base and top) serve as electrodes.

Modifications which were made to this type of flat sample holder are the following 1: i) We have added by cold fitting tiny electrical connector pins on the upper edge of the two sample holder pieces. After screwing the sample holder to the sample stick, these allow to connect the wires for the DE- measurement. ii) We isolate electrically the electrodes (top and base) from each other by thin Teflon sheets on which the central part is cut out in order to leave most of the neutron window free. When closing the sample holder, the top cover pulls the thin teflon foils into the base plate so that it is lining equally the side walls of the sample volume. We have used 2 or 3 such very thin window foils of only $10\mu m$ thickness. This minimises the risk of shearing off the teflon foil when closing the sample holder. It also minimises the neutron background arising from the coherent scattering (Bragg peaks) of Teflon (PTFE), which is important because minor parts of the foil near the border of the neutron window might still reach into the neutron beam. iii) For sealing liquid samples we squeeze an Indium wire, placed in between the foils around the sample volume. The PTFE foils also protect the Indium from contact with the sample as we aim for measuring acidic liquids. At first Aluminium screws are used for sealing the sample cell (squeezing the Indium wire), which after tight closing are then exchanged one by one by electrically insulating Nylon screws. iv) Our aim is to measure acidic samples which would corrode the Aluminium quite fast. Therefore the neutron windows with their side walls were coated on the inside of the sample holder with a very thin Au layer ($0.34\mu m$) in order to minimise neutron activation of the sample holder. v) As the major source for potential neutron background stems from the nylon screws (protonated carbon chain) we attach, for the neutron scattering experiments only, a Cadmium mask on top of the sample holder facing the neutron beam, taking care not to create electrical contact between the electrodes.

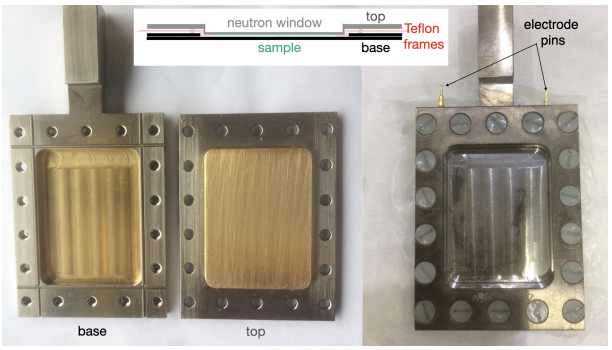

Figure 1. left photo: gold coated sample holder: bottom part (l.h.s.) and top cover (r.h.s.); right photo: filled sample holder with Nylon screws and electrode pins on top. Inset: schematic view how the sample is squeezed between base and top plate and how the 3 thin Teflon foils are placed.

2.3 Sample preparation

All air sensitive samples were handled within a glove bag under Argon flow, including in a few cases melting the crystalline samples on a heat plate, weighing the appropriate sample amount and pipetting it into the sample holder. Sample handling took place only after a low humidity level had been reached (typically 2.5% RH at about 20C). RH and temperature were registered continuously close to the sample with a Sensirion humidity sensor. The exposure time of the samples to the dry atmosphere was minimised to several ten seconds until the sample holder was closed and initially kept together with a special tool until it was definitively closed with screws outside of the Argon bag.

Critical and delicate phases are the preparation of the sample holder with the very thin Teflon foils and the Indium wires in between, the transfer of this assembly to the glove bag, and the closing of the sample holder within the bag, where the foils are hardly anymore visible. During closing the sample holder with screws, care had to be taken not to pull the Teflon foils with the screws into the threads which could rupture the foils and create electrical contact. Punching holes into the very thin foils before assembly seemed difficult, therefore we have perforated the foils with a needle in the center of each screw hole after assembly and then placed the Aluminium screws. In some cases a short circuit was detected after the sample assembly and then the described tedious procedure had to be repeated. In that respect there is room for improving the sample holder design and handling.

3 Dielectric tests on standard samples

In order to test our sample holder design we have carried out dielectric spectroscopy on well known samples and on empty sample holders in the IN16B standard cryofurnace and with the sample stick described above. As test samples

we have used Milli-Q-water, glycerol and a glycerol-water mixture. Finally we report on a phosphorous acid - water mixture, belonging to the group of samples which meet closest our main objective, namely measuring the low temperature conductivity of PA-water systems simultaneously with neutron spectroscopy. Systematic measurements on this series will be reported elsewhere. Here we show that our experimental setup is well suited for dielectric measurements on standard samples. But we also point out the experimental limitations of our setup for samples with extremely high conductivity similar to that of PA.

3.1 Tests on glycerol

As an example for the DE-data quality achievable with our n-DE-setup we show in Fig.2 dielectric spectra measured in a frequency range from $2.710^{-1} - 10^6$ Hz on glycerol between 209 K and 240 K at temperatures similar to the ones reported in literature (e.g. [17]) which show the α-relaxation peak in the imaginary part of the dielectric permittivity ϵ''.

For two temperatures (T = 209 K and 219 K) we show in Fig.3 fits of the α-relaxation peak observed in the imaginary part of the dielectric permittivity ϵ'' of glycerol. We have fitted ϵ'' applying a single Havriliak-Negami (HN) model fit function with an additional conductivity term, resulting in HN shape parameters β = 0.97 and γ= 0.48. β is found to be very similar to the value given in Ref.[2] (β = 0.95), but the smaller γ found by us (γ= 0.6 in Ref.[2]) indicates a lower slope in the high frequency wing. We attribute this to the fact that we have not fitted an additional HN-function to the high frequency wing as it was done in Ref.[2].

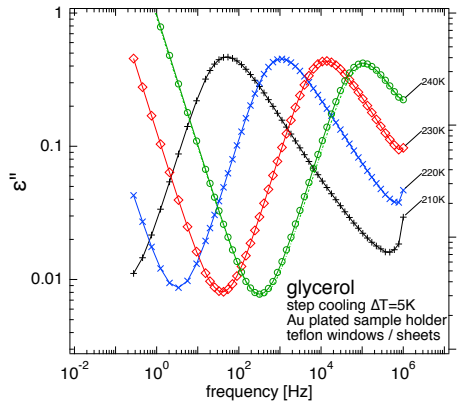

Figure 2. Frequency dependence of the imaginary permittivity of a glycerol sample, measured in a gold coated flat sample holder, placed in an IN16B cryofurnace, suited for simultaneous neutron scattering.

In neutron spectroscopy a powerful way to get an overview over the onset of different relaxation processes as a function of the sample temperature or pressure are so-called (elastic or inelastic) fixed window scans (EFWS, IFWS, FWS) [10]. Such FWS are most efficiently carried out on reactor backscattering spectrometers using a linear-motor Doppler drive, where the incident neutron

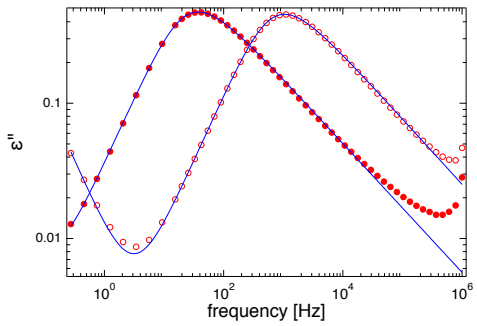

Figure 3. Test fits with a HN-function including conductivity of the α-relaxation peak of glycerol at T = 209 K and T = 219 K.

wavelength $\lambda_{inc}(t) = \lambda_M \pm \Delta\lambda_D = \lambda_M \mp \frac{h}{m_n}\frac{1}{v_D(t)}$ can be flexibly set offset with respect to the fixed wavelength $\lambda_M = \lambda_A$ of the static monochromator and the analysers by choosing an appropriate periodic Doppler velocity profile $v_D(t) \approx \pm const.$ for the backscattering monochromator which, when discarding the regions near the reversal points, is constant [10].

This way most of the neutron detection time is spent in the corresponding energy transfer channel $E = \frac{\hbar^2}{2m_n}((1/\lambda_A)^2 - (1/\lambda_{inc})^2)$ which is probed with sub-μeV energy resolution and thus with the longest relaxation times currently available on neutron spectrometers operating in frequency space. In view of the short neutron measuring times and the superior statistics of FWS compared to QENS, carrying out the fast DE-spectroscopy simultaneously with FWS might be of highest interest (e.g.[18]).

In order to prepare for such n-DE-experiments we have carried out off-line temperature scans on glycerol in cooling from 330 K to 15 K with a continuous cooling ramp of -0.5 K/min (see Fig.4a), followed by continuous heating (Fig.4b) with the same ramp speed of 0.5 K/min using a gold plated flat sample holder and the IN16B standard cryofurnace. In a ramp the sample temperature set point was adapted continuously every 6 seconds. A frequency sweep for the dielectric spectra was chosen to last about 2 min in the range 0.2 to 1 MHz, followed by a waiting time of 1 min, which should be compared with neutron measuring times (not reported here) of about 30 s for an EFWS and 60-180 s for an IFWS step. The time for a DE frequency sweep would become much longer and would no longer match a temperature step of the FWS if lower frequencies were chosen (e.g. one period at 1 μHz equals 1000 s).

For both sets of scans it can be seen in Fig.4 how the -relaxation peak moves in the intermediate T-range through the dielectric frequency window. With increasing temperature the spectra are dominated towards lower frequency by strong DC conductivity leading to $\epsilon'' \propto 1/\omega$. The spectra in Fig.4 show also the limitations of our experimental setup at low temperatures and at frequencies above 10^5 Hz where the systematic errors increase (see also empty can measurements). Some temperatures are highlighted by colours to show their different behaviour.

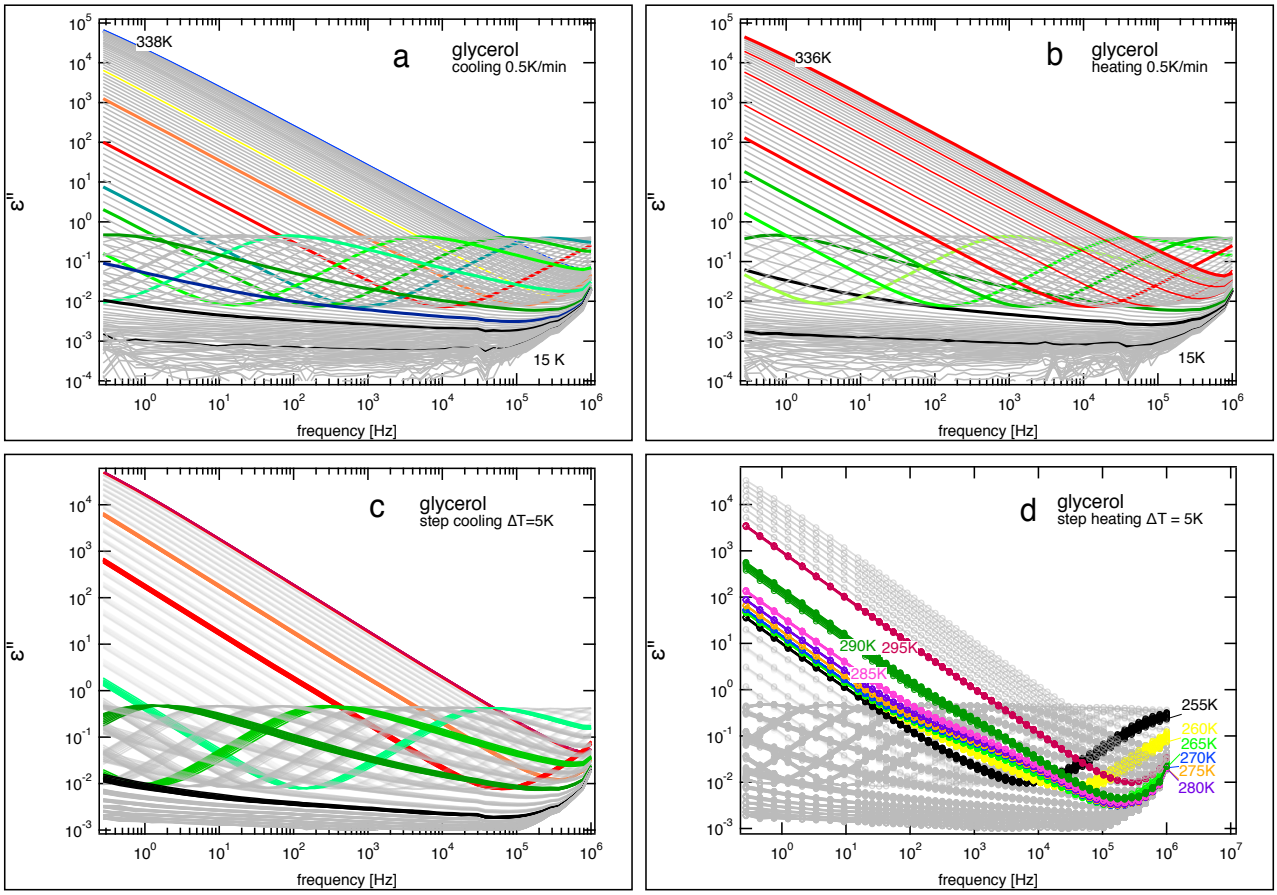

Figure 4. Frequency dependent dielectric permittivity at temperatures measured in: (a) continuous cooling scan with a ramp of 0.5 K/min, (b) continuous heating with the same rate, (c) in step cooling with ΔT=5K, followed by scans during temperature equilibration and (d) in step heating, followed by scans during temperature equilibration. With the slower rate in step heating crystallisation of glycerol is observed.

Depending on the heating or cooling rate a temperature equilibrium at the sample may not always be guaranteed. This depends on the details of the experimental setup and in our case the thermal equilibration is prolongated with respect to normal FWS conditions on IN16B because an electrically and thermally insulating PEEK adapter is placed between the sample and the sample stick (see experimental details). In order to get information on temperature equilibration we have also carried out measurements in step cooling and heating with much longer temperature equilibration times. We judge the equilibration time from the dielectric sample response which is recorded for a nominally identical sample temperature. Such step scans, which followed without sample change the continuous temperature scans (Fig.4a,b), are shown in Fig.4c and Fig.4d. Here the temperature set point was lowered or increased in steps of ±5 K. After a waiting time of 10 min a frequency sweep of the dielectric signal was recorded which took about 2 min and was repeated ten times before changing to the next sample set point temperature.

From Fig.4c) it seems that the sample reaches thermal equilibrium faster at higher temperatures than at low temperatures near the glass transition of glycerol ($T_g \approx 185K$), which could be a kind of aging effect. It might, however, as well reflect that at low temperatures, when approaching the glass transition, an equivalent sample temperature change causes a larger frequency shift of the ϵ'' signal than at higher temperature. In fact the data points in the temperature plot of Fig. 5 below are more spread in the α-peak region where the most pronounced temperature shift is expected on ϵ''.

During the step heating scans of glycerol (Fig.4d) a somewhat different behaviour was found, which is highlighted by the coloured curves. A nearly temperature independent shoulder developed near 260 K in the frequency range $10^2 - 10^5$ Hz, followed by a major rapid increase of ϵ'' in the whole frequency range near 290 K. We ascribe these features to (partial) crystallisation phenomena, followed by melting at higher temperatures in heating. The equilibrium melting temperature for glycerol from literature is about $T_m = 291K$. In cooling or in the faster continuous heating glycerol doesn't show any sign of crystallisation in our measurements.

A detailed analysis of the crystallisation kinetics of glycerol by DE-spectroscopy with dedicated equipment can be found elsewhere (see e.g. Ref.[19],[20] and references therein) and is not the purpose of the present paper. We don't offer a quantitative analysis of the glyc-

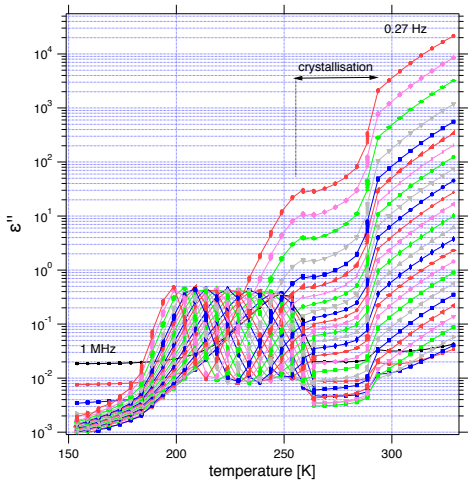

Figure 5. Temperature dependence of the dielectric permittivity of glycerol at selected frequencies measured in step heating.

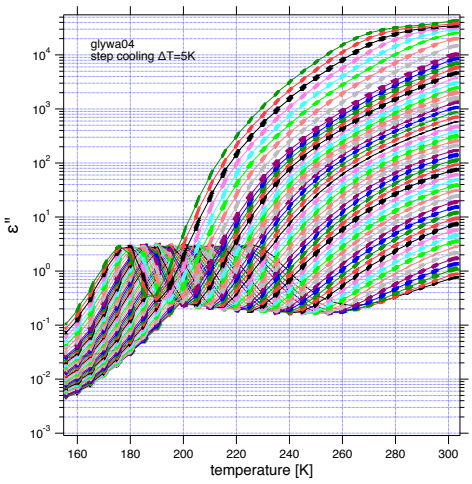

Figure 6. Temperature dependence of the dielectric permittivity of a glycerol-water mixture with a 0.4 molar fraction of glycerol as measured in step cooling.

erol signal but only strengthen our hypothesis that we observe (partial) crystallisation by plotting the temperature dependence at different constant frequencies between 0.27 Hz and 1 MHz (Fig.5). The temperature at which the α-relaxation peak maximum is observed in heating is strongly frequency dependent as expected; it is located near 200K for 0.27 Hz and near 250 K for 1 MHz. With the thermal protocol applied in our study glycerol crystallises near 260 K indicated by a frequency independent feature in Fig.5, a temperature region in which ϵ'' increases only moderately compared to the temperature increase below 260 K. At the end of this crystallisation region, near the melting temperature T_m = 291 K, ϵ'' jumps back to a higher value which can be considered as the extrapolation of the ϵ'' values below the crystallisation region.

3.2 Tests on glycerol-water

A detailed study of the glycerol-water system by DE and neutron spectroscopy as a function of both temperature and pressure is part of a PhD thesis by D.N. [15]. For testing our setup we show here the measurement on a glycerol-water sample with 0.4 molar fraction of glycerol in our flat sample holder, following the same protocol as described for neat glycerol described above. No crystallisation was observed in any of the cooling or heating scans. Fig.6 shows the corresponding temperature dependence for all measured frequencies between 0.27 Hz and 1 MHz and for step cooling with ΔT = 5 K.

3.3 Influence of Teflon

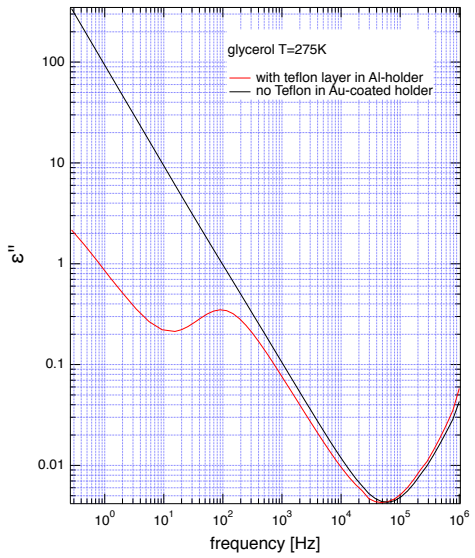

Figure 7. Imaginary part of the dielectric permittivity of glycerol with and without a Teflon covered electrode. A peak appears with Teflon coverage as discussed in the text. ϵ'' for glycerol with standard Teflon windows (black curve) is scaled down by 0.55 to match roughly the minimum seen near $5 \cdot 10^4$ Hz

There is some discussion in literature about the possibility to cover one electrode with a teflon layer for extracting a signal which might be hidden below a high DC-conductivity contribution ('blocking electrode') as published for glycerol by Bergman [17] and commented by Ref.[21] with reply by Ref.[22]. We are not aiming to contribute to this controversial discussion. But for our n-DE-sample holder we used Teflon foil frames for electrical insulation between the electrodes (2 or mostly 3 foils, thus 20 or 30 μm in total) with nominally no Teflon in the neutron window, but only sample (see inset in Fig.1). However, assuming that the 3 foils may not always be perfectly superposed, there could be a possibility that a little part near the edge of the neutron window (capacitor) of our sample holder might have a 10 μm teflon with some sample on one or both sides. Thus we have tested by purpose to increase the electrode coverage with teflon by decreasing drastically the window size which we cut into a single

10 μm thick teflon foil (in the order of 1 cm^2 window). We show in Fig.7 that in that case we detect a peak with the partially teflon covered electrode, which is absent if we use our standard Teflon frames with proper opening as described in ch.2.2. This check and the absence of such a peak is important for our data measured on PA-water, which we will discuss below.

3.4 Tests on Milli-Q water

As another characterisation of our nDS setup we have measured pure Millipore water (see Fig.8). The imaginary permittivity versus frequency, measured in continuous cooling with 0.5 K/min, changes abruptly from a smooth frequency dependence at temperatures above a registered sample temperature of 266.6 K to curves exhibiting at least one peak, which moves with further cooling to lower frequencies. We assign this observation to a freezing of the supercooled milliQ water in this type of cooling scan and at lower temperatures the observation of relaxation peak(s) in ice. In heating with 0.1K/min the melting is found near T = 273K as shown in Fig.8, r.h.s.

Similar to glycerol we have carried out in a limited temperature range on MilliQ-water DE-scans in step cooling (Fig.8c, bottom, l.h.s.) and also during much slower continuous heating with 0.1 K/min (Fig.8c, bottom, r.h.s.)), which confirm the presence of relaxation peaks in the crystal. As the empty sample holder does not show such peaks and as we didn't see relaxation peaks with teflon in the normal setup on glycerol, we can be fairly sure that the small peaks seen at low temperatures in the ϵ''-signal stems from ice water.

3.5 Comparison of the empty holder with glycerol

In order to get an indication of how much the empty sample holder may contribute to the measured ϵ''-signal we have measured an empty sample holder prepared in the same way as the filled samples, but on air. In these measurements the ϵ''-signal of the empty cell (lines in Fig.9) was smaller than 10^{-3} and thus significantly lower than the permittivity of glycerol (symbols in Fig.9) measured under similar conditions. The empty cell signal decreases with decreasing temperature. At high frequencies we see for all temperatures an increase of ϵ'' towards 1 MHz, the upper limit of the frequency range we decided to probe, ending in a similarly high ϵ'' value.

3.6 Tests on PA-water

All DE-measurements reported in the previous sections were carried out on standard samples and suggest that our sample holder design should be suited for simultaneous neutron and dielectric spectroscopy. As our project aim is to measure on phosphoric acid - water (PA-w) mixtures simultaneously conductivity spectra by DE-spectroscopy and proton dynamics by n-spectroscopy, we show here an example of the DE-scans taken on PA with our n-DE-setup. We refer the discussion concerning the physics of PA and PA-w-mixtures to a later publication and discuss

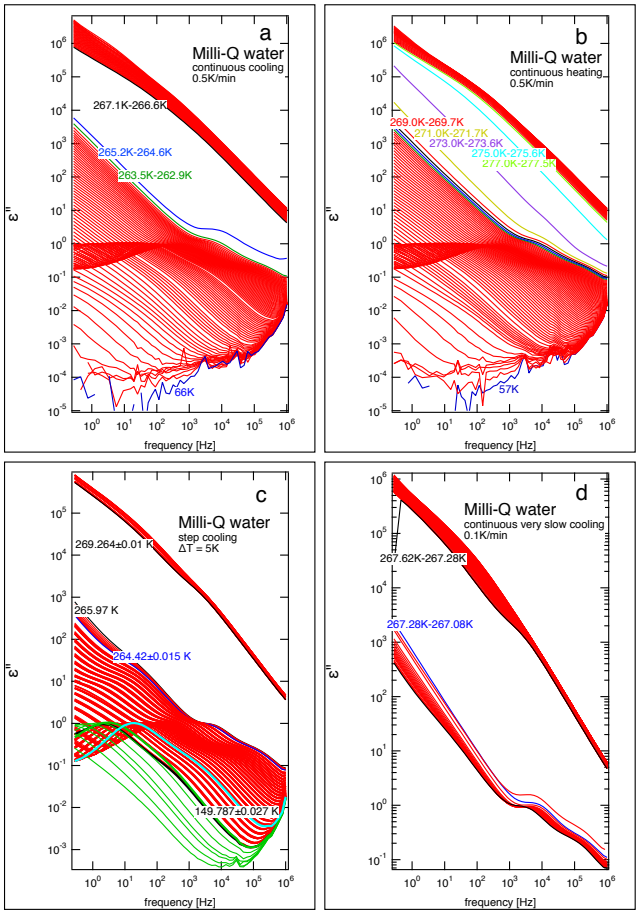

Figure 8. Imaginary part of the dielectric permittivity of Milli-Q water, measured during temperature scan in continuous cooling and heating with rates of ± 0.5 K/min (top), in cooling with steps of $\Delta T = 5K$ followed by equilibration (bottom, left) and around the melting / crystallisation with a slower cooling ramp of 0.1K/min (bottom/right).

here the limitations of our setup which we found on theses systems at high temperatures and high sample conductivity. As a note in passing we mention that phosphoric acid (PA) is known to exhibit an extremely high intrinsic proton conductivity, which can be further enhanced only by the addition of water (see e.g. [23], [24], [25]).

In Fig.10 we show dielectric spectra taken on dry PA. We observe for PA and PA-water mixtures (not shown here) at high temperatures a sharp decrease of the imaginary part of the permittivity ϵ'' in the high frequency range (highlighted within the dashed frame in Fig.10), which is not present at lower temperatures. In Fig.10 and the following we explain why the apparent peak formed is most probably an artefact. This is also suggested by the real part ϵ', which decreases sharply and which takes on negative values at high frequency and high temperatures (for frequencies above the vertical dashed line). This becomes more clear by plotting for 271 K additionally the modulus of ϵ', shown by the dots in the upper part of the figure.

To underline this we add a figure with the measured impedances Z, where Z'_s and Z''_s corresponds to the serial real and imaginary part of the impedance as it is output by

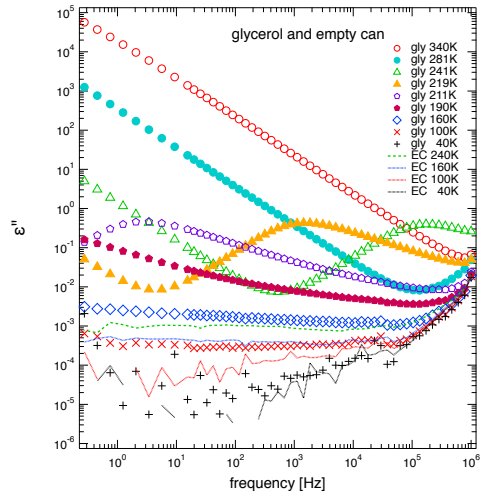

Figure 9. Dielectric scan on empty can (lines) and glycerol (symbols) for comparison are shown at several temperatures (see legend; same colour indicates same temperature).

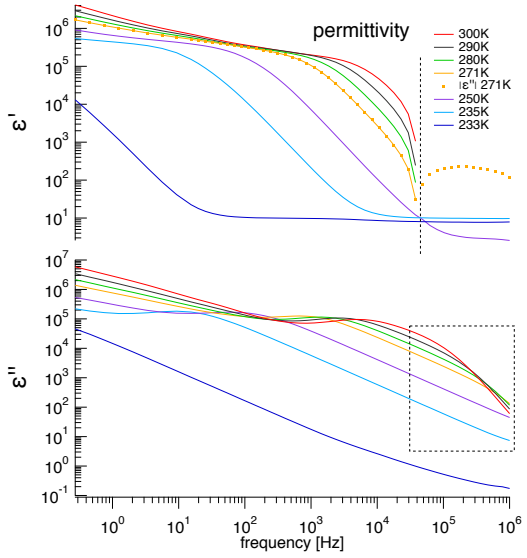

Figure 10. Real and imaginary part of the dielectric permittivity of phosphoric acid (PA), measured in cooling with the setup for simultaneous n-DE-spectroscopy and showing anomalies for high temperatures at high frequency. For ϵ'' we find at high frequency with increasing temperature an increasingly steeper decay (lower figure; dashed square region). In the same temperature-frequency region the real part of the permittivity ϵ' turns negative (upper part: r.h.s. of the dashed line). As the data are plotted on a log-log scale, we have highlighted this by adding for 271 K the absolute values of ϵ' (dots). Note also that crystallisation has appeared between T = 235 K and 233 K.

the Novocontrol WINDETA [8]. Z_s'' changes from negative to positive sign above this frequency as shown in the lower part of Fig.11.

As the onset of the ϵ''-decrease with frequency varies systematically with conductivity, i.e.with increasing temperature and with increasing water content, we suspect that due to the extremely high conductivity of PA-water induc-

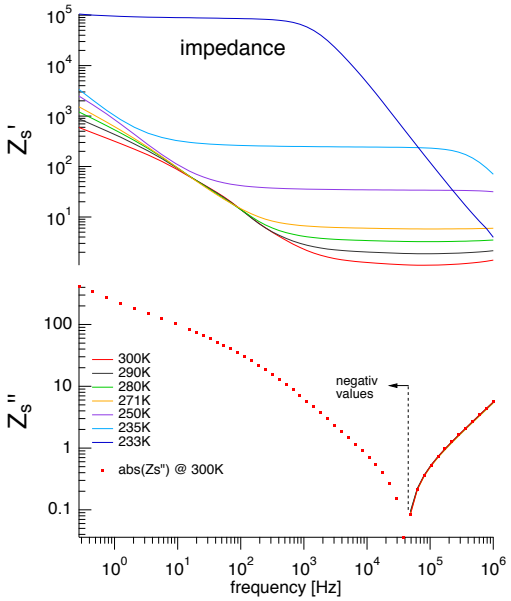

Figure 11. Impedances Z as measured on phosphoric acid (PA) with the setup for simultaneous n-DE-spectroscopy. Upper figure: real part of the serial impedance Z_s'. Lower part of the figure: imaginary counterpart Z_s'' which changes sign at the frequency indicated by a dashed vertical line (positive at high and negative at low frequencies). Dots in the lower figure correspond to the absolute value of Z_s'' shown for T = 300 K only.

tion contributions from the cables might become important, in spite of the 4-wire connection. It is known that it may be difficult to measure highly conducting liquids by dielectric spectroscopy, especially at higher frequency, if the measuring cell is not suited [8]. For DE-spectroscopy a much larger spacing between the electrodes can then be chosen, which however would conflict, at least for protonated samples, with the requirement of simultaneous neutron spectroscopy for which the thickness should be chosen to minimise multiple scattering.

Another possibility which we can't exclude completely as explanation of this artefact could be that our Teflon frames could produce a peak in ϵ' as discussed above in section 3.3 and in Ref.[21]. However, as the temperature scans were measured in cooling, we can expect that the sample geometry (rearrangement of electrodes/Teflon/sample which might depend on viscosity) does not change when cooling to lower temperature and therefore the same feature would be visible as well at lower temperature. These described artefacts unfortunately limit the useful frequency range at high temperatures and for high conductivies for our planned PA-water measurements.

Nevertheless, as can be seen by calculating the conductivity σ' in Fig.12, we are able to determine well the DC-conductivity plateau level with our simultaneous n-DE-setup. Thus we will be able to deduce valuable information by comparing the temperature and water concentration dependence of the DC-conductivity plateau with the neutron scan data, even though it would have been better to see the transition from DC- to AC- conductivity in

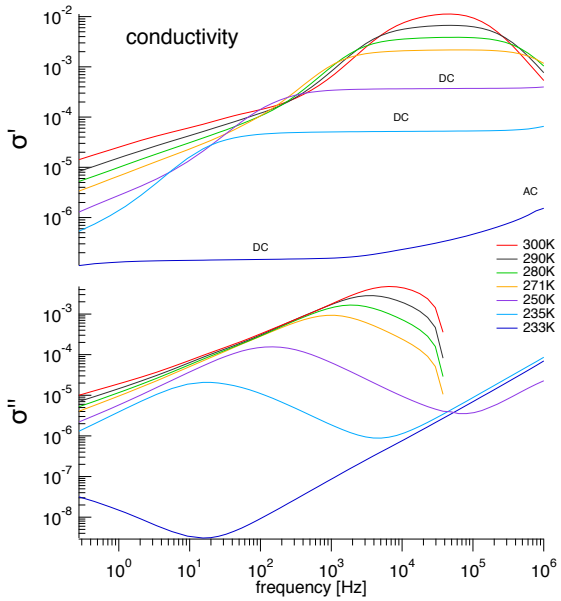

Figure 12. Conductivities as measured on phosphoric acid (PA) with the setup for simultaneous n-DE-spectroscopy. Upper figure: real part of the conductivity σ' and lower part of the figure the imaginary part σ''

a wide frequency range. Such simultaneous comparison is important as we have shown above by step cooling that temperature equilibration can be long and that temperatures recorded in the continuous cooling or heating FWS scans are no equilibrium sample temperatures.

4 Conclusion

We have presented a design for a flat sample holder which can serve as a sample cell (capacitor) for dielectric spectroscopy and in which the same sample volume permits scattering neutrons, thus allowing for simultaneous neutron spectroscopy. The presented type of sample holder allows for measuring normal, air sensitive and acidic liquids, i.e. it is a sealed sample cell which we assembled for some samples in a dry Argon atmosphere - noting that this operation is delicate. The upper temperature range is limited by the Indium seal to about 340K. Dielectric test scans in a wide frequency (0.27 Hz - 1 MHz) and temperature range (2 K - 340 K) on several standard samples (glycerol, water, glycerol-water) and under conditions similar to neutron fixed window scans (FWS) show that our flat cell design, in connection with ILL's DE-equipment, is working well, albeit not being competitive with a dedicated DE-spectroscopy or a dedicated neutron scattering setup, which is what we had expected.

We have pointed out some limitations of our n-DE-setup comprising the empty cell, like systematic errors which become important at higher frequencies. For samples with very high conductivity, like the PA sample tested in this work, another severe restriction in the high frequency range is observed at high temperatures. We ascribe this to the inductivity of cables becoming important for high sample conductivity.

Another limitation which we should stress is that absolute values of the dielectric permittivity or the conductivity are difficult to obtain with our setup. This can be judged e.g. from Fig.2 and Fig.3 were the permittivity of glycerol is found to be lower than regularly reported in literature. Although somehow expected, taking into account that we don't use a dedicated dielectric spectroscopy equipment, it is instructive to learn about the most probable reasons. Certainly the sample holder, originally designed for neutron scattering only, adds a non-negligible contribution as we have shown. Another important contribution comes from imperfect sample filling, which is nearly unavoidable with the present design but which could have been further optimised for the glycerol data shown. The sample is filled in the liquid state near room temperature and the needed sample quantity is calculated from the nominal sample holder dimensions. However, mechanical precision and the necessary play between the top and bottom pieces, uncertainties in the sample thickness due to the squeezed Indium seals and Teflon or minor deformation of the thin Aluminium neutron windows will contribute mostly to underestimate the sample quantity needed. Thus some void or gaz filled volume and an imperfect sample geometry are difficult to avoid and cause more problems for highly viscous samples. Thus one should be aware of the uncertain absolute value of the dielectric permittivity and envisage a more quantitative determination of the deviations in cases where it seems necessary.

In summary, the presented flat sample cell and setup for n-DE-spectroscopy will allow us tackling problems where simultaneous spectroscopy is of interest and we hope that the tests which we report here will help to develop a further improved generation of sample cells for simultaneous n-DE-spectroscopy.

We would like to thank Jérôme Rimet, IN16B ILL, the sample environment group SANE of ILL and the ILL for technical and financial support. We are thankful to Anette Fuchs, MPI Stuttgart, for the sample preparation of phosphoric acid (PA) and KDD Kreuer, MPI Stuttgart and A. Alegria, San Sebastian for discussing the possible origin of a high frequency artefact presented in this paper for PA.

References

[1] M. Bée, *Quasielastic neutron scattering: principles and applications in solid state chemistry, biology and materials science* (Adam Hilger, 1988)
[2] F. Kremer, A. Schönhals, *Theory of Dielectric Relaxation Spectra in Broadband Dielectric Spectroscopy* (Springer: Berlin, 2002)
[3] H.W. Hansen, A. Sanz, K. Adrjanowicz, B. Frick, K. Niss, Nature Communications **9**, 518 (2018)
[4] K. Niss et al., 10.5291/ILL-DATA.LTP-6-7 (2015)
[5] A. Sanz, H.W. Hansen, B. Jakobsen, I.H. Pedersen, S. Capaccioli, K. Adrjanowicz, M. Paluch, J. Gonthier, B. Frick, E. Lelièvre-Berna et al., Review Of Scientific Instruments **89**, 023904 (2018)

[6] H.W. Hansen, B. Frick, S. Capaccioli, A. Sanz, K. Niss, The Journal of Chemical Physics **149**, 214503 (2018)
[7] H.W. Hansen, F. Lundin, K. Adrjanowicz, B. Frick, A. Matic, K. Niss, Physical Chemistry Chemical Physics **137**, 080901 (2020)
[8] *WinDETA 6.02 - Program's Manual*, Novocontrol Technologies Germany (2017)
[9] *https://www.ill.eu/users/support-labs-infrastructure/instrument-control-service/remote-instrument-control* (last viewed 2022)
[10] B. Frick., J. Combet, L. van Eijck, Nuclear Instruments & Methods In Physics Research Section A-Accelerators Spectrometers Detectors And Associated Equipment **669**, 7 (2012)
[11] *https://www.ill.eu/in16b* (last viewed 2022)
[12] K. Niss et al (to be published)
[13] G. Squires, *Introduction to the Theory of Thermal Neutron Scattering* (Cambridge University Press, 1978)
[14] S. Lovesey, *Theory of neutron scattering from condensed matter* (Clarendon Press: United Kingdom, 1984)
[15] D. Noirat, *PhD thesis Roskilde University* (in progress)
[16] M. Jiménez-Ruiz, A. Sanz, A. Nogales, T. Ezquerra, Review of Scientific Instruments **76**, 043901 (2005)
[17] R. Bergman, H. Jansson, J. Swenson, The Journal of Chemical Physics **132**, 044504 (2010)
[18] H.W. Hansen, B. Frick, T. Hecksher, J.C. Dyre, K. Niss, Physical Review B **95**, 104202 (2017)
[19] A. Sanz, K. Niss, Crystal Growth & Design **17**, 4628 (2017)
[20] A. Sanz, K. Niss, The Journal of Chemical Physics **146** (2017)
[21] M. Paluch, S. Pawlus, K. Kaminski, The Journal of Chemical Physics **134**, 037101 (2011)
[22] R. Bergman, H. Jansson, J. Swenson, The Journal of Chemical Physics **134**, 037102 (2011)
[23] K.D. Kreuer, Chemistry Of Materials **17**, 610 (1996)
[24] J-P. Melchior, K-D. Kreuer, J. Maier, Physical Chemistry Chemical Physics **19**, 587 (2016)
[25] J-P. Melchior, B. Frick, Physical Chemistry Chemical Physics **19**, 28540 (2017)